

AFOSR-TR-81-0609

LEVEL III

(2)

6 EXPERIMENTAL AND ANALYTICAL STUDY OF EROSION
BURNING OF SOLID PROPELLANTS

10 Merrill K. King
Research and Technology Division
Atlantic Research Corporation
5390 Cherokee Avenue
Alexandria, Virginia 22314

A079618

Kenneth/Kuo
Rohit/Arora Robert/Beddini
The Pennsylvania State University
University Park, PA 16802

Robert Beddini
Aeronautical Research Associates of Princeton, Inc.
Princeton, NJ 08540

9 FINAL REPORT
October 1, 1978 - January 30, 1981

20
Contract/F49620-78-C-0016

15
Air Force Office of Scientific Research (AFSC)
Building 410
Bolling AFB, DC 20332

11 June 1981

12 114

Approved for public release;
distribution unlimited.

DTIC
ELECTRONIC
S
AUG 14 1981
C

AD A102850

DTIC FILE COPY

81 8 14 010

403

SECURITY CLASSIFICATION OF THIS PAGE (When Data Entered)

REPORT DOCUMENTATION PAGE		READ INSTRUCTIONS BEFORE COMPLETING FORM
1. REPORT NUMBER AFOSR-TR- 81 - 0609	2. GOVT ACCESSION NO. AD-102 850	3. RECIPIENT'S CATALOG NUMBER
4. TITLE (and Subtitle) "EXPERIMENTAL AND ANALYTICAL STUDY OF EROSION BURNING OF SOLID PROPELLANTS"		5. TYPE OF REPORT & PERIOD COVERED FINAL 1 OCT 78-31 JAN 81
		6. PERFORMING ORG. REPORT NUMBER
7. AUTHOR(s) M K KING R ARORA R BEDDINI K KUO		8. CONTRACT OR GRANT NUMBER(s) F49620-78-C-0016V
9. PERFORMING ORGANIZATION NAME AND ADDRESS ATLANTIC RESEARCH CORPORATION 5390 CHEROKEE AVENUE ALEXANDRIA, VA 22314		10. PROGRAM ELEMENT, PROJECT, TASK AREA & WORK UNIT NUMBERS 2308/A1 61102F
11. CONTROLLING OFFICE NAME AND ADDRESS AIR FORCE OFFICE OF SCIENTIFIC RESEARCH/NA BOLLING AFB, DC 20332		12. REPORT DATE JUNE 1981
		13. NUMBER OF PAGES 111
14. MONITORING AGENCY NAME & ADDRESS (if different from Controlling Office)		15. SECURITY CLASS. (of this report) UNCLASSIFIED
		15a. DECLASSIFICATION/DOWNGRADING SCHEDULE
16. DISTRIBUTION STATEMENT (of this Report) Approved for public release; distribution unlimited		
17. DISTRIBUTION STATEMENT (of the abstract entered in Block 20, if different from Report)		
18. SUPPLEMENTARY NOTES		
19. KEY WORDS (Continue on reverse side if necessary and identify by block number) EROSIVE BURNING SOLID PROPELLANT COMBUSTION REACTIVE FLOWS TURBULENT BOUNDARY LAYER TURBULENT COMBUSTION		
20. ABSTRACT (Continue on reverse side if necessary and identify by block number) Experimental and analytical, modeling studies of the erosive burning of solid propellants were conducted at Atlantic Research and Penn State University, with additional modeling efforts at Aeronautical Research Associates of Princeton. At Atlantic Research, erosive burning characteristics of approximately 15 AP-composite solid propellant formulations with systematically varied compositions and ingredient particle sizes were determined over a wide range of pressure		

and crossflow velocity. It was found that the most important parameter in determining sensitivity of burn rate to crossflow is the no-crossflow (base) burning rate versus pressure behavior of the formulation. An analytical model of the erosive burning of AP-composite formulations was developed and found to yield good a priori predictions of burn rate as a function of pressure and crossflow velocity, given only composition and ingredient particle sizes. This model was also found to predict an observed decrease in crossflow sensitivity with increasing grain port diameter. In addition, an analytical model of erosive burning of double-base propellants was developed and found to give good agreement with literature data. In the case of double-base propellants both this mechanism and tilting over a columnar diffusion flames appear to contribute. At PSU, erosive burning behavior of four AP-composite propellants was experimentally studied and erosive burning rate correlations relating r/r_0 to velocity and pressure were developed. $K-\epsilon$ turbulence closure, along with Spalding's eddy-breakup concept was used in a reacting turbulent boundary layer analysis which was coupled with a core region flow analysis into an erosive burning model. Theoretical results agreed well with data obtained at PSU and elsewhere. Erosive burning is attributed to increased turbulence activity near the propellant surface with increasing core axial velocity. At ARAP, modeled differential equations for combustion, turbulence, and mean-flow development within a grain port were numerically solved, enabling prediction of flow development and erosive burning. An improved scaling procedure for predicting erosive burning in large motors, involving prediction of mean-flow transition behavior, was developed. An assessment of the contribution of AP to erosive burning of composite propellants indicated strong sensitivity to the type of combustion model used. Direct effects of turbulence on homogeneous propellant gas-phase combustion were found to have negligible influence on erosive burning.

UNCLASSIFIED

INTRODUCTION - RESEARCH OBJECTIVES

Erosive burning, the augmentation of solid propellant burning rate by the flow of products across a burning surface, has become increasingly important with use of lower port-to-throat area ratio motors and nozzleless motors, both of which result in high velocity crossflows. The response of various propellants to such crossflows must be known by the motor designer in order for him to perform adequate motor design. In addition, it is important that the propellant formulator understand the effect of various formulation parameters on the sensitivity of a propellant to crossflows so that he may tailor his propellants to the desired characteristics. For example, in a nozzleless rocket motor, the decrease in pressure from the head end to the aft end of the grain tends to result in slower burning at the aft end in the absence of erosive effects. Depending upon the sensitivity of the formulation to crossflow, the increasing Mach number along the grain port may lead to undercompensation, exact cancellation, or overcompensation of the pressure effect. A detailed discussion of the effects of erosive burning on solid propellant rocket interior ballistics for low port-to-throat area ratio motors and nozzleless motors was presented by this author in Reference 1. Under this contract, experimental and analytical studies of erosive burning have been conducted at Atlantic Research and Pennsylvania State University along with additional modeling efforts at Aeronautical Research Associates of Princeton (ARAP). A comprehensive list of research objectives for this program is presented below:

A. Atlantic Research Objectives (Task A)

1. Develop a theoretical model of steady state erosive burning to permit prediction of composite propellant burning rate as a function of pressure and crossflow velocity, given only propellant composition and particle size distribution, and extend this model to handle cases involving multimodal oxidizer (ammonium perchlorate) and metalized propellants.
2. Work on development of an improved theoretical model of the effects of oscillatory crossflow on composite propellant combustion.

AIR FORCE OFFICE OF SCIENTIFIC RESEARCH (AFSC)
NOTICE OF TRANSMITTAL TO DDC
This technical report has been reviewed and is
approved for public release IAW AFR 190-12 (7b).
Distribution is unlimited.
A. D. BLOSE
Technical Information Officer

3. Conduct approximately 50 testing firings with approximately 10 different composite propellant formulations in the erosive burning test apparatus.

4. Formulate suitable quantities of composite propellants of various types to perform the erosive burning test program of Task A (3) in an experimental apparatus developed by Atlantic Research under AFOSR Contract F44620-76-C-0023.

5. Gather and correlate burning rate versus pressure versus crossflow velocity data from the tests of Task A (3).

6. Make continuing comparisons between experimental data and the developed erosive burning theoretical model, using these comparisons to upgrade the model as needed.

7. Incorporate in theoretical modeling of erosive burning by flame bending the effects of high blowing velocities and increased turbulence, characteristic of cylindrically perforated motors as opposed to test devices.

8. Develop at least a preliminary model for erosive burning of double-base propellants.

9. Investigate the need for modeling erosive burning in HMX-oxidized propellants.

10. Perform special motor tests to investigate the change in erosive burning sensitivity caused by a large change in the ratio of blowing velocity to crossflow velocity.

11. Perform preliminary design for a cold-flow test apparatus to study boundary layer shapes and turbulence distributions in internally perforated solid propellant grains.

12. Proceed with final design, construction and use of the cold flow apparatus for the purpose shown in Item A (11) above; or alternatively, perform 30 additional tests in the Atlantic Research erosive burning hardware, using about five selected HMX and double-base formulations.

B. Aeronautical Research Associates of Princeton Objectives (Task B)

1. Improve the grain port or test section flowfield modeling part of the erosive burning model located at Aeronautical Research Associates of Princeton, by removing the inviscid outer boundary layer assumption, and compare the results with existing flow experimental data.

2. Implement at least one commonly used composite propellant combustion model, and compare the results with appropriate data.

3. Remove the Shvab-Zeldovich assumptions from the Aeronautical Research Associates of Princeton erosive burning model and ascertain the limits of insensitivity to driver propellant temperature.
4. Develop a computer code with the ability to perform a quasitime dependent analysis of the burning of cylindrical and two-dimensional grains, depending upon the model's satisfactory performance under task B (1) and (2).
5. Parameterize the velocity profile results from the SPEC model in graphical or algebraic form.
6. Formulate the system of equations necessary to model particulate behavior and turbulence interaction within the grain port.
7. Incorporate the modeled particulate flow equations of subparagraph (6) into the SPEC code and demonstrate their solution.
8. Assess the effects of tubular motor length to diameter ratio and turbulence on particulate number-density profiles within the grain port.
9. Include an imposed acoustic field in the SPEC model and assess the effects of frequency and velocity on propellant burning.

C. Pennsylvania State University Objectives (Task C)

1. Perform checkout tests of the erosive burning model computer program located at Pennsylvania State University.
2. Perform a set of "computer experiments" to determine the best set of coefficients for turbulence correlations in the Pennsylvania State erosive burning model.
3. Perform a set of parametric calculations with the resulting final erosive burning model to study the effects of conditions such as gas velocity, flame temperature, chamber pressure, pressure gradient, and oxidizer particle size on erosive burning.
4. Investigate possible improvements in the turbulence closure procedures involved in the Pennsylvania State erosive burning model.
5. Use the resulting computer program to generate an erosive burning formula of use to propellant grain designers.
6. Perform a series of erosive burning experiments in a test apparatus, located at Pennsylvania State University. Parameters to be varied in this study include free-stream velocity, pressure, pressure gradient, oxidizer particle size, and propellant types.

Best Available Copy

Accession for	<input checked="" type="checkbox"/>	<input type="checkbox"/>	<input type="checkbox"/>
THIS FILE			
DISC FILE			
Unannounced			
Justification			
By			
Distribution/			
Availability Codes			
Avail and/or			
Dist Special			

A

7. Further improve the Pennsylvania State erosive burning model by improving the way reaction rate is included, and by taking account of high Mach number flow and surface roughness.
8. Extend the erosive burning model from flat-plate geometry to axisymmetric flow.
9. Validate the 2-D model of erosive burning by experimental firings and measurements.
10. Incorporate the erosive burning model into an existing rocket performance prediction code and test the resulting coupled erosive burning rocket performance code.

OVERALL SUMMARY

General approaches taken at the three different facilities are summarized in Figure 1. Two test devices, employing markedly different flow geometries as regards boundary layer development, were used to collect data at ARC and PSU. Composite propellant models were developed at ARC and PSU, while homogeneous propellant models were developed at ARAP and ARC. A major contrast between the modeling approaches lay in the emphasis at ARC on flame structure details, with a relatively simple mixing-length turbulence description, while more comprehensive turbulence models but simplified flame structure models were used at ARAP and PSU.

Results are summarized in Fig. 2. At ARAP, modeled differential equations for combustion, turbulence, and mean-flow development within a grain port were numerically solved, enabling prediction of flow development and erosive burning. An improved scaling procedure for predicting erosive burning in large motors, involving prediction of mean-flow transition behavior, was developed. An assessment of the contribution of AP to erosive burning of composite propellants indicated strong sensitivity to the type of combustion model used. Direct effects of turbulence on homogeneous propellant gas-phase combustion were found to have negligible influence on erosive burning.

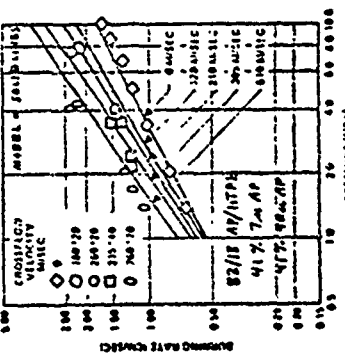
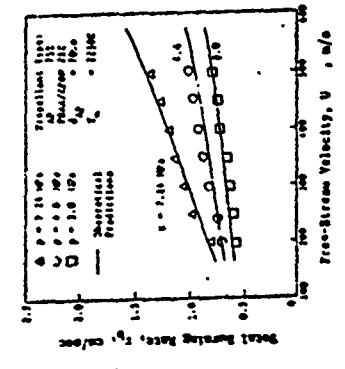
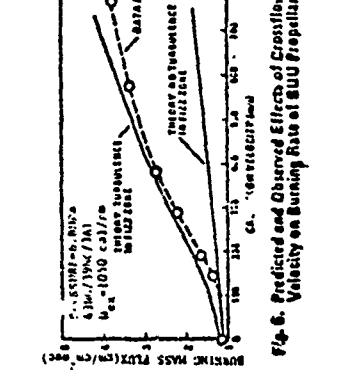
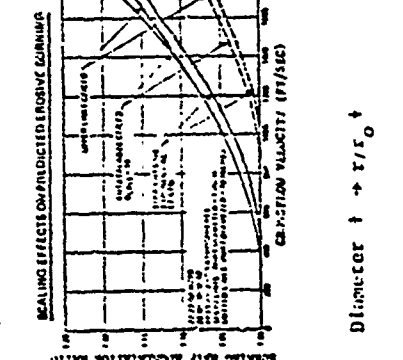
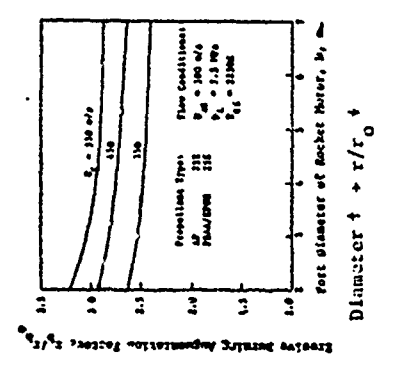
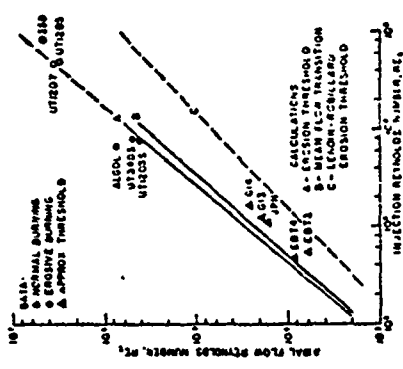
At PSU, erosive burning behavior of four AP-composite propellants was experimentally studied and erosive burning rate correlations relating r/r_0 to velocity and pressure were developed. K- ϵ turbulence closure, along with Spalding's eddy-breakup concept was used in a reacting turbulent boundary layer analysis which was coupled with a core region flow analysis into an erosive burning model. Theoretical results agreed well with data obtained at PSU and elsewhere. Erosive burning is attributed to increased turbulence activity near the propellant surface with increasing core axial velocity.

At ARC, models of erosive burning of AP composite propellants and homogeneous double-base propellants were developed and found to agree well with data. Both models permit prediction of no-cross-flow burn rate as well as erosive effects for uncatalyzed propellants. Postulated mechanisms are listed in Fig. 1. Both models predict a decrease in erosive burning effects with increasing port diameter, in agreement with observation. Erosive burning characteristics of approximately 15 composite formulations with systematically varied compositions and ingredient particle sizes have been measured over a wide range of pressure and crossflow velocity. It appears that the most important parameter in determining sensitivity of burn rate to crossflow is the no-crossflow (base) burning rate versus pressure behavior of the formulation.

FIGURE 1. APPROACHES USED IN EROSION BURNING STUDIES BY INVESTIGATORS AT ARC, ARAP, AND FSU.

ITEMS	ARC (1)		PSU		ARAP		ARC (2)	
	Theoretical and Experimental	Composite	Theoretical and experimental	Composite	Theoretical	Theoretical	Theoretical	Theoretical
Propellant Type								
Basic mechanisms considered in theoretical modeling	Crossflow-induced tilting of columnar diffusion flames. Also, crossflow-induced turbulent transport property augmentation + accelerated mixing of fuel and oxidizer and to increased heat transfer.	Composite	Turbulent shear flow interacts with the diffusion flame plus higher turbulent kinetic energy near surface + better mixing and higher rates of turbulent transport + higher heat feedback + higher r_b .		Homogeneous (AP or DB)	Homogeneous (Double base)		
Model Emphasis	Combustion Zone Details		Turbulent fluid dynamics					
Gas Phase Chemical Heat Release Rate Considerations	Modified BUP Model: O/F Diffusion Flame Plus AP Monopropellant Flame		Eddy breakup model of Spalding		Arrhenius Reaction Rate Law Applied to Single Global Reaction.	Combustion Zone Details		
Major Governing Equations	Heat Balance at Surface Including feedback from AP and O/F flames. Geometric location of O/F flame related to crossflow velocity. Eddy viscosity Prandtl mixing length approach used to describe turbulence distribution.		Conservation equations for mass, momentum, species, and energy are considered for mean flow variables. Turbulence closure was achieved by K- ϵ two-equation model.		Conservation equations for mass, momentum, species, and energy are considered for mean flow variables. Turbulence closure was achieved by multi-equation second-order closure.			Fourier Equations used to correct surface, fizz zone flame sheet and final flame sheet. Eddy viscosity Prandtl mixing length approach used to calculate turbulent transport property distribution.
Physical Model Configuration	2D or Axisymmetric		2D or Axisymmetric		2D or Axisymmetric	2D or Axisymmetric		2D or Axisymmetric
Important Features of Test Rig in Terms of Type of Flow.	Propellant sample connected to upstream driver grain to allow boundary layer development before the test section.		Propellant sample mounted on fixed leading edge so that boundary layer develops along it.					
Burn Rate Measurement Procedure	Direct measurement using high-speed photography through quartz windows		Direct measurement using high-speed photography through Plexiglas windows.					

FIGURE 2. MAJOR RESULTS

ITEMS	ARC (1)	PSU	ARAP	ARC (2)
<p>Comparison of data and theory (typical)</p>			<p>Only qualitative comparisons made</p>	
<p>Definition of parameters strongly influencing erosive burning sensitivity, (Experimental)</p>	<p>Strongly dependent on base rate. Small residual effect of AP size. Other parameters appear to have effect only through their effect on base rate</p>	<p>Strongly dependent on base rate. Other parameters not studied extensively.</p>		<p>Fig. 6. Predicted and Observed Effects of Crossflow Velocity on Burning Rate of BBU Propellant.</p>
<p>Scale Effects Predicted By Models</p>				<p>Diameter $\rightarrow r/r_0 \rightarrow$</p>
<p>Other</p>	<p>Model includes capability of predicting un-crossflow (base) burn rate versus pressure for uncatalyzed AP/HTPB formulations.</p>	<p>Effects of nonuniform port diameter and roughness on erosive burning examined and found to be non-negligible.</p>	<p>Direct effects of turbulence on gas-phase combustion are shown to have negligible influence on erosive burning of homogeneous propellants.</p>	<p>Model includes capability of predicting no-crossflow (base) burn rate as a function of pressure and Hex for uncatalyzed double-base propellants.</p>

A brief summary of the work accomplished at Atlantic Research along with a list of publications and a description of interactions with other activities is presented below. Similar presentations of the Penn State and ARAP efforts are presented in Appendices A and B. Finally, copies of several of the more important publications generated during this program, providing the interested reader with a fairly comprehensive picture of the various experimental and modeling efforts, are included as Appendices C - F.

SUMMARY OF WORK ACCOMPLISHED AT ATLANTIC RESEARCH

The major emphases of the work carried out at Atlantic Research involved development of a comprehensive composite propellant burning rate model capable of yielding accurate predictions of burn rates of such propellants as a function of pressure and crossflow velocity, given only propellant composition and ingredient particle sizes, and creation of a systematic data base regarding the effects of crossflow on burning rate as a function of formulation parameters. A fairly comprehensive summary of these efforts appears in Appendix C, a copy of a paper presented by the first author at the 17th JANNAF Combustion Meeting⁽²⁾. During the program, erosive burning characteristics of approximately 15 AP-composite formulations with systematically varied compositions and ingredient particle sizes were measured over a wide range of pressure and crossflow velocity. Data for all but four of these formulations appear in Appendix C. (Data for two polyester binder formulations appear in Reference 3, while data for two aluminized formulations tested subsequent to preparation of Reference 2 have not yet been published elsewhere and are included herein as Figures 3 and 4.) As a result of these tests, it was concluded that the most important parameter in determining sensitivity of burn rate to crossflow is the base (no-crossflow) burning rate versus pressure behavior of the formulation, independent of what formulation variations are used to fix this behavior. In general, the AP-composite propellant burning rate model developed during this program was found to give excellent predictions of the no-crossflow burn rate versus pressure behavior of the propellants tested and good-to-excellent prediction of the erosive burning characteristics. In addition (and very importantly) the model predicts a decrease in sensitivity of burn rate to cross flow with increasing port diameter, in agreement with the observations of motor developers. The modeling effort described in Appendix C (and earlier references) was limited to two-dimensional channels: during the last year of the program, the model was straightforwardly modified to treat axisymmetric port geometries as well. In addition, the capability of treating the effects of zirconium as an ingredient (though only on a heat-sink basis) was added.

During the final year of the contract, an additional model, for prediction of the effects of pressure, crossflow velocity, and heat of explosion on the burning rates of NC/NG double-base propellants was developed and tested against existing data. This effort is described in Appendix D, a copy of a paper to be presented at the AIAA/SAE/ASME 17th Joint Propulsion Conference in July, 1981. In this study, a flame-sheet model of double-base propellant burning rate as a function of pressure and heat of explosion was first developed and found to give excellent agreement with data except at extremely low pressures. Two models of the effects of crossflow were then developed as extensions of this base model.

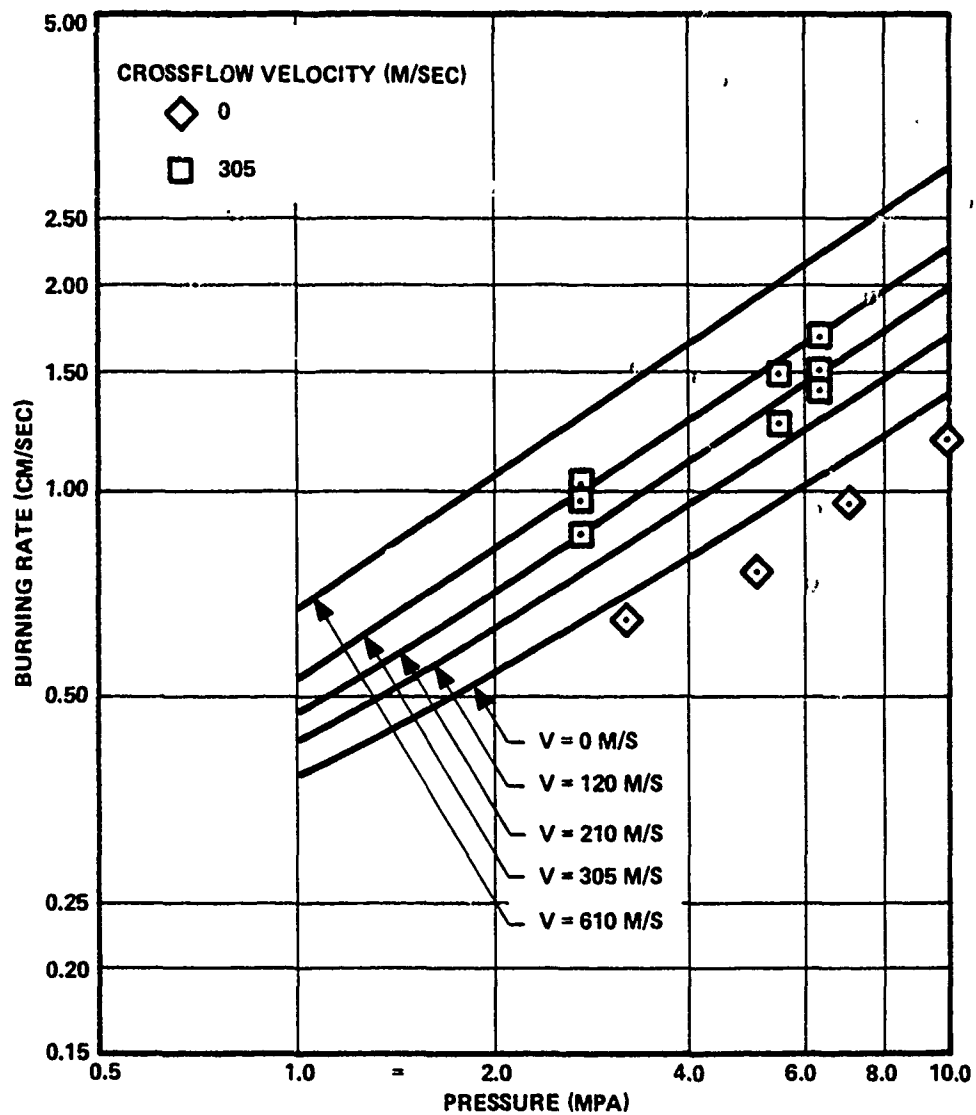


Figure 3. Burning Rate Predictions (Solid Lines) and Data (Points) for Formulation 9316 (80/5/15 AP/Al/HTPB, 24% 20 μ AP, 30% 200 μ AP, 26% 400 μ AP)

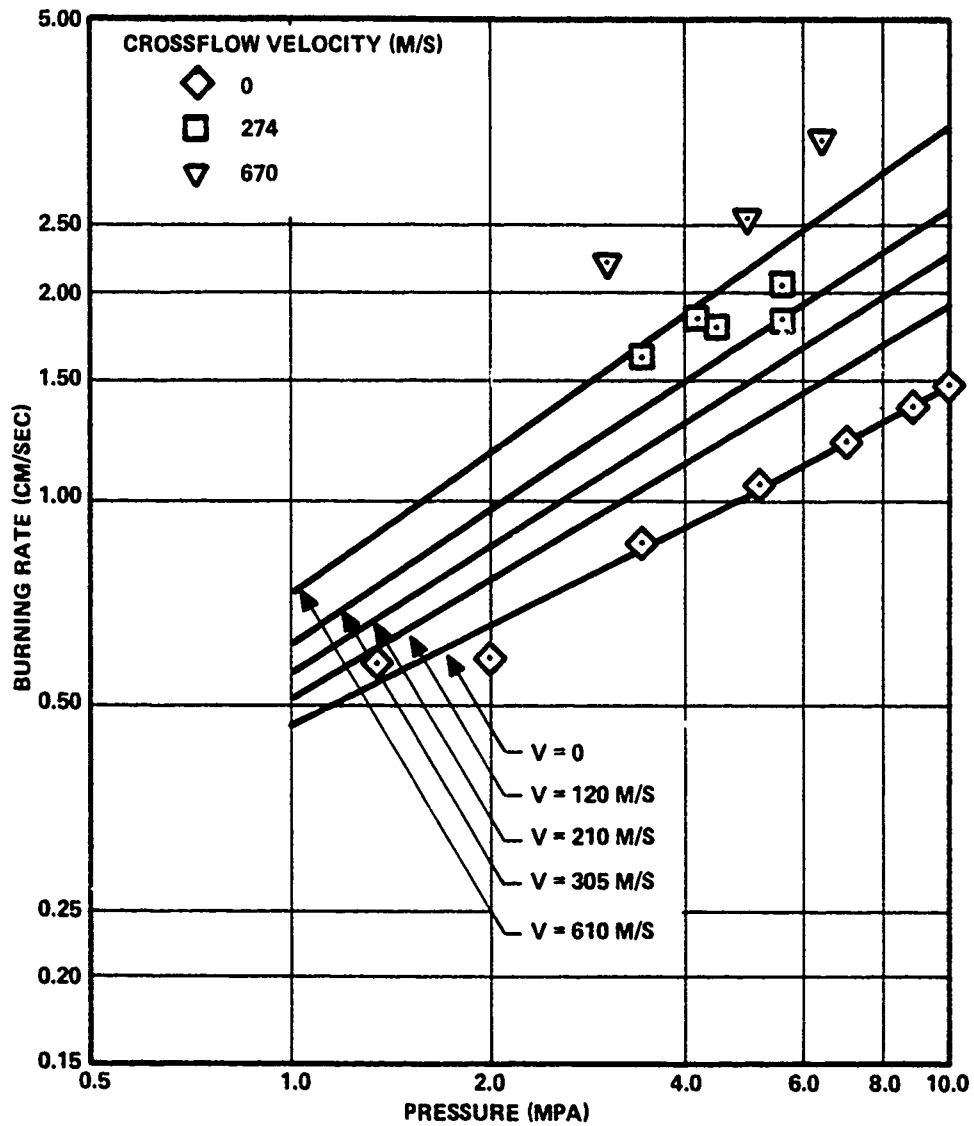


Figure 4. Burning Rate Predictions (Solid Lines) and Data (Points) for Formulation Webcomp 19M (70/18/12 AP/Al/HTPB, 10% 200 μ AP, 39% 90 μ AP, 21% 20 μ AP.

In the first, the fizz zone was assumed to be sufficiently structured to prevent turbulence penetration, the only burn rate augmentation mechanism being amplification of transport properties in the dark zone (sufficient to cause final flame influence) by crossflow-induced turbulence. This model seriously underpredicts crossflow effects. In the second model, the fizz zone was treated as a gas in terms of fluid dynamics with resultant amplification of transport properties in both the fizz and dark zones. This approach gave reasonably good agreement between predicted and measured burning rates over a wide range of crossflow conditions.

References:

1. King, M. "Effects of Crossflow on Solid Propellant Combustion: Interior Ballistic Design Implications", 1976 JANNAF Propulsion Meeting, Atlanta Georgia, December 1976, CPIA Publ. 280, Vol. V, p. 342.
2. King, M.K., "Predicted and Measured Effects of Pressure and Crossflow Velocity on Composite Propellant Burning Rate", 17th JANNAF Combustion Meeting, Hampton, Va., September, 1980. CPIA p. 61. 329, Vol. I, Nov. 1980, p. 99
3. King, M.K., "An Investigation of the Effects of Formulation Parameters on Erosive Burning of Composite Propellants", 16th JANNAF Combustion Meeting, Monterey, Calif., Sept., 1979. CPIA Publ. 308, Vol. II, Dec., 1979, p. 171

PUBLICATIONS GENERATED BY ATLANTIC RESEARCH UNDER
CONTRACT F49620-78-C-0016*

King, M. K., "Model for Steady State Combustion of Unimodal Composite Solid Propellants," AIAA 16th Aerospace Sciences Meeting, Huntsville, Alabama, January 1978, AIAA Paper No. 78-216.

King, M. K., "Erosive Burning of Composite Solid Propellants: Experimental and Modeling Studies," AIAA/SAE 14th Joint Propulsion Conference, Los Vegas, Nevada, July, 1978. Also, Journal Of Spacecraft and Rockets, 16, 3, May-June, 1979. p. 154.

King, M. K., "Erosive Burning of Composite Solid Propellants," 15th JANNAF Combustion Meeting, Newport, R.I., September, 1978, CP'A Publication 297, Vol. II, pp. 179-88, Feb., 1979.

King, M. K., "A Model of the Effects of Pressure and Crossflow Velocity on Composite Propellant Burning Rate," AIAA Paper 79-1171, AIAA/SAE/ASME 15th Joint Propulsion Conference, June, 1979, Las Vegas, Nevada.

King, M.K., "An Investigation of the Effects of Formulation Parameters on Erosive Burning of Composite Propellants," 16th JANNAF Combustion Meeting, Monterey, California, Sept. 1979. CPIA Publication 308, Vol. II, Dec., 1979, p. 171.

King, M.K., "Experimental and Theoretical Study of the Effects of Pressure and Crossflow Velocity on Composite Propellant Burning Rate," 18th Symposium (International) on Combustion, Waterloo, Canada, 1980. To be printed in Meeting Proceedings.

King, M.K., "Predicted and Measured Effects of Pressure and Crossflow Velocity on Composite Propellant Burning Rate", 17th JANNAF Combustion Meeting, Hampton, Va., Sept. 1980, CPIA Publ. 329, Vol. I, Nov., 1980, p. 99.

King, M.K., "A Burning Rate Model For Double-Base Propellants With and Without Product Crossflow," 1st International Specialists Meeting of the Combustion Institute, Bordeaux, France, July, 1981. To appear in Proceedings Volume.

King, M.K., "A Model For Prediction of Effects of Pressure, Crossflow Velocity, and Heat of Explosion on Double-Base Propellant Burning Rate", AIAA Paper 81-1555, AIAA/SAE/ASME 17th Joint Propulsion Conference, Colorado, Springs, Colorado, July, 1981.

* See Appendices A and B for Publications Generated by Penn State and ARAP Under contract F49620-78-C-0016

PROFESSIONAL PERSONNEL ASSOCIATED WITH
ATLANTIC RESEARCH EFFORT UNDER CONTRACT F49620-78-C-0016

1. Dr. Merrill K. King - Principal Investigator, Analytical Modeling,
Test Selection, Data Analysis
2. Mr. Stephen Kunkel - Test Direction
3. Mr. Phillip Graham - Propellant Formulation
4. Mr. Merlin Larimer - Propellant Formulation
5. Mr. Robert Wallace - Testing

INTERACTIONS (COUPLING ACTIVITIES) INVOLVING
ATLANTIC RESEARCH PERSONNEL*

1. Dr. King participated in the Velocity-Coupled Combustion Instability Workshop held at the US Naval Postgraduate School during the 16th JANNAF Combustion Meeting, September, 1979.
2. Dr. King had several conversations with Dr. Robert Hermesen (CSD) during August-September, 1979, regarding both the first and second generation erosive burning models and the Atlantic Research erosive burning data base developed under this program, with the object of incorporating this information into the Solid Rocket Performance Program being developed by CSD and Software Engineering Associates for AFRPL.
3. H. P. Sauerwein, A. Lampert, and R. H. Schmucker (Bayern Chemie, West Germany) have incorporated our first generation erosive burning model into an interior ballistics code to very successfully predict performance of small tactical rockets. Results of this work were presented at the 53rd AGARD Propulsion and Energetics Symposium in Oslo.
4. Atlantic Research, with SEA as a subcontractor, is currently developing a Nozzleless Motor Performance Computer code under contract to AFRPL. A major part of this development involves incorporation of Dr. King's second generation erosive burning model into the code for prediction of burning rate as a function of pressure, crossflow velocity, grain port diameter, and axial location along the port.

* See Appendices A and B for similar information regarding the Penn State and ARAP subcontracts.

APPENDIX A

FINAL REPORT FROM PENNSYLVANIA STATE UNIVERSITY

TO

ATLANTIC RESEARCH CORPORATION

TURBULENT BOUNDARY-LAYER ANALYSIS
AND EXPERIMENTAL INVESTIGATION OF
EROSIVE BURNING OF COMPOSITE SOLID PROPELLANTS*

Final Report

to

Atlantic Research Corporation
Alexandria, Virginia 22314

Contract No. F49620-78-C-0016

Prepared by:

Kenneth K. Kuo

and

Rohit Arora

Mechanical Engineering Department
The Pennsylvania State University
University Park, Pennsylvania 16802

April 1, 1981

* This research work was conducted under a subcontract from the Atlantic Research Corporation which is the prime contractor for AFOSR under the management of Dr. L. H. Caveny. The processing of propellant samples arranged by Dr. D. George at AFRPL and by Dr. M. K. King at Atlantic Research Corporation is highly appreciated. The assistance of Dr. M. K. Razdan, Mr. F. X. White, Mr. H. Kamath and T. White of The Pennsylvania State University is acknowledged.

Summary and Conclusions

The purpose of this study was to investigate the frequently encountered phenomenon of erosive burning of composite solid propellants in rocket motors. Both theoretical and experimental investigations were conducted to acquire a deeper understanding of the basic mechanism of erosive burning. In the experimental work, two-dimensional propellant slabs were used in a windowed test chamber with hot combustion product gases flowing over the sample at various velocities (subsonic and supersonic) and chamber pressures for four different AP-based composite propellants. The instantaneous regression rate of the propellant was recorded by a high speed movie camera and deduced through a motion analyzer. Erosive burning rate correlations were developed which relate the burning-rate augmentation factor to velocity and pressure.

In the theoretical work, the propellant burning process was described by considering a quasi-steady two-dimensional (planar or axisymmetric) chemically reacting, turbulent boundary layer over a propellant surface. For the axisymmetric case, the flow in the core region was solved with the flow in the viscous boundary layer region. K- ϵ turbulence closure, along with the eddy-breakup concept of Spalding was used for the reacting turbulent boundary layer analysis. The theoretical model, comprised of a set of partial differential equations, was solved numerically.

Comparison of the theoretical results with the experimental data obtained under the present contract and that obtained from existing literature, showed a close agreement. From the results of this study, the mechanism of erosive burning is believed to be the increased turbulence activity near the regressing propellant surface as the cross flow velocity is increased.

Both experimental and theoretical results show that the erosive burning rate is more pronounced at higher pressures than that at lower pressures. Erosive burning rate of a rocket motor is found to decrease as the inner diameter of the propellant grain increases. The erosive burning rate was found to correlate well with pressure and freestream velocity for all four of the different composite propellants studied.

Publications

The papers and reports, representing the results obtained through the sponsorship of this program, which were published or accepted for publication and presentation are attached with this report and listed below.

1. Razdan, M. K. and Kuo, K. K., "Erosive Burning Study of Composite Solid Propellants by Turbulent Boundary-Layer Approach," AIAA Journal, Vol. 17, No. 11, November 1979, pp. 1225-1233.
2. Razdan, M. K. and Kuo, K. K., "Measurements and Model Validation for Composite Propellants Burning Under Cross Flow of Gases," AIAA Journal, Vol. 18, No. 6, June 1980, pp. 669-677.

3. Razdan, M. K. and Kuo, K. K., "Turbulent-Flow Analysis and Measurements of Erosive-Burning Rates of Composite Solid Propellants," AIAA Paper No. 80-1209, AIAA/SAE/ASME 16th Joint Propulsion Conference, Hartford, CT, June 30-July 2, 1980.
4. Razdan, M. K. and Kuo, K. K., "Turbulent Boundary Layer Analysis and Experimental Investigation of Erosive Burning Problem of Composite Solid Propellants," Scientific Report to AFOSR, March 1980 (192 pages).(not attached)
5. Kuo, K. K. and Razdan, M. K., "Erosive Burning of Solid Propellants," accepted as a chapter of the book entitled Fundamentals of Solid Propellant Combustion being edited by K. K. Kuo and M. Summerfield for AIAA Progress Series, 1980.
6. R. Arora, F. X. White, and K. K. Kuo, "Erosive Burning of Composite Propellants Under High-Velocity Cross Flow Conditions," AIAA Paper No. 81-1581, to be presented in the AIAA/SAE/ASME 17th Joint Propulsion Conference, Colorado Springs, CO, July 26-29, 1981.

Linkage with Other DoD Sponsored Programs

The erosive burning chamber designed and fabricated under this contract has been demonstrated to be useful in obtaining erosive burning data. This test rig is being used currently for measuring the erosive burning characteristics of a Navy propellant under a contract sponsored by Naval Ordnance Station, Indian Head, Maryland.

This facility will also be used for future research programs sponsored by DoD agencies in the area of propellant combustion and propulsion.

64

APPENDIX B
FINAL REPORT FROM AERONAUTICAL RESEARCH ASSOCIATES
OF PRINCETON
TO ATLANTIC RESEARCH CORPORATION

ANALYSIS OF INJECTION - INDUCED FLOWS IN POROUS - WALLED DUCTS
WITH APPLICATION TO THE AEROTHERMOCHEMISTRY OF
SOLID - PROPELLANT MOTORS

A final report prepared under contract ARC-P.O.12181

for

Atlantic Research Corporation

5390 Cherokee Avenue

Alexandria, Virginia 22314

by

Robert A. Beddini

Aeronautical Research Associates of Princeton, Inc.

P.O. Box 2229

50 Washington Road

Princeton, New Jersey 08540

May, 1981

SUMMARY

A theoretical analysis of injection-induced flows in porous ducts has been presented with application to the aerothermochemistry of solid propellant motors. Major assumptions and analytical restrictions are summarized in Table 2.1.

A literature review of injection-induced flows in porous tubes indicates that for large injection Reynolds numbers the flow development may be characterized by three distinct regimes. Within a relative axial distance of $x/R = 5-10$, as measured from the closed (head) end, the axial velocity profile attains the form predicted by laminar similarity theory. For relative axial distances of this same order, the flow can undergo a turbulent transition with turbulence intensities greater than 10% of the axial velocity component observed. Within this second regime the mean axial velocity profile continues to correspond with laminar similarity theory, while the turbulence intensity profile undergoes further development. The pronounced maximum in the turbulence intensity profile lies midway between the centerline and inner surface of the tube at values of $x/R < 10$. The height above the surface at which this maximum occurs decreases with increasing axial distance. Finally, a third flow regime has been observed in one experimental apparatus (that of Olson, 1964, and Huesmann-Eckert, 1968), and is initiated by transition of the mean axial velocity-profile.

Table 2.1. Summary of Assumptions

Preliminary Gas-Phase Assumptions

- a) External body forces and the coefficient of bulk viscosity are negligible.
- b) Effects of radiation on mass, momentum, and heat transfer are negligible.
- c) Species diffusion due to thermal and pressure gradient effects is negligible, and all binary diffusion coefficients are equal.
- d) The Lewis number is unity.
- e) Specific heats of the chemical species are equal and independent of temperature.
- f) The flow is steady in the mean, and the contribution of the time derivative of pressure appearing in the total enthalpy equation (Eq. (2.3)) is negligible.
- g) The term in brackets in the total enthalpy equation (Eq. (2.3)) is negligible. This condition is satisfied if either
 - 1) Combustion occurs in a low Mach number region of the flow, or
 - 2) The Prandtl number is nearly unity, the mean flow is of boundary layer type (gradients are large in a direction normal to the principal flow direction) and the contributions of turbulent dissipation and velocity divergence effects appearing in the total enthalpy equation are negligible.
- h) Combustion of a homogeneous reactant mixture proceeds through a single step, irreversible, chemical reaction.

Condensed Phase Assumptions

- i) The condensed phase is homogeneous.
- j) The condensed phase is stationary in the reference coordinate system.
- k) Material properties are constant.
 - l) Species diffusion is negligible.
- m) Radiation effects at the interface and in the condensed phase are negligible.
- n) The interface velocity is small relative to the characteristic flow velocity.
- o) Subsurface chemical reactions, if present, are in equilibrium with the surface mass flux.
- p) The surface reaction is rate-limited and governed by a zeroth-order, irreversible Arrhenius kinetic expression.
- q) Condensed phase processes are quasi-steady.

- r) Heat transfer in the condensed phase occurs only in the direction normal to the interface and is confined to a boundary layer which is thin compared with the local interface radius of curvature and the mean fluid dynamic length scales.

Final Assumptions

- s) The gas-phase species-average molecular weight is equal to the molecular weight of the mixture at equilibrium.
- t) The effects of turbulence are modeled using a second-order-closure technique with the effects of turbulence on the gas-phase reaction rate correlations (combustion-turbulence interaction) consistently included in the analysis.
- u) The flow is two-dimensional in the mean and is either axially symmetric or symmetric about the centerline of a planar duct.
- v) The radius (R) of the cylindrical duct or the half-height (δ) of a planar duct is independent of axial position.
- w) The flow is of boundary layer type; viz., gradients of the dependent variable normal to the surface are assumed much larger than axial gradients, with the normal gradient of static pressure assumed negligible.

Theoretical results from the present analysis are found to be in good agreement with laminar similarity theory and the mean axial velocity profile data of Yamada, et al., and Dunlap, et al., (Regime 2). Agreement to within several percent is obtained in comparison with the transitional mean flow data of Huesmann and Eckert which, in view of the hydrodynamic sensitivity of this phenomenon, is considered quite encouraging. Agreement between the present calculations and turbulence intensity data in Regime 2 ranges from qualitative (for the intensity profiles reported by Yamada, et al.) to quantitative (within approximately 20% for the other maximum intensity data of Yamada, et al., and the profile data of Dunlap, et al.). Detailed measurements of mean flow and turbulence structure in Regime 3 have not been reported. The character of the flow within Regime 3 is predicted to be similar, in some respects, to wall-bounded turbulent shear flows with injection (e.g., the behavior of friction coefficient), with turbulent Poiseuille-flow conditions asymptotically approached as x/R increases.

The sensitivity of turbulence development in Regime 2 and the attendant mean-flow transition process have been assessed for two types of disturbance. The first type originates within the head-end region ($x/R \sim 1$), as caused, for example, by the vortex shedding off the impermeable head-end surface observed by Yagodkin. This type is simulated by specifying finite relative turbulence intensity distributions as computational "initial" conditions at $x/R = 1-10$. The second type of disturbance is caused by high fluid injection rates through a porous medium - the "jet coalescence" phenomenon experimentally observed by Pimenta and Moffat and others. This type of

pseudo-turbulent disturbance has not been theoretically examined in prior work on porous tube flows or more general boundary-layers with injection. It is modeled in the present analysis as a finite value of the transverse velocity autocorrelation at the tube surface; the root mean square of this value assumed (in the absence of detailed experimental data) to be proportionate to the mean injection velocity.

The results of the sensitivity studies may be summarized as follows.

- (a) For either type of disturbance and for any of the disturbance levels investigated, the present results for the loci of axial-flow Reynolds number at mean-flow transition ($Re_{c,tr}$) as a function of injection Reynolds number (Re_s) follow the trend predicted by planar linear stability-theory for the initial destabilization (turbulent transition) of the flow. In particular, for large values of Re_s (> 300) the present results indicate the linear relation

$$Re_{c,tr} \sim Re_s$$

with the constant of proportionality generally dependent on the magnitude and type of disturbance. The linear high Reynolds number relation for transition of the mean velocity profile in nonreactive porous-tube flows also implies that the axial distance required for transition is independent of injection Reynolds number.

- (b) The growth rate of the maximum value of turbulence and the downstream location of mean flow transition are quite sensitive to the relative turbulence level specified at the initial station when this level is small (less than 5% of the mean speed). In such cases the tube lengths required for mean-flow transition can be relatively large ($x/R > 50$), and the present compressible flow calculations indicate that the flow can "choke" before mean-flow transition is attained.
- (c) The location of transition becomes nearly insensitive to relative initial turbulence levels when such levels are large (greater than approximately 15%). The "excess" turbulence is found to linearly decay in the upstream portion of Regime 2. Evidence of this behavior is found in some of the experimental data of Yamada, et al. This result indicates that quasi-equilibrium turbulence development can occur in Regime 2, and that while the mechanisms of flow destabilization in Regime 1 and turbulence development in Regime 2 may be different, the processes exhibit a similar dependence on injection Reynolds number.
- (d) Disturbances introduced at the porous tube surface are predicted to be much more effective in inducing mean flow transition than are disturbances introduced within the upstream region of the flow. For example, a moderate level of disturbance (3.5% of the mean injection velocity) is theoretically found to reduce the mean-flow transition length to $x/R = 16$.

(e) There is little effect of the roughness of the porous tube surface (typically, 10-100 μ m) on mean flow transition. The disturbance level and length scale caused by fluid injection through a porous medium (d) appears to create a virtual roughness much larger than the actual physical roughness.

(f) There is little quantitative difference between the porous tube and channel results for mean flow transition, when expressed in terms of the axial-flow and injection Reynolds numbers defined herein.

With respect to application of the present theory to the aerothermochemistry of the solid propellant motor (viz., the erosive burning problem), the following conclusions may be drawn.

(g) Good agreement has been obtained in comparisons of theoretical results with axial pressure distribution data in a laboratory motor experiencing severe erosive burning. The predicted behavior and magnitude of erosive burning is found comparable to that displayed by the Lenoir-Robillard theory. Both theories require some form of calibration or estimation of empirical constants or physical parameters. For the Lenoir-Robillard theory, the empirical coefficients were evaluated by Stokes, et al., using a least-squares procedure to correlate the pressure distribution data. For the present theory, the thermochemical parameters required to approximate the nonerosive combustion of the propellant are first estimated. Exposing the propellant to the theoretically predicted flow within the laboratory motor yields an erosive

burning response, the magnitude of which is sensitive (in part) to the assumed value of propellant surface roughness. The values of surface-roughness height which provide the best agreement with experimental data are believed quite reasonable.

- (h) The essential features of the flow within a solid propellant motor are found to be similar to those predicted for nonreactive injection-induced porous duct flows. In particular, the initiation of erosive burning (the threshold condition) is consistently found to be preceded by transition of the mean axial velocity profile within the grain port. Comparing the present predictions with the classical and conventional concept, i.e., that erosive burning is due to enhanced (turbulent) thermal diffusion within a coexistent viscous sublayer/combustion zone, it is noted that no revolutionary mechanism of erosive burning is proposed. Rather, the present results, together with cold-flow data, imply that unless the mean flow undergoes transition, one does not have a well-defined sublayer to support conventional assumptions and approaches to the erosive burning problem.
- (i) The transition and threshold phenomena are found to vary with the size and, more generally, the Reynolds numbers of the flow. The threshold scaling may be expressed as

$$Re_{c, \text{threshold}} \sim Re_x^\chi$$

where χ is found to be approximately 1.26 in calculations for

specific, but representative propellant conditions. The mean flow transition behavior is found to scale similarly, but with the slightly lower value of $\chi = 1.22$. The predicted dependence of the threshold condition on injection Reynolds number is found to be larger than that exhibited by other theories examined (particularly the Lenoir-Robillard theory, for which $\chi = 1$) and reflects the physical processes considered. The present results appear to provide better agreement with scale-up of the threshold condition from laboratory and sub-scale to full-scale motors, and hence appear to reconcile the absence of erosive burning observed in large (booster-type) motors.

It is also noted that the predicted value of $\chi = 1.0$ for mean flow transition scaling in nonreactive flows differs from the $\chi = 1.22$ value obtained for a reactive system. This indicates that the presence of a combustion zone, though quite close to the surface, is nevertheless able to interact with the fluid dynamics so as to alter both the magnitude and scaling of transition. The latter effect is not believed to be exhibited by prior erosive burning theories.

- (j) Two models which have been proposed for the normal combustion of ammonium perchlorate (AP) have been examined with regard to their predicted erosive burning response under similar flow conditions. Since both combustion models (due to Beckstead, et al., 1971; and Guirao-Williams, 1971) are able to correlate the normal burning-rate behavior of AP, it is difficult to establish the validity of either model on this basis. However, the two

combustion models are found to yield substantially different predictions for erosive burning, which is principally due to the different estimates of reaction zone thickness (flame height) intrinsic to the models. The difference in erosive burning produced by the two established combustion models illustrates the importance of this aspect of the problem - apart from the description of fluid dynamics, and the need for further research in this area.

- (k) The effects of turbulence on the gas-phase reaction rate (combustion-turbulence interaction) have been assessed. The analysis includes the contributions of both the mean reaction-rate and the reaction-rate correlations appearing in the turbulence transport equations. In comparison with results obtained without the effects of CTI, the results obtained with CTI show negligible effect on the propellant burning rate under erosion conditions. In particular, no evidence has been found that CTI causes a reduction in burning rate at lower axial-velocity conditions ("negative erosion"), as hypothesized by Vilyunov and Dvoruashin.

Despite the negligible effects on burning rate, CTI is found to cause appreciable changes in the temperature autocorrelation, turbulent heat flux, and mean reaction-rate profiles. For the two sets of parametric conditions principally investigated, regions wherein the mean reaction rate is approximately doubled or halved by CTI are predicted. The competitive physical processes which maintain a nearly constant burning (deflagration) rate under these circumstances are obscured by the numerical solution procedure, and

arouse considerable curiosity. Qualitatively similar numerical results have recently been reported by Borghi and Dutoya (1979) for a completely gas-phase problems.

For further detail, the reader is referred to A.R.A.P. Report No. 449, May 1981, from which the above summary was extracted.

PUBLICATIONS

Beddini, R.A. and Varma, A.K., "Analysis of Combustion-Turbulence Interaction with Application to the Deflagration of a Solid Monopropellant," in preparation. Submitted to Combustion Science and Technology in December, 1979.

Beddini, R.A., and Varma, A.K., "Analysis of Ammonium Perchlorate Combustion in Turbulent Flow", 16th JANNAF Combustion Meeting, Monterey, Calif., Sept., 1979. CPIA Publication No. 308, Vol. II, p. 193, Dec. 1979.

Beddini, R.A., "On the Scaling of Erosive Burning: The Threshold Condition," 15th JANNAF Combustion Meeting, Newport, Rhode Island, Sept. 1978, CPIA Publication 297, Vol. II, p. 199, Feb., 1979.

Beddini, R.A., "Aerothermochemical Analysis of Erosive Burning in a Laboratory Solid-Rocket Motor," AIAAJ, 18, 11, Nov. 1980, p. 1346.

Beddini, R.A., "A Reacting Turbulent Boundary Layer Approach to Solid Propellant Erosive Burning, AIAA Journal, Vol. 16, No. 9, September, 1978.

INTERACTIONS

- 1.) Mr. Beddini presented results from the combustion-turbulent interaction phase of research at the 16th JANNAF Combustion Meeting, Naval Postgraduate School, Monterrey, CA, Sept. 10-14, 1979.
- 2.) While at that meeting, he discussed various aspects of flowfield-interaction effects on velocity coupling. The individuals principally involved in the technical discussion were Mr. Jay N. Levine of AFRPL and Dr. Ronald Derr of NWC/China Lake.
- 3.) Dr. Robert Hermsen (of United Technologies/Chemical Systems Div.) and Mr. Beddini had several discussions during July - September, 1979. Dr. Hermsen forwarded a revised copy of a graph showing the scaling of the erosive burning threshold condition that was previously published by Mr. Beddini. Dr. Hermsen had added new data from several CSD motors and indicated that this provided further support for the scaling relation developed under AFOSR sponsorship. Dr. Hermsen was investigating the implementation of the threshold criterion in the Solid Rocket Performance Program being developed by CSD for AFRPL.
- 4.) While at the AFOSR/RPL Reserarch Meeting (March 20-22, 1979), discussions were held with Dr. Dawell George of AFRPL concerning the applicability of the SPEC model to the upcoming RPF "Nozzleless Performance Program." Mr. Beddini indicated that direct incorporation of the SPEC model in the NNP would be somewhat premature in the time-frame of interest to AFRPL. However, results from the SPEC model could be used as a guide in the selection of suitable erosive burning models.

APPENDIX C

Technical Paper Summarizing
Atlantic Research Experimental
and Analytical Studies of Erosive
Burning of AP-Composite
Propellants

(Presented at the 17th JANNAF
Combustion Meeting
September, 1980)

PREDICTED AND MEASURED EFFECTS OF PRESSURE
AND CROSSFLOW VELOCITY ON COMPOSITE
PROPELLANT BURNING RATE*

Merrill K. King
Atlantic Research Corporation
Alexandria, Virginia 22314

ABSTRACT

A theoretical model for prediction of burning rates of composite (ammonium perchlorate oxidizer) solid propellants as a function of pressure and crossflow velocity has been developed. Included in this model is the capability for treatment of multimodal oxidizer particle sizes and metalized formulations. In addition, an experimental device for measuring the effects of crossflow velocity on propellant burning rate has been developed and used to characterize a series of AP/HTPB propellants with systematically varied formulation parameters. Model predictions of zero-crossflow burning rate versus pressure characteristics have been found to be in excellent agreement with data, while the agreement between erosive burning predictions and data is in general good. The experimental data indicate that the dominant factor influencing the sensitivity of composite propellant burning rate to crossflow is the base (no-crossflow) burning rate versus pressure characteristics of the propellant (lower base burning rate leading to increased crossflow sensitivity) with other factors having at most a second order effect outside their influence on base burning rate. For example, three formulations with widely different compositional and ingredient particle size parameters but with nearly identical base burning characteristics exhibited very similar erosive burning characteristics. Finally, the model has been used to examine the effects of motor scaling on erosive burning: erosive burning is predicted to diminish with increasing motor size, in agreement with experience.

INTRODUCTION AND BACKGROUND

Erosive burning, the alteration of propellant burning rate by high velocity product flow across the burning surface, has become an increasingly important phenomenon with the advent of very low port-to-throat area ratio cylindrically perforated motors and nozzleless motors. The motor designer must be able to predict this burning rate modification and in particular understand the effects of motor scaling and length/diameter ratio on erosive burning in order to properly carry out his function. In addition, the propellant chemist needs to understand the effects of various formulation parameters on the sensitivity of a propellant to crossflow in order to tailor propellants to desired ballistic characteristics.

*Research sponsored by the Air Force Office of Scientific Research (AFSC), United States Air Force, under Contract F49620-78-C-0016. The United States Government is authorized to reproduce and distribute reprints for Governmental purposes notwithstanding any copyright notation hereon.

Approved for Public Release. Distribution Unlimited.

Over the past several years, this investigator has been conducting an experimental and analytical study of the erosive burning of composite propellants with the aims of determining how various formulation parameters influence the sensitivity of propellant burning rate to crossflow, developing an *a priori* burning rate model (second generation model) which will permit accurate prediction of composite propellant burning rate as a function of pressure and crossflow velocity given only the formulation composition and solid ingredient particle sizes, and developing scaling laws to permit extrapolation of erosive burning data obtained in test devices and small motors to larger motor situations. Details of the model development, with the exception of the treatment of effects of aluminum additive on burning rate, are presented in References 1 and 2. During the past year, the model has been slightly modified to more accurately treat the augmentation of transport properties by crossflow-induced turbulence, and it has been extended to treat aluminized formulations as well as non-metalized ones.

Since there is a dearth of systematic experimental erosive burning data in the literature, a test device has been developed and used to characterize the erosive burning behavior of a series of AP/HTPB composite propellants with systematically varied formulation properties. Zero-crossflow predictions and data have been generated for thirteen non-catalyzed AP/HTPB formulations (four containing aluminum) while crossflow data and predictions have been obtained for ten of these formulations to date. A brief description of the model (with emphasis on its extension to treat metalized propellants), comparison of theoretical predictions with data, and definition of major parameters affecting composite propellant crossflow sensitivity are presented in the following sections.

MODEL DESCRIPTION

The major elements involved in development of a complete *a priori* model for prediction of composite propellant burning rate as a function of pressure and crossflow velocity include development of a no-crossflow composite propellant model (embodying many of the concepts of the Beckstead-Derr-Price⁽³⁾ model) for prediction of burning rate as a function of pressure in the absence of crossflow, followed by incorporation of modifications based on two postulated mechanisms for augmentation of heat feedback from flames in the gas phase above the propellant surface by crossflow. (See Figure 1). As discussed in Reference 2, several variants of a basic no-crossflow model were developed for unimodal-oxidizer non-metalized propellants, with one variant finally being selected for extension to treatment of formulations containing multi-modal oxidizer and metal fuel.

The basic model centers around an energy balance at the propellant surface. In this balance, the product of the propellant burning mass flow and the heat required to raise the ingredients from ambient temperature to the surface temperature (related to the burning rate by an Arrhenius function) plus the heat required to vaporize that fraction of the ingredients which do not exothermically react just below the surface is equated to the sum of the heat release rate from subsurface reactions and the rate of heat feedback from the two gas flame zones depicted in Figure 1. (For metalized formulations, as discussed later, an additional heat release zone associated with burning of the metal in the gas above the propellant surface, not depicted in Figure 1, is also considered.) Thus, the burning rate of non-metalized formulations is

controlled by three principal heat release zones: (1) heat release in a thin subsurface zone just adjacent to the propellant surface; (2) heat release in the gas phase above the propellant from ammonium perchlorate decomposition products burning as a nonpropellant; and (3) heat release from a diffusion flame between the AP decomposition (and monopropellant flame) products and fuel vapor released by binder pyrolysis.

The subsurface heat release is calculated by an iterative process, coupled with the remainder of the model, in which an estimate of the subsurface temperature profile is made and substituted into an Arrhenius rate expression representing subsurface heat release data measured by Waesche and Wenograd⁽⁴⁾, which is then integrated from the surface to a depth where the temperature drops below the melting point of AP to obtain the total subsurface heat release per unit mass of propellant. This is then multiplied by the burning mass flux to yield a heat release rate. This procedure differs markedly from that of the BDP model in which the amount of subsurface heat release per unit mass of propellant is assumed to be a constant, independent of such parameters as burning rate, and is included with the binder heat of vaporization. Since the subsurface temperature profile steepens rapidly with increasing burning rate, while surface temperature increases with burning rate, the procedure used herein results in the subsurface heat release per unit mass of propellant varying with the burning rate.

For the gas phase, a two-flame approach was chosen for this model, the two flames being an AP monopropellant flame and a columnar diffusion (Burke-Schumann⁽⁵⁾) flame. As indicated in Figure 1, three distance parameters ($FH90\sin\theta$, L_{AP} , and L_{RX}) are important in calculating heat feedback from these gas flames to the propellant surface. $FH90$ refers to the distance associated with completion of mixing of 90 percent of the fuel and oxidizer gas products, while L_{RX} and L_{AP} are reaction distances (products of reaction times and gas velocity away from the surface) associated with the binder gas-oxidizer gas flame and the monopropellant AP gas flame, respectively. As discussed below, flame bending associated with crossflow is postulated to reduce the distance from the surface to the end of the mixing region, measured perpendicular to the surface, by the factor $\sin\theta$, where θ is the angle between the surface and the resultant vector of the transpiration and crossflow velocities.

Heat release from the AP monopropellant flame is assumed to occur at one plane, resulting in a discontinuity in the temperature derivative at its point of release, while the columnar diffusion flame is assumed to release its heat in a distributed fashion (the distribution being defined by a Burke-Schumann⁽⁵⁾ analysis) between distances L_{RX} and $L_{RX} + FH90\sin\theta$ from the surface.

Details of the equation development for the unimodal oxidizer, non-metalized propellant model and the solution procedure are presented in References 1 and 2. Included in the model are three "free" constants to be chosen by optimization against data. These three constants are pre-exponentials associated with the subsurface heat release rate expression and the two rate expressions used to calculate the gas-phase reaction times. These constants were chosen on the basis of no-crossflow burning rate versus pressure data for four unimodal oxidizer AP/HTPB (hydroxyterminated polybutadiene) formulations and then used unchanged for no-crossflow and crossflow calculation for multimodal oxidizer and metalized formulations.

Extension of the basic model to treat multimodal oxidizer propellants was carried out in a very straightforward manner using a minor variation on Glick's "petit ensemble" approach⁽⁶⁾. In Glick's approach, a propellant containing oxidizer particles of different sizes is broken into a series of subpropellants, each of which contains oxidizer of only one size. The subpropellants are assumed to burn non-interactively, with the unimodal oxidizer model being used to calculate a mass flux for each, and straightforward averaging weighted according to fractional surface areas associated with each subpropellant then being used to obtain an overall propellant average linear regression rate. The only manner in which oxidizer of one size is allowed to affect the burning rate of a subpropellant containing oxidizer of another size is through possible influence on the assignment of fuel to that subpropellant. That is, rather than fuel having to be assigned to each oxidizer size category in direct proportion to the amount of oxidizer in that category, the capability of allowing uneven assignment of fuel to various oxidizer size subpropellants is included by means of a power law:

$$V_{f,d_i} = C_2 (D_o)^{XEXPOF} \quad (1)$$

where V_{f,d_i} is the volume of fuel assigned to a particle of diameter $(D_o)_i$, XEXPOF is an arbitrary input power law constant, and C_2 is a constant determined by application of overall continuity. It may easily be shown that XEXPOF = 3 will result in each subpropellant having the same oxidizer/fuel ratio as the overall propellant. XEXPOF < 3, on the other hand, will result in subpropellants with small oxidizer being more fuel-rich than the overall propellant and subpropellants with large oxidizer being more fuel-lean, with the reverse occurring for XEXPOF > 3. (Based on preliminary calculations, XEXPOF has been set equal to 3 in the calculations presented herein.)

As mentioned, one modification to the Glick approach has been introduced. His averaging procedure involves an implicit assumption that the average fractional surface area of the total propellant which is subpropellant i is equal to the volume fraction of the propellant which is subpropellant i . However, careful examination of the situation indicates that if there are subpropellants burning at different rates, the slower burning ones will at any given time occupy a higher fraction of the surface than indicated by their volume fraction: thus, it seems that an averaging approach based on residence time distributions is more appropriate. Development of this concept leads to the average burning rate for XEXPOF=3 cases being given by:

$$\bar{r} = 1/\sum x_i/r_i \quad (2)$$

rather than by Glick's formula:

$$\bar{r} = \sum x_i r_i \quad (3)$$

r_i = burning rate of subpropellant i

x_i = mass fraction of propellant in subpropellant i

\bar{r} = average burning rate

The model described in detail in Reference 2 has recently been extended to treat the effects of aluminum additive on propellant burning rate. The metal is allowed to affect burning rate both through heat sink effects (altered

heatup terms in the overall energy balance and a depressed gas diffusion flame temperature relative to that which would be achieved by the oxidizer and fuel in the absence of the metal heat sink) and via conductive and radiative feedback of heat released by the metal particles burning with the gas flame products above the propellant surface. Among the phenomena treated in this model are aluminum agglomeration at the surface, particle velocity lag relative to the gases leaving the propellant surface, particle ignition delay, particle combustion, conductive feedback from incremental heat release zones at various distances from the propellant surface, and radiative feedback. In the case of multimodal oxidizer propellants, the assignment of various fractions of the aluminum to the various subpropellants is treated in the same manner as the assignment of fuel (binder) to these subpropellants. (As with the assignment of binder to subpropellants containing different size oxidizer particles, in the calculations presented herein, the assignment of metal was carried out such that all subpropellants were of the same composition as the overall formulation.)

Aluminum particles are assumed to leave the propellant surface in two forms, agglomerated and unagglomerated (virgin), with the agglomerate fraction and size being calculated using empirical formulae developed by Beckstead⁽⁷⁾.

$$D_{AG} = \text{MAX} (D_{UN}, \left[(1-\epsilon) \frac{\zeta_{Al}}{\zeta_{OX,C}} \right]^{1/3} D_{OX,C}) \quad (4)$$

$$\epsilon = 1 - 0.0005 D_{OX,C} D_{UN}^{0.25} \left[\frac{1+30(F/C)}{1+80(F/C)^2} \right] \quad (5)$$

ϵ = Fraction aluminum not agglomerated

D_{AG} = Agglomerate diameter (microns)

D_{UN} = Virgin metal diameter (microns)

$D_{OX,C}$ = Coarse fraction oxidizer diameter (microns)

ζ_{Al} = Volume fraction Aluminum in Propellant

$\zeta_{OX,C}$ = Volume Fraction Coarse Oxidizer in Propellant

F/C = Weight of Finest Oxidizer Cut/Weight of Coarsest Oxidizer Cut

Based on preliminary calculations, agglomerates were assumed to contribute negligible conductive feedback to the propellant surface due to long ignition and combustion times. Ignition delay times for virgin particles subsequent to leaving the surface are calculated from a simple heatup formula:

$$t_{ign} = \frac{\rho_{Al} D_{UN}^2}{12 \lambda_{gas}} \left[C_{p,Al} \ln \left(\frac{T_{Final}-T_s}{T_{Final}-T_{ign}} \right) + \frac{L_{melt}}{T_{Final}-T_{melt}} \right] \quad (6)$$

t_{ign} = Ignition delay time

ρ_{Al} = Aluminum particle density

- λ_{gas} = gas thermal conductivity
- $C_{p,\text{Al}}$ = Aluminum specific heat
- T_{Final} = Equilibrium flame temperature subsequent to Al combustion
- T_s = Propellant Surface Temperature
- T_{ign} = Aluminum particle ignition temperature (2100°K)
- T_{melt} = Aluminum melting temperature
- L_{melt} = Aluminum heat of fusion

After ignition, the particle diameter-time history (and thus burning rate) is calculated using a rearranged form of the Belyaev (8) burning time formula:

$$D_{t+\Delta t} = \left[D_t^{1.5} - (a_k^{0.9}/670) \Delta t \right]^{0.667} \quad (7)$$

D_t = particle diameter (cm) at time t

$D_{t+\Delta t}$ = particle diameter at time $t+\Delta t$

Δt = time increment (seconds)

a_k = $100 (n_{\text{CO}_2} + n_{\text{H}_2\text{O}} + n_{\text{O}_2}) / \sum n_i$

Thus, from Equations 6 and 7, the fractional consumption of aluminum as a function of time subsequent to its leaving the surface is calculated. (Note that implicit in Equation 6 is an assumption that the aluminum particle temperature is equal to the propellant surface temperature when it leaves the surface.)

For calculation of the distance of the particle from the surface versus time (required for calculation of the metal heat release distribution) the gas velocity component normal to the surface is first calculated as a function of distance from the surface using the propellant burning flux calculated in the previous loop of the overall trial and error solution procedure along with assumption of a linear temperature profile from the propellant surface to the end of the columnar diffusion flame zone with subsequent constant temperature. Next, a force balance on the particle (with a buoyancy term neglected on the basis of preliminary estimates for particle sizes of interest):

$$\frac{\Delta V_p}{\Delta t} = \frac{0.75 \rho_g C_D (v_g - v_p)^2}{\rho_{\text{Al}} D} \quad (8)$$

ΔV_p = change in particle velocity in time increment Δt

ρ_g = gas density

C_D = drag coefficient

- V_g = gas velocity component normal to surface
 V_p = particle velocity component normal to surface
 D = particle diameter

is integrated outward from the surface, utilizing a fitted drag coefficient versus Reynolds' Number expression, with this coefficient assumed (based on the work of Marshall (9)) to increase by a factor of 2.5 for ignited particles. (Actually, Equations 7 and 8 have to be integrated simultaneously subsequent to particle ignition since they are coupled through the changing particle diameter.) With coupling of Equations 5-8, the fraction of the total aluminum in the propellant burned is calculated as a function of distance from the propellant surface. This is then multiplied by the heat of combustion of aluminum in the oxidizer/fuel products, calculated as:

$$Q_{AL} = c_{pm} (T_{Final} - T^*) / X_{Al} \quad (9)$$

- Q_{Al} = aluminum heat of combustion per unit mass
 c_{pm} = mixture specific heat
 T^* = equilibrium flame temperature with non-reacting aluminum
 X_{Al} = weight fraction aluminum in the propellant

to yield a distribution of heat release from aluminum combustion versus distance from the propellant surface. Conductive feedback flux from the aluminum combustion to the propellant surface is then calculated from:

$$q_{fdbk, Al, c} = \dot{m} \sum_j \left\{ Q_j \prod_{i=1}^j \exp(-\dot{m} c_p \Delta x_i / \lambda_i) \right\} \quad (10)$$

- \dot{m} = propellant burning mass flux (gm/cm²sec)
 $q_{fdbk, Al, c}$ = aluminum feedback flux cal/cm²sec)
 Q_j = aluminum heat release per unit mass of propellant at jth node from the surface (cal/gm)
 c_p = product heat capacity
 Δx_i = size of ith increment
 λ_i = total thermal conductivity (laminar plus turbulent) associated with ith increment

Preliminary calculations indicated that radiative feedback should in general be small, but a very simplified analysis for estimating this feedback was included. In this analysis, an effective distance from the surface is input as a free parameter and an effective cloud emissivity based on the fractional area subtended by particles in that region is then calculated: for motors, the distance is chosen to be the port radius while for strands it is arbitrarily set equal to 1 to 2 centimeters (with the assumption that cooling due to entrained nitrogen from the surroundings makes particles further away ineffective). For the metalized formulations tested and discussed in this paper, radiative transfer is predicted to have an insignificant effect on predicted burning rate.

It was originally postulated by this author that the augmentation of composite propellant burning rate due to crossflow resulted solely from shortening of the distance, measured normal to the propellant surface, associated with mixing of the fuel and oxidizer gases through distortion of the mixing cone, as depicted in Figure 2. A detailed discussion of this mechanism is given in Reference 10. From tall-flame theory, for no crossflow, the mixing distance is related to the burning mass flux and oxidizer particle diameter by:

$$FH90 = k \dot{m}_p d_p^2 \quad (11)$$

With crossflow (refer to Figure 2) the mass flux in the direction of the resultant flow is:

$$\dot{m} = \dot{m}_p / \sin\theta \quad (12)$$

where θ is the resultant flow angle. However, the characteristic mixing time is decreased since the average mixing concentration gradient is increased by the circular mixing cross-section (in the absence of crossflow) being converted to an elliptical cross-section with major axis d_p and minor axis $d_p \sin\theta$. An exact mixing calculation for this geometry is of course quite difficult, but replacement of the circle diameter d_p by the geometric mean ellipse diameter, $\sqrt{d_p^2 \sin\theta}$ in Equation 11 does not seem unreasonable. With substitution of (12) into (11), one finds:

$$FH90 = \frac{k \dot{m}_p}{\sin\theta} (d_p^2 \sin\theta) = k \dot{m}_p d_p^2 \quad (13)$$

as in the case of no crossflow. However, this FH90 is now measured along the resultant flow vector: accordingly, the distance from the surface to the end of the mixing zone is reduced to $FH90 \sin\theta$.

Use of an erosive burning package based solely on this mechanism in the different Generation 2 model variants led in all cases to major under-prediction of the effect of crossflow on burning rate, indicating that the flame-bending mechanism was by itself insufficient. Accordingly, a second possible mechanism, augmentation of turbulence transport properties in the region between the propellant surface and the gas-phase flames was invoked and combined with the flame-bending mechanism. In this approach, it was assumed that both the effective thermal conductivity (governing feedback from the various gas flames) and the effective mass diffusivity (an important parameter in determining the thickness of the diffusion flame) were increased in crossflow situations by crossflow-induced turbulence. A flow profile analysis

permitting calculation of eddy viscosity (and, by analogy, total effective thermal conductivity and diffusivity) as a function of distance from the propellant surface for a given crossflow velocity, transpiration velocity (determined by the propellant burning rate), and temperature field (depending on the location of gas-phase heat release zones) was developed and coupled with the combustion model for erosive burning calculations. An improved calculation of diffusion flame-bending angle was also incorporated in this analysis.

Details of the flow profile analysis procedures are presented in Reference 2. (A summary of the equations used and the solution procedure employed are given in Table I and II.) The outputs from this analysis are used to calculate:

$$\lambda_{\text{effective}}/\lambda_{\text{laminar}} = D_{\text{effective}}/D_{\text{laminar}} = 1 + \rho\epsilon/\mu = F(y) \quad (14)$$

That is, the ratio of total transport properties to laminar transport properties are calculated as a function of distance from the surface. Average total transport property values between appropriate zones are then calculated and substituted for the laminar values in the diffusional mixing equations and the heat feedback equations in the original model, revised burn rates and flame distances are calculated, and the procedure is repeated until convergence is achieved. As might be expected, this looping procedure is considerably more complex in the case of multimodal propellants than for unimodal propellants since solution of the individual subpropellant cases becomes interactive in the case of crossflow. This interaction occurs because there is only one boundary layer for the overall propellant (that is, one cannot calculate a different boundary layer profile for each subpropellant) with the boundary layer details being controlled by the average transpiration velocity, flame height, surface temperature, etc. for the overall propellant rather than by the individual values of these parameters for each subpropellant.

It should be noted that the procedures used for calculating average transport properties between zones from the distribution of these properties have been modified from those procedures used in calculation of predicted burning rates presented in References 2 and 11. In the earlier work, linear averaging was employed, while the modified procedure allows for the fact that the effect of the gas-phase heat release on burning rate decreases exponentially with the distance of that release from the surface. In addition, in calculation of results presented previously, the bent flame was approximated as being straight with the effective angle being determined by integration of the velocity vector profile from the surface to the end of the diffusion flame zone while the effects of flame curvature are included in the current model.

Several options for closure of the boundary layer analysis through specification of an eddy viscosity equation were built into the model: all entailed use of a Prandtl mixing-length expression of the general form:

$$\epsilon = .168 (y+y_{\Delta})^2 (DF)^2 du/dy \quad (15)$$

where DF is a damping factor which is a function of such parameters as blowing ratio, axial pressure gradient, and roughness height while y_{Δ} is an offset factor dependent on roughness height. Most satisfactory results were found

with DF set equal to unity (no damping) and γ_0 set equal to zero (no roughness effect).

EXPERIMENTAL

The experimental test apparatus (Figure 3) and procedures for measuring burning rates with crossflow are described in detail in Reference 12. A cylindrically perforated "driver" grain whose length is chosen to give the desired operating pressure produces a high velocity gas flow through a transition section into a rectangular channel which contains the test grain. The test grain extends through the transition section to butt against the driver grain to eliminate leading edge effects. The test grain is approximately 40 cm long, 1.90 cm wide, and 2.50 cm deep (web) and burns only on the 1.90 cm face. The flow channel is initially 1.90 x 1.90 cm, opening up to 1.90 cm x 4.40 cm as the test propellant burns. For high crossflow velocity tests, the apparatus is operated without a nozzle while for lower velocity tests, a two-dimensional nozzle is employed.

The burning rate is directly measured by photographing the ablating grain with a high-speed motion picture camera through a series of four quartz windows located along the length of the test section. Frame by frame analysis of the films permits determination of instantaneous burning rate as a function of time at each of the four window locations.

For nozzled cases, the measured location of the burning propellant surface at each window as a function of time, together with the known constant throat area, permits straightforward calculation of the crossflow velocity as a function of time. However, the very sensitive dependence of Mach number on area ratio for $M > 0.5$ makes calculation of crossflow velocity from area ratio measurement quite poor for nozzleless cases. Accordingly, for these tests, stagnation pressure is determined at the aft end of the test section and used in combination with the driver chamber pressure for calculation of the stagnation pressure in the test section as a function of time and position. Static pressure wall taps at each window location are used for measurement of static pressure as a function of time for both nozzled and nozzleless cases. From the static and stagnation pressure values determined as a function of time and position down the test section, crossflow Mach Number and velocity are calculated as a function of time at each window location in the test section for the nozzleless cases.

The erosive burning characteristics of a series of 11 AP/HTPB formulations (4 with unimodal AP and no catalyst or metal, 5 with multimodal AP and no catalyst or metal, 1 with multimodal AP and aluminum but no catalyst, and 1 with unimodal AP plus catalyst) with systematically varied parameters have been measured in this device to date. In addition, standard strand-burning procedures have been used to determine zero-crossflow burning rate versus pressure characteristics for these 11 formulations plus 3 additional multimodal AP, aluminized (no catalyst) formulations. The propellant matrix tested, including the rationale for its selection, is presented in Table III.

EXPERIMENTAL RESULTS AND COMPARISON WITH MODEL PREDICTIONS

Predicted and measured zero-crossflow burning rate versus pressure characteristics of 13 of the 14 formulations are presented in Figure 4-6.

(Predictions were not made for the catalyzed formulation since the catalyst should cause shifting of one or more of the three aforementioned kinetic constants and it was felt that the catalyzed formulation data base was insufficient for re-evaluation of these constants.) As may be seen, agreement between predicted and measured 200 psia burning rates is excellent, with all predictions, covering a wide range of non-metalized and metalized AP/HTPB formulations, falling within 10 percent of the measured values. Similarly, the 1000 psia burning rate predictions and data show excellent agreement, with only one point falling outside the 20 percent error band and one falling between the 10 and 20 percent bands, the remainder agreeing within 10 percent. As indicated by Figure 6, the 1000 psia predicted versus measured value comparisons of burning rate pressure exponent are also quite good, all lying within the 20 percent error bands and most within the 10 percent bands. Accordingly, it appears that development of an accurate zero-crossflow model, necessary as a first step in developing an adequate erosive burning model, has been satisfied.

Erosive burning test results are presented in Figures 7-17, in the form of burning rate versus pressure at various crossflow velocities. In addition, theoretical predictions are presented for all but the catalyzed formulation (4869) in these figures. As may be seen, the agreement between data and predictions for the no-crossflow conditions is excellent, as indicated earlier, for all formulations except 7996, where the theoretically predicted burning rates are 10 to 20 percent high. In addition, the crossflow effect predictions agree reasonably well with the data in general. With the baseline formulation (4525), the theory slightly underpredicts the effect of crossflow on burning rate while with 5051, 4685, and 5542 (the other three non-catalyzed unimodal oxidizer formulations) agreement between theory and data is excellent. The model predicts that the high burning rate formulation (5555) should be quite insensitive to crossflow velocity, in excellent agreement with experiment. Formulation 5565, on the other hand, appears to be slightly less sensitive to crossflow than predicted, particularly at the lower pressures (1-3 MPa). Agreement between theory and data for the remaining three multimodal oxidizer, non-metalized formulations is good, except that the zero-crossflow offset between theory and data for 7996 appears to be maintained for the crossflow cases. Finally, the rather limited data for the metalized formulation (6626) appear to be in general agreement with predictions.

Results for the various formulations may be compared to identify parameters dominating the sensitivity of burning rate to crossflow. Formulations 4525, 5051, and 4685 were identical except for oxidizer particle size (and, as a consequence) base (no-crossflow) burning rate. Examination of Figures 7-9 reveals that the crossflow sensitivity increases with increasing particle size (decreasing base burning rate). For example, at 200 m/sec and 5 MPa, the augmentation ratios for 4685, 4525 and 5051 are about 1.10, 1.60 and 2.00 respectively.

Comparison of data for 4525 and 4869, differing only in use of catalyst in the latter (with consequent higher base burn rate) again shows an increase in crossflow sensitivity with decreasing base rate. At 5 MPa and 200 m/sec, their respective burn rate augmentation ratios are 1.60 and 1.10, while at 600 m/sec, the r/r_0 values are 2.3 and 1.7. Thus, base burn rate is seen to affect erosion sensitivity even at constant oxidizer size.

Formulations 4685 and 4869 have approximately the same base burning rate at 8 MPa although their oxidizer sizes are different. Data comparison indicates that these formulations have nearly the same sensitivity to low crossflow velocities at 8 MPa, with the catalyzed propellant being only slightly more sensitive at higher velocities. Thus, it appears that it is the base burning rate rather than the oxidizer particle size which dominates the sensitivity of this series of four 73/27 AP/HTPB formulations to crossflow, though oxidizer size itself does appear to have a slight additional effect, crossflow sensitivity decreasing with decreasing size at constant base rate.

Formulation 5542 differs from 4525 in oxidizer/fuel ratio and consequently flame temperature. Since oxidizer particle size was held constant, the higher O/F ratio results in higher base rate for 5542. The data (Figure 7 and 11) indicate that the crossflow sensitivity of 5542 is considerably lower over the entire range of conditions studied. Comparison of results for 5565 and 4525, which differ in O/F ratio, but have the same base burning behavior (due to compensating AP particle size differences) indicates that the sensitivity of these two formulations to crossflow is nearly identical. Accordingly, it may be concluded that O/F ratio (and consequently flame temperature) changes do not directly effect the erosion sensitivity of these formulations, but only affect it through their effect on base burning rate.

As indicated in Table III, Formulation 6626 (metalized) has nearly the same base burning characteristics as 4525 and 5565 and approximately the same flame temperature as 5565. The data of Figures 7, 12 and 17 reveal that all three formulations have quite similar erosive burning characteristics. For example, at 760 m/sec and 2.8 MPa, the augmentation ratios for 4525, 5565, and 6626 are 2.1, 2.25, and 2.1, while at 260 m/sec and 4.0 MPa, they are 1.65, 1.55 and 1.60. These results support a conclusion that the dominant factor affecting crossflow sensitivity of composite propellants is base burning rate, largely independent of the factors determining that base rate.

Formulations 5555, 5565, 7993, 7996, and 8019 are identical in composition (82/18 AP/HTPB) differing only in oxidizer particle size blends, which were adjusted to give a range of base (zero-crossflow) burning rate versus pressure characteristics. In Figure 18, data extracted from Figures 12-16 are plotted in the form of burning rate augmentation factor (r/r_0) versus base burning rate for three combinations of pressure and crossflow velocity. As may be seen, the augmentation factor decreases monotonically and fairly smoothly with increasing base burning rate, again indicating the importance of that parameter on crossflow sensitivity.

A summary of the above comparisons, delineating the effects of various parameters on crossflow sensitivity of burning rate is presented in Table IV.

MOTOR SCALING EFFECTS

It has been observed in the past that erosive burning effects tend to diminish with increasing motor size, all other parameters being held constant. It is therefore of interest to ascertain whether the model described above can predict such a trend. Accordingly, a series of calculations have been run for equal crossflow velocities and pressures with different motor diameters. Typical results are plotted in Figures 19 and 20, comparison being made between motors with port diameters of 1.0 and 10 inches. As may be seen, erosive

burning effects are indeed predicted to decrease significantly with increasing motor size. Another point of interest may be made from Figure 20. One of the weakest links in the use of the flow profile analysis routine outlined earlier for calculation of the flame bending angle and turbulent transport property distribution is specification of the ratio of skin friction coefficient with blowing to that without blowing as a function of the blowing ratio, as discussed in detail in Reference 2. Accordingly, several different empirical expressions have been examined (See Figure 21). As shown in Figure 20, the predicted burning rate augmentation ratio is in general fairly insensitive to the choice of expression among those considered as reasonable possibilities.

CONCLUSIONS

A fundamental composite propellant combustion model capable of predicting burning rate as a function of pressure and crossflow velocity, given only propellant composition and ingredient particle size has been developed. Testing against zero-crossflow data for a series of 13 non-catalyzed AP/HTPB formulations (4 containing aluminum additive) indicates that the model does an excellent job in predicting the non-erosive burning rate versus pressure characteristics of such formulations. In addition, erosive burning data have been obtained for 10 of these formulations: the model also does a good job in predicting the observed erosive burning behavior of these propellants.

The data obtained to date indicate that the base (no-crossflow) burning rate characteristics of the propellant have a predominant affect on its sensitivity to crossflow, high burning rate formulations being considerably less susceptible to erosive burning than low burning rate formulations, whether the base burning rate alterations are produced by oxidizer particle size variation, oxidizer/fuel ratio variation, addition of metal, or use of catalysts. Thus propellants with widely differing oxidizer size distribution, O/F ratios, metal loadings, etc tend to show identical erosive burning behavior as long as they have identical base (no crossflow) burning rate characteristics. Oxidizer particle size does appear to have some residual effect (but only a slight one) beyond its effect on base burning rate, erosion sensitivity increasing with increasing particle size. An important preliminary conclusion is that aluminum (at least at low levels) does not affect erosion sensitivity other than through its effect on base burning rate.

The model also predicts a decrease in erosive effects with increasing motor port size (at equal pressure and crossflow velocity) in agreement with observations by other investigators.

REFERENCES

1. King, M., "Model for Steady State Combustion of Unimodal Composite Solid Propellants," AIAA Paper 78-216, Jan., 1978. Available from Engineering Societies Library, 245 East 47th Street, NY, NY 10017.

2. King, M., "A Model of the Effects of Pressure and Crossflow Velocity on Composite Propellant Burning Rate," AIAA Paper 79-1171, June, 1979. Available from Engineering Societies Library, 345 East 47th Street NY, NY 10017.
3. Beckstead, M.W., Derr, R.L. and Price, C.F. Thirteenth Symposium (International) on Combustion, p. 1047, the Combustion Institute, 1971.
4. Waesche, R.H.W. and Wenograd, J., "Calculation of Solid Propellant Burning Rates from Condensed-Phase Decomposition Kinetics," AIAA Paper 69-145, January 1969. Available from Engineering Societies Library, 345 East 47th Street, NY, NY 10017.
5. Burke, S.P. and Schumann, T.E.W., Ind Eng Chem, 20, 998 (1928); also First/Second Symposium Combustion, p. 2, The Combustion Institute, Reprinted 1965.
6. Glick, R.L. and Condon, J.A., "Statistical Analysis of Polydisperse, Heterogeneous Propellant Combustion: Steady-State," 13th JANNAF Combustion Meeting, CPIA Publication No. 281, Vol. II, p. 313, December, 1976.
7. Beckstead, M.W., "A Model for Solid Propellant Combustion," 14th JANNAF Combustion Meeting, CPIA Publication No. 292, Vol. I, p. 281, December, 1977.
8. Belyaev, A.F., Frolov, Yu.V., and Korotkov, A.I., Fizika Goreniya i Vzryva, 4, 3, 323-329 (1968).
9. Marshall, R.L., Pellet, G.L. and Saunders, A.S., "An Experimental Study of the Drag Coefficient of Burning Aluminum Droplets," Air Force Rocket Propulsion Laboratory Report AFRPL-TR-67-223, Vol II, p. 843, August, 1967.
10. King, M.K. "Erosive Burning of Composite Solid Propellants," 15th JANNAF Combustion Meeting, CPIA Publication 297, Vol. II, p. 179-188, February, 1979.
11. King, M.K., "An Investigation of the Effects of Formulation Parameters On Erosive Burning of Composite Propellants," 16th JANNAF Combustion Meeting, Monterey, California, September, 1979. CPIA Publication 308, Vol. II, pp. 171-191, December 1979.
12. King, M., "Erosive Burning of Composite Propellants," 13th JANNAF Propulsion Meeting, CPIA Publication 281, Vol. II, p. 407, December, 1976.

Table I. Main Equations used in Flow Profile Analysis (Coupled with Burning Rate Analysis Through Temperature Dependence of Density and Viscosity).

1. $C_{f0} = f_1 (Re, D_0/k)$
2. $C_f/C_{f0} = f_2 (B)$ $B = (\dot{m}_{inj}/\dot{m}_{crossflow})/(C_{f0}/2)$
3. $\tau_{wall} = (C_f/2) \rho_{fs} U_{fs}^2$
4. $\tau_y = \tau_{wall} + \dot{m}_{inj} U - K_{mom} \int_0^y \tau_y dy$
5. $\tau_y = (\mu + \rho \epsilon) dU/dY$
6. $\epsilon = [f_3 (Y, \dot{m}_{inj}, dP/dx, k)] dU/dY$
 FOR ZERO ROUGHNESS AND NO DAMPING, FOR EXAMPLE
 $\epsilon = .168 Y^2 (dU/dY)$
7. $\rho = P(MW)/RT$
8. $\mu = kT^{0.8}$
9. $T = T_s + (T_f - T_s)Y/(L_{RX} + FH90 \sin \theta)$
10. $V = \dot{m}_{inj}/\rho$

Table II. Application of Flow Profile Analysis Equations.

1. USE EQNS 1-4 TO OBTAIN $\tau = g(u,y)$
 2. *INTEGRATE EQN 5, WITH USE OF EQNS 4 AND 6-9, FROM THE WALL (SURFACE) TO OBTAIN $u, du/dy, \epsilon$ AS FUNCTION OF y
 3. KNOWING $\epsilon(y)$, COMBINE THIS WITH EQNS 7-9 TO OBTAIN $[1 + \rho\epsilon/\mu]$ AS A FUNCTION OF y
 4. USE THIS FUNCTION TO OBTAIN AVERAGE AUGMENTATION RATIOS FOR LAMINAR TRANSPORT PROPERTIES OVER VARIOUS REGIONS AND USE THESE TO ADJUST EFFECTIVE FLAME OFFSET DISTANCES
 5. HAVING $u(y)$ AND $v(y)$ INTEGRATE ALONG A STREAMLINE TO DETERMINE THE EFFECTIVE REDUCTION OF DIFFUSIONAL DISTANCE DUE TO FLAME BENDING.
 6. LOOP - FAIRLY COMPLEX FOR UNIMODAL AP CASES; EVEN MORE SO FOR MULTIMODAL AP CASES, WHERE INTERACTION BETWEEN THE MODES MUST NOW BE CONSIDERED
- *FOR LOW CROSS FLOW, HIGH BLOWING RATIO CASES, THE $-K_y$ TERM IN EQN 4 CAUSES τ TO GO NEGATIVE, A RESULT WE INTERPRET AS INDICATING BOUNDARY LAYER BLOWOFF - IF THIS OCCURS, WE USE A COSINE LAW VELOCITY PROFILE FOR OUR ANALYSIS IN PLACE OF INTEGRATION OF EQN 5.

Table III. Propellant Matrix (AP/HTPB) Tested.

FORMULATION	COMPOSITION	RATIONALE
4825	73/27 AP/HTPB, 20 MICRON AP	BASILINE FORMULATION, FLAME TEMPERATURE = 1967°K
5051	73/27 AP/HTPB, 200 MICRON AP	COMPARE WITH 4825 FOR AP SIZE EFFECT AND BASE BURNING RATE EFFECT
4885	73/27 AP/HTPB, 5 MICRON AP	COMPARE WITH 4825 AND 5051 FOR AP SIZE EFFECT AND BASE BURNING RATE EFFECT
4889	72/28/2 AP/HTPB/F ₂ O ₃ , 20 MICRON AP	COMPARE WITH 4825 FOR BASE BURNING RATE EFFECT AT CONSTANT AP SIZE
5542	77/23 AP/HTPB, 20 MICRON AP	COMPARE WITH 4825 FOR MIXTURE RATIO AND FLAME TEMPERATURE EFFECT AT CONSTANT AP SIZE. T=2058°K
5885	82/18 AP/HTPB, 13.88% 90 MICRON AP, 86.12% 200 MICRON AP	AP SIZES CHOSEN TO MATCH BASE BURNING RATE OF 4825. COMPARE WITH 4825 FOR MIXTURE RATIO AND FLAME TEMPERATURE EFFECT. T=2575°K
5885	82/18 AP/HTPB, 41% 1 MICRON AP, 41% 7 MICRON AP	COMPARE WITH 5885 FOR EFFECT OF BASE BURNING RATE.
7883	82/18 AP/HTPB, 41% 7 MICRON AP, 41% 90 MICRON AP	} FURTHER STUDY OF AP SIZE AND BASE BURNING RATE EFFECTS
7886	82/18 AP/HTPB, 41% 20 MICRON AP, 41% 200 MICRON AP	
8019	82/18 AP/HTPB, 27.3% 1 MICRON AP, 27.3% 20 MICRON AP, 27.4% 200 MICRON AP	
8026	74/21/5 AP/HTPB/Al, 70% 90 MICRON AP, 4% 200 MICRON AP	
8485	73/17/10 AP/HTPB/Al, 7.3% 90 MICRON AP, 58.4% 200 MICRON AP, 7.3% 400 MICRON AP	} STUDY OF EFFECTS OF VARIOUS ALUMINUM LOADINGS AND O/F RATIOS ON EROSION BURNING BEHAVIOR.
8487	80/18/5 AP/HTPB/Al, 8.0% 90 MICRON AP, 84.0% 200 MICRON AP, 8.0% 400 MICRON AP	
WC19M	70/12/18 AP/HTPB/Al, 21.0% 20 MICRON AP, 38.0% 90 MICRON AP, 10.0% 200 MICRON AP	

Table IV. Effects of Various Parameters on Sensitivity of Formulations to Crossflow.

COMPARISON	PARAMETERS STUDIED	EFFECT ON EROSION BURNING
4825, 5051, 4885	VARIED d_p, r_p AT FIXED BINDER TYPE, FIXED FLAME TEMPERATURE	$d_p \uparrow \rightarrow r_p \uparrow \rightarrow E \downarrow$
4824, 4889	VARIED r_p AT FIXED AP SIZE, BINDER TYPE, AND FLAME TEMPERATURE	$r_p \uparrow \rightarrow E \downarrow$
4823, 4889	VARIED d_p AT FIXED r_p , BINDER TYPE, AND FLAME TEMPERATURE	$d_p \downarrow \rightarrow E \downarrow$ SLIGHTLY
4825, 5542	VARIED O/F RATIO (AND THUS FLAME TEMPERATURE) AND r_p AT FIXED BINDER TYPE AND FIXED AP SIZE	$T_f \uparrow \leftrightarrow r_p \uparrow \rightarrow E \downarrow$
5885, 4825	VARIED O/F RATIO (AND THUS FLAME TEMPERATURE) AT FIXED BINDER TYPE AND FIXED r_p	$T_f \uparrow \rightarrow E$ UNCHANGED
5885, 5885, 7883, 7886, 8019	VARIED d_p, r_p AT FIXED BINDER TYPE, FIXED FLAME TEMPERATURE	$d_p \downarrow \rightarrow r_p \uparrow \rightarrow E \downarrow$
5885, 8026	ALUMINUM VERSUS NON-ALUMINUM AT FIXED r_p , BINDER TYPE, AND FLAME TEMPERATURE	E UNCHANGED

CONCLUSIONS FROM ABOVE COMPARISONS

1. THE AMMUNITION FACTOR IS STRONGLY DEPENDENT ON BASE BURNING RATE.
2. THERE IS A SMALL RESIDUAL EFFECT OF OXIDIZER PARTICLE SIZE, AT FIXED BURNING RATE.
3. O/F (FLAME TEMPERATURE) EFFECTS E FOR HTPB SYSTEMS ONLY THROUGH EFFECT ON BASE BURNING RATE.
4. AT FIXED BASE BURNING RATE, ALUMINUM HAS NO EFFECT ON E .

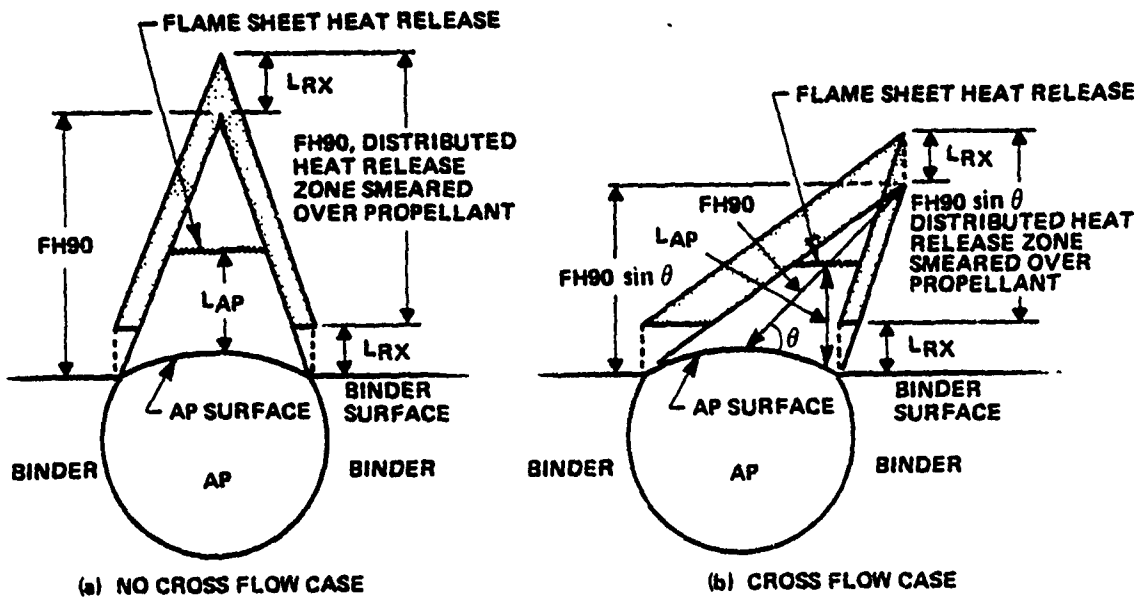


Figure 1. Schematic of Burning Composite Propellant Postulated Flame Structure, with and without Crossflow.

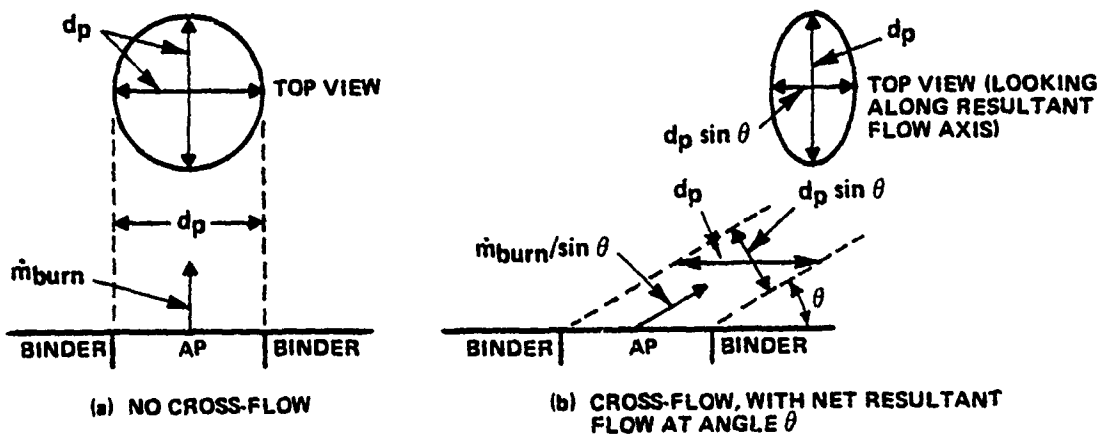


Figure 2. Modification of Diffusion Flame Shape by Crossflow.

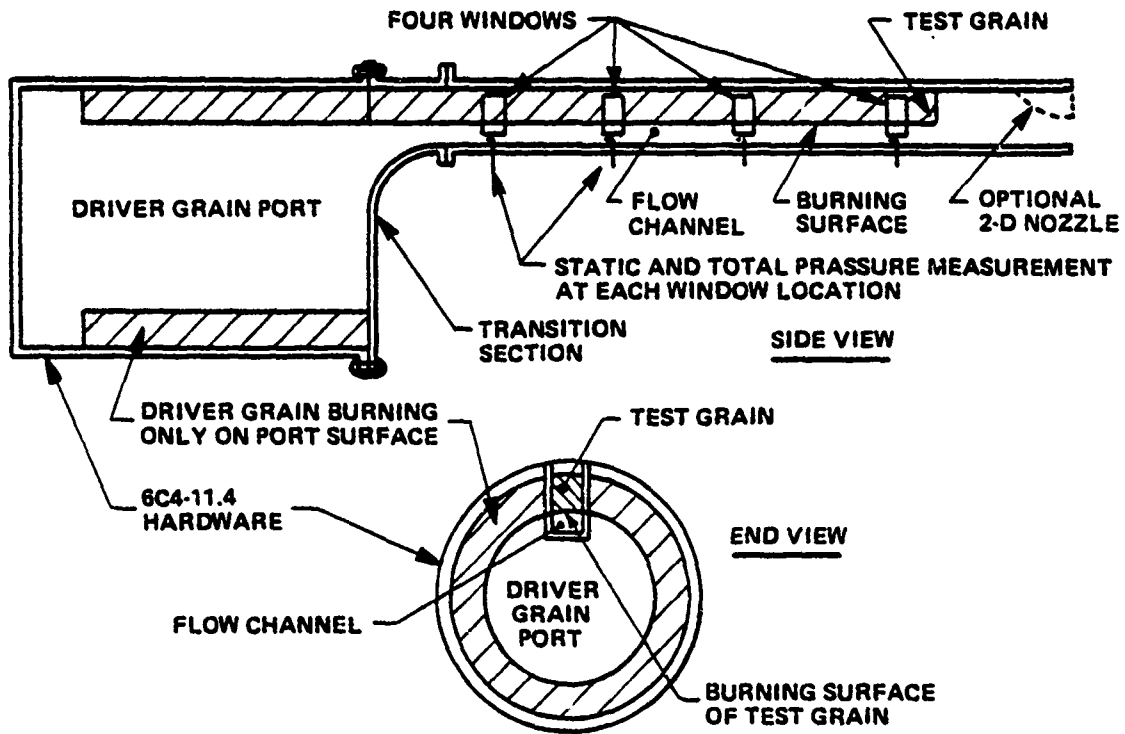


Figure 3. Schematic Drawing of Erosive Burning Test Apparatus.

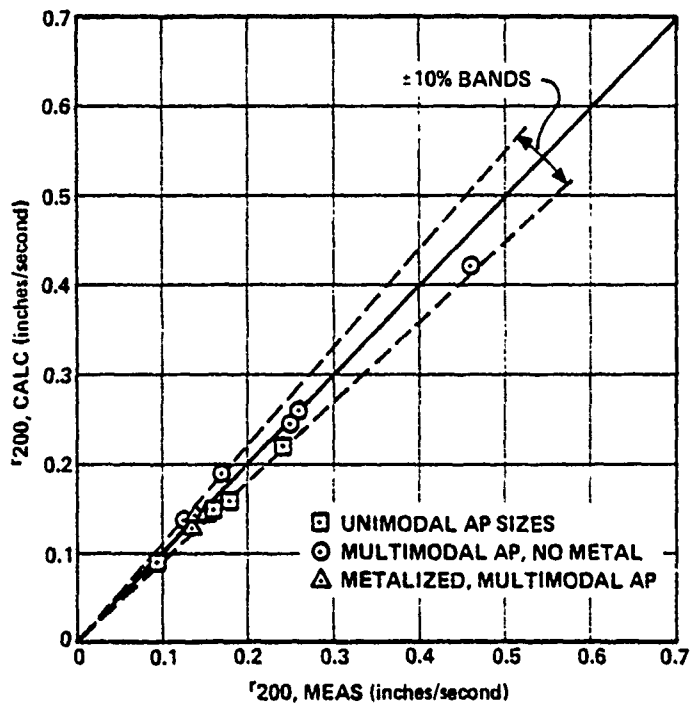


Figure 4. Zero-Crossflow Burning Rates at 200 psia, Data and Predictions.

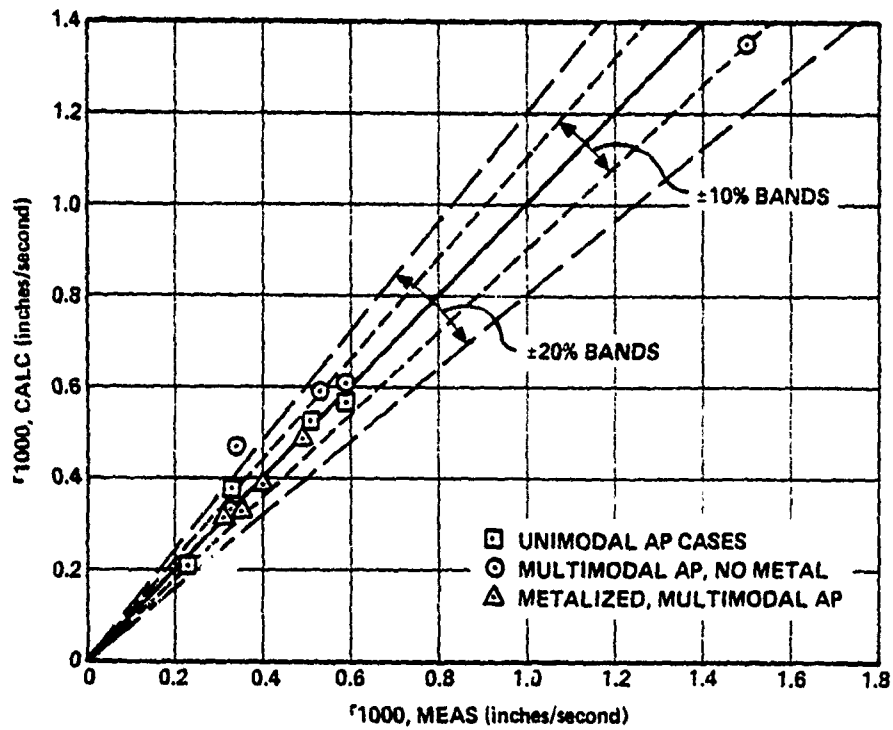


Figure 5. Zero-Crossflow Burning Rates at 1000 psia, Data and Predictions.

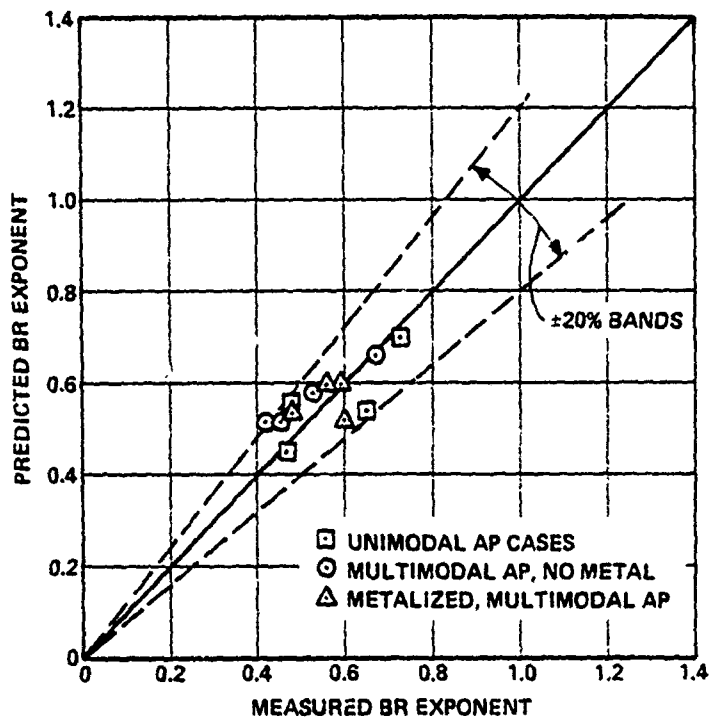


Figure 6. Zero-Crossflow Burning Rate-Pressure Exponent at 1000 psia, Data and Predictions.

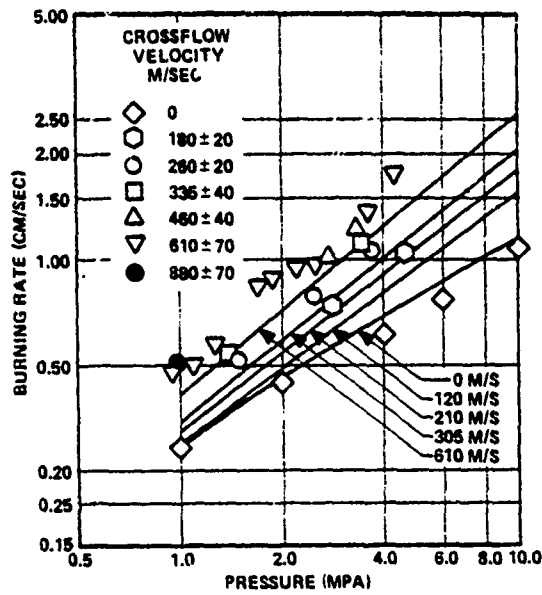


Figure 7. Burning Rate Predictions (Solid Lines) and Data (Points) for Formulation 4525 (73/27 AP/HTPB, 20 MICRON AP).

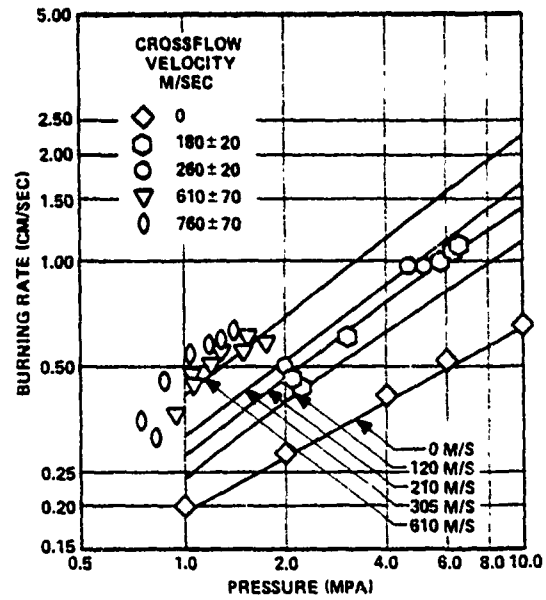


Figure 8. Burning Rate Predictions (Solid Lines) and Data (Points) for Formulation 5051 (73/27 AP/HTPB, 200 Micron AP).

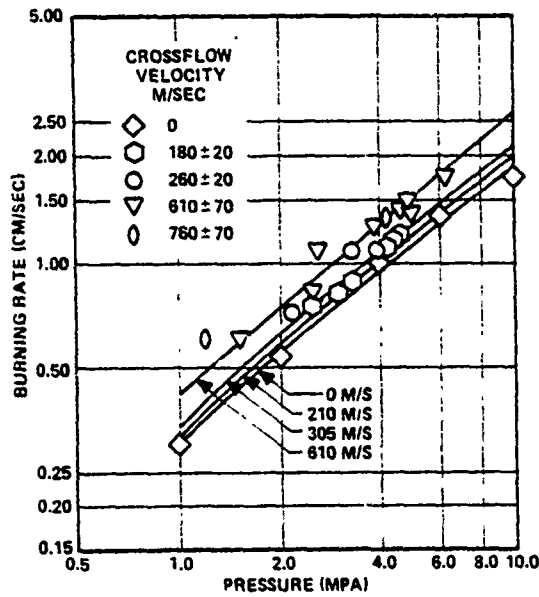


Figure 9. Burning Rate Predictions (Solid Lines) and Data (Points) for Formulation 4685 (73/27 AP/HTPB, 5 Micron AP).

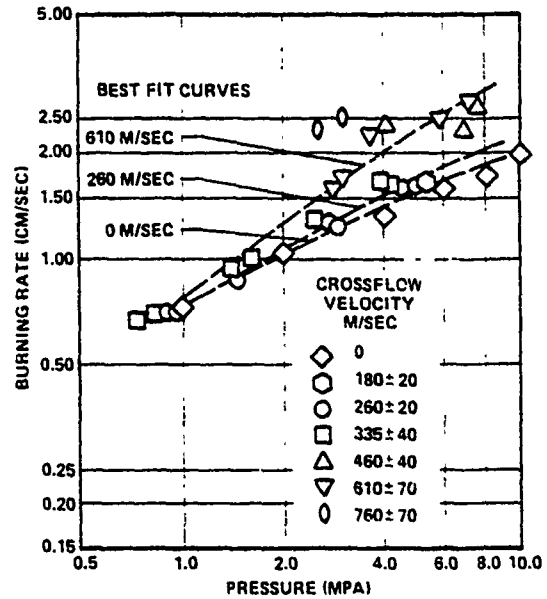


Figure 10. Burning Rate (No Predictions) for Formulation 4869 (72/26/2 AP/HTPB/Fe₂O₃, 20 Micron AP).

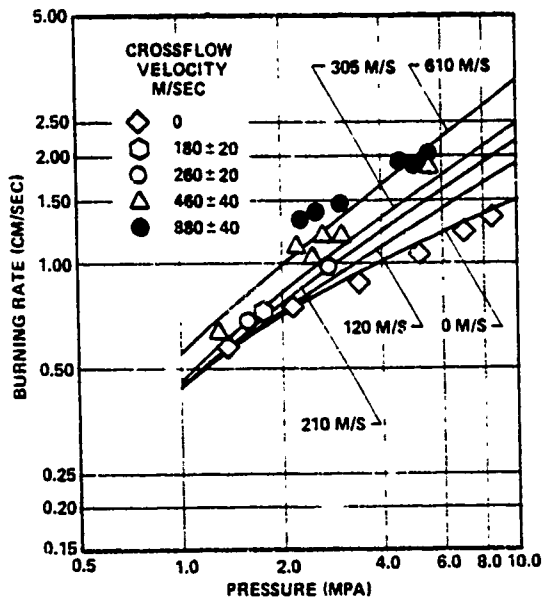


Figure 11. Burning Rate Predictions (Solid Lines) and Data (Points) for Formulation 5542 (77/23 AP/HTPB, 20 Micron AP).

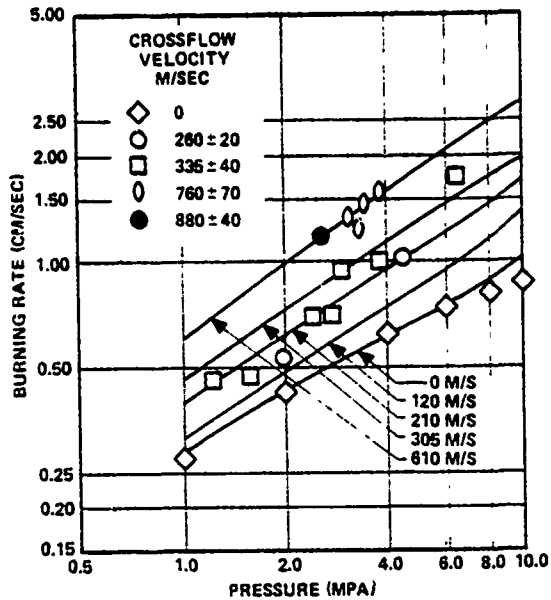


Figure 12. Burning Rate Predictions (Solid Lines) and Data (Points) for Formulation 5565 (82/18 AP/HTPB, 13.65% 90 Micron AP, 68.35% 200 Micron AP).

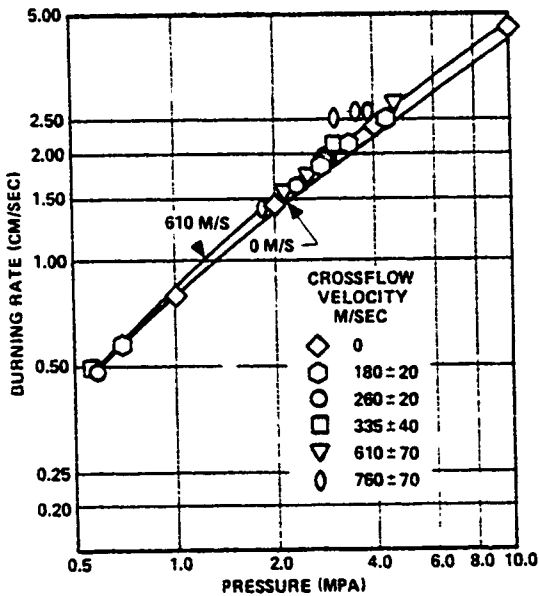


Figure 13. Burning Rate Predictions (Solid Lines) for Formulation 5555 (82/18 AP/HTPB, 41% 1 Micron AP, 41% 7 Micron AP).

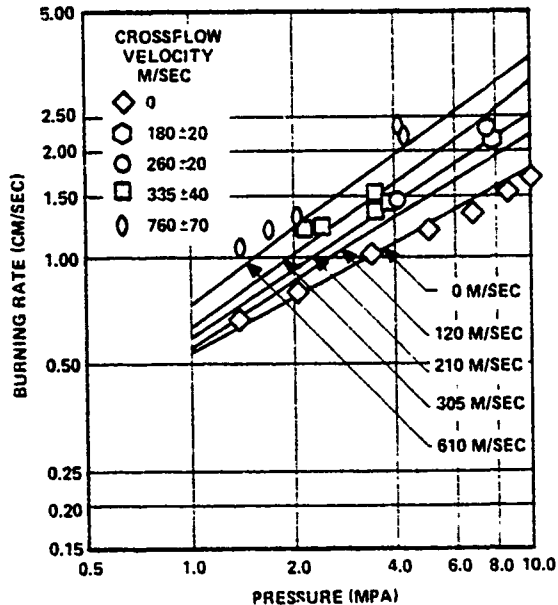


Figure 14. Burning Rate Predictions (Solid Lines) and Data (Points) for Formulation 7993 (82/18 AP/HTPB, 41% 7 μ AP, 41% 90 μ AP).

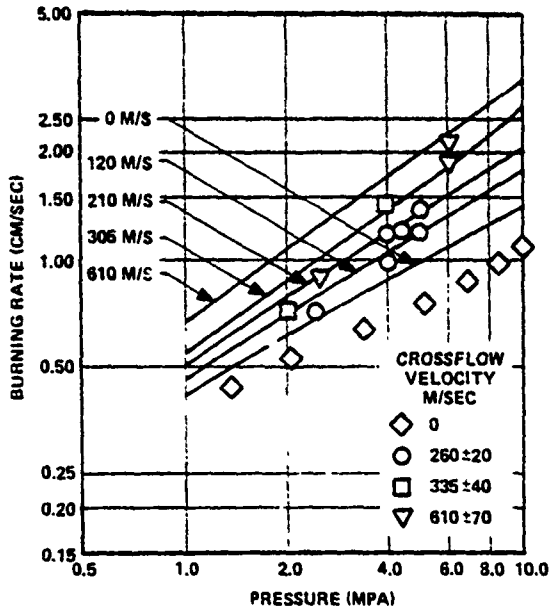


Figure 15. Burning Rate Predictions (Solid Lines) and Data (Points) for Formulation 7996 (82/18 AP/HTPB, 41% 20 μ AP, 41% 290 μ AP).

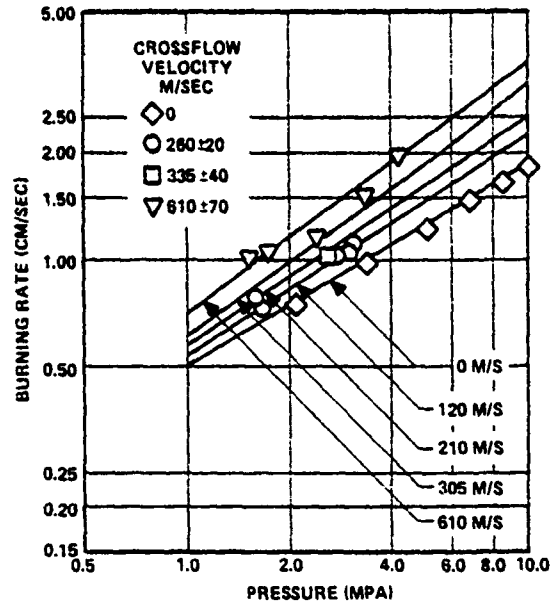


Figure 16. Burning Rate Predictions (Solid Lines) for Formulation 8019 (82/18 AP/HTPB, 27.3% 1 μ AP, 27.3% 20 μ AP, 27.4% 200 μ AP).

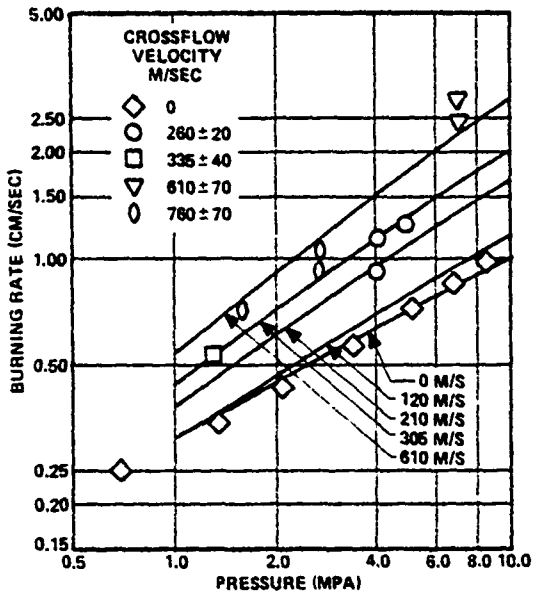


Figure 17. Burning Rate Predictions (Solid Lines) and Data (Points) for Formulation 6626 (74/21/5 AP/HTPB/Al, 5 Micron Al, 70% 90 Micron AP, 4% 200 Micron AP).

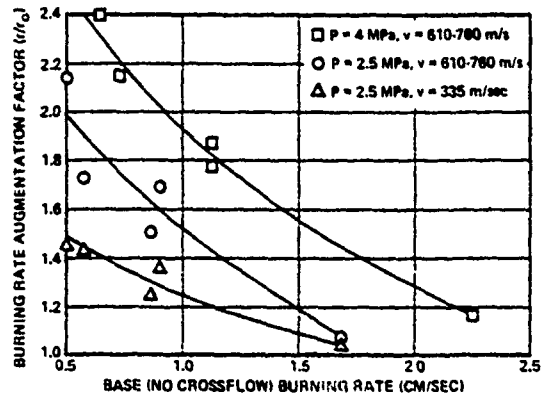


Figure 18. Summary of Results for 82/18 AP/HTPB Formulations.

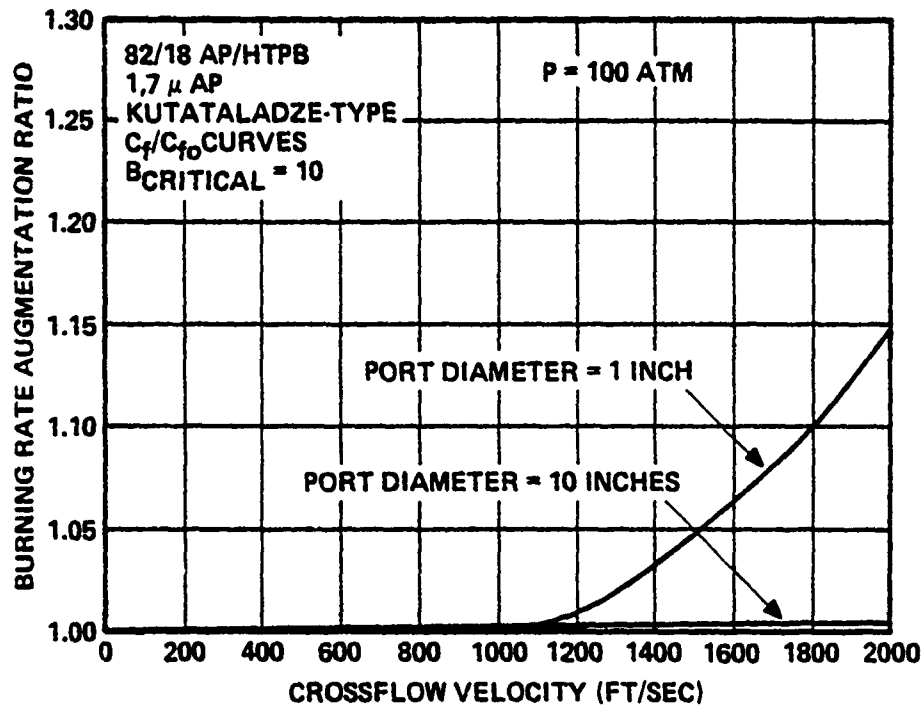


Figure 19. Scaling Effects on Predicted Erosive Burning.

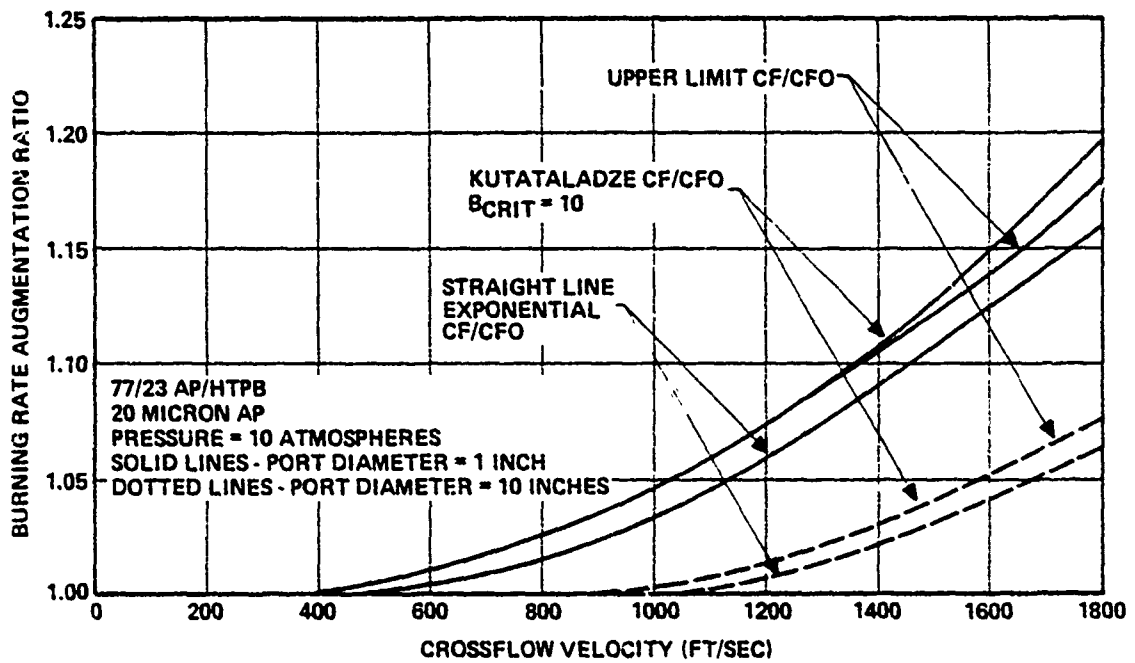


Figure 20. Scaling Effects on Predicted Erosive Burning.

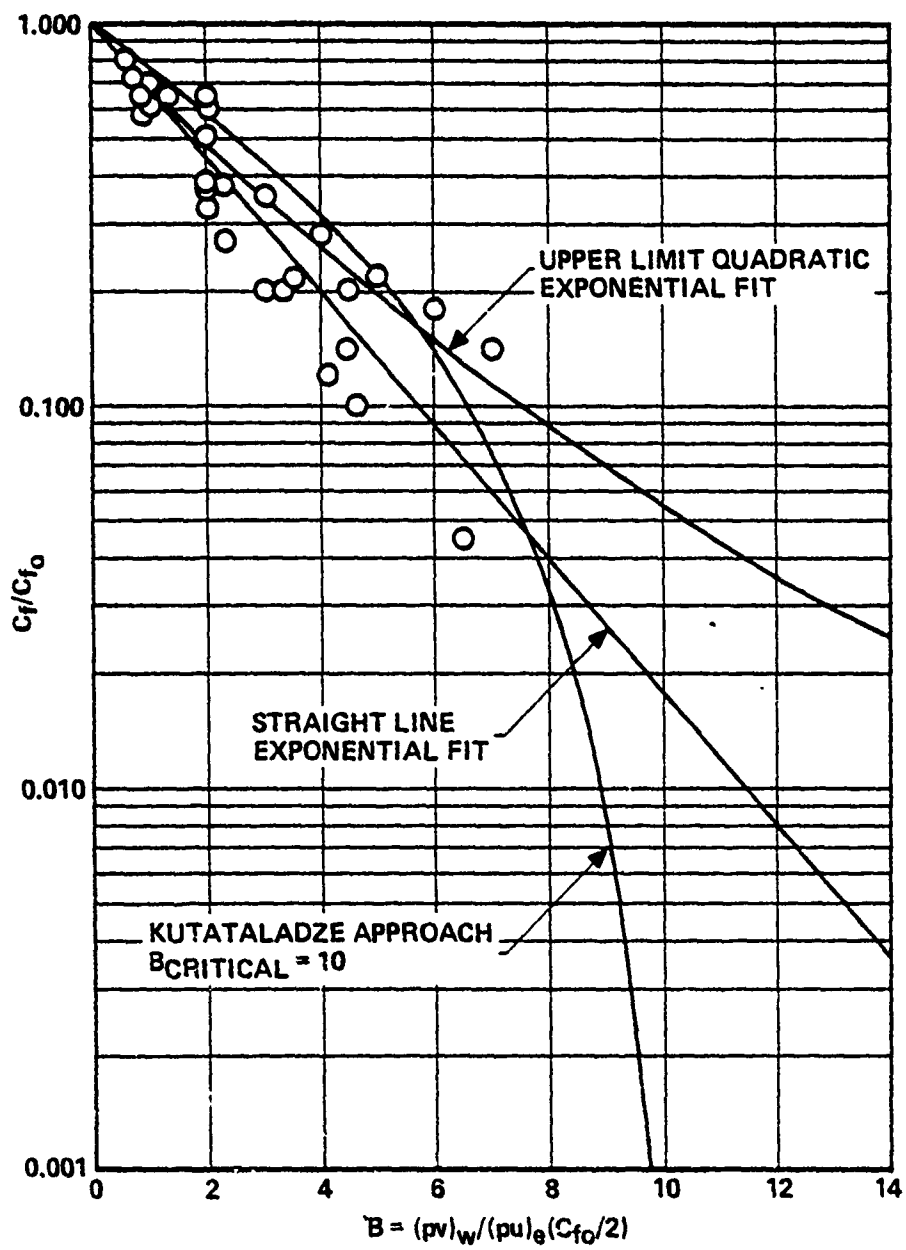


Figure 21. Skin Friction Coefficient Reduction Versus Blowing Parameter.

APPENDIX D

Technical Paper Summarizing
Atlantic Research Modeling
Efforts Re Erosive Burning of
Double-Base Propellants

(To be presented at the AIAA/
SAE/ASME 17th Joint
Propulsion Conference, July, 1981)

A MODEL FOR PREDICTION OF EFFECTS OF
PRESSURE, CROSSFLOW VELOCITY, AND HEAT OF EXPLOSION
ON DOUBLE-BASE PROPELLANT BURNING RATE

Merrill K. King
Atlantic Research Corporation
Alexandria, Virginia

ABSTRACT

A model permitting the prediction of mass burning rate of uncatalyzed NG/NC double-base propellants as a function of crossflow velocity, pressure, and formulation heat of explosion has been developed. Two crossflow model variants, differing in assumptions regarding the penetration of crossflow-induced turbulence into the fizz zone, were examined. In the first variant, the fizz zone was treated as being sufficiently structured to prevent turbulence penetration, with the only burning rate augmentation mechanism then being the amplification of transport properties in the dark zone (sufficient to cause the final flame to influence the inner zones) by crossflow-induced turbulence. This model variant was found to result in serious under prediction of crossflow effects. In the other variant, the fizz zone was treated as a gas in terms of its fluid dynamic behavior, with resultant turbulence amplification of transport properties in both the fizz and dark zones. With this approach, reasonably good agreement between predicted and measured burning rates over a wide range of crossflow velocities was obtained. Under zero-crossflow conditions, the models were found to give good agreement with data for burning mass fluxes in excess of $0.5 \text{ gm/cm}^2 \text{ sec}$ without introduction of a pressure-dependency for surface/sub-surface condensed-phase heat release. Inclusion of pressure dependency in this term permitted extension of the region of good agreement between data and theory down to $0.3 \text{ gm/cm}^2 \text{ sec}$.

BACKGROUND

Over the past twenty years, numerous models for prediction of solid propellant burning rate augmentation due to crossflow of combustion product gases across the propellant surface have been developed. Most of those developed prior to 1977 are referenced and reviewed in Reference 1,

while more recent models appear in References 2-11. These models may be divided into several categories: (1) models based on heat transfer from a "core" gas to the propellant surface by forced convection; (2) models based on the alteration of transport properties between a gas-phase flame zone and the propellant surface by crossflow-induced turbulence; (3) models based on chemically reacting boundary layer theory; and, (4) models based on alteration of flame geometry by crossflow. Some of these models have been developed specifically for homogeneous propellants and others for heterogeneous propellants, while in some of the heat transfer models, the propellant type is not even considered. For the most part, these models emphasize the fluid dynamic aspects of the problem with little attention being paid to the combustion wave structure, a major shortcoming in this author's opinion. Recently, however, several models of composite propellant erosive burning (notably those of King⁽²⁻⁴⁾, Renie, et al⁽⁵⁾, and Legelle⁽¹²⁾) with emphasis on the flame structure have been developed.

It does not appear to this writer that any of the existing homogeneous (double-base) propellant erosive burning models adequately treat the observed mechanistic details of double-base propellant combustion, notably the existence of multiple heat release regions separated by zones in which little reaction takes place. Instead, the existing models of double-base propellant erosive burning either simply treat forced convective heat transfer from the mainstream core flow to the propellant surface or, at best, analyze heat feedback from a single flame zone whose location is defined by analysis of one simple global reaction. In the current effort, the effects of crossflow on a multiple-flame double-base propellant combustion wave as described by Rice and Ginnell⁽¹³⁾, among others, are examined.

The proposed double-base propellant flame structure is depicted in Figure 1. As indicated, there are three major reaction zones, separated by regions in which negligible reaction occurs, sometimes referred to as induction zones. Deep below the surface, the propellant is simply preheated from its conditioning temperature until it reaches a temperature, near the surface, at which reaction to preliminary gaseous or gas/liquid spray products

takes place. These fragments are further heated by the thermal wave until a second set of reactions producing NO and simple organic molecules (notably formaldehyde) occurs in a second reaction zone (which may be quite thin or may occupy a large fraction of the fizz zone, depending on the temperature sensitivity of the reaction rates). Finally, there is a long induction zone, generally referred to as the "dark zone" terminated by a final luminous flame zone in which the intermediates are converted to equilibrium products. It is generally claimed that this last reaction zone is quite thin, allowing it to be reasonably approximated as a flame sheet.

As indicated in Figure 1, the second derivative of temperature is positive in the non-reactive regions and negative in the reaction zones. In the absence of crossflow, it may be easily shown that the long distance separating the final flame zone from the fizz zone, combined with the relatively low gas molecular conductivity results in negligible heat feedback from the final flame zone to the inner zones, thus causing the temperature-distance derivative to be essentially zero at the inner edge of the dark zone, with resultant decoupling of the final flame zone processes from the burn-rate-controlling fizz zone and subsurface zone reaction processes. However, in the presence of strong crossflow, induced turbulence can cause the average effective turbulent thermal conductivity across the dark zone to be raised one to two orders of magnitude above the molecular thermal conductivity. Preliminary calculations performed using empirical expressions for the dark zone width based on the work of Aoki and Kubota⁽¹⁴⁾ indicate that such an increase results in the final flame region contributing appreciable heat flux back to the fizz zone, thus raising its temperature markedly. This, in turn, accelerates the reactions in this zone causing greatly increased heat feedback to the propellant surface with a resultant increase in burning rate.

A second potential mechanism by which crossflow can accelerate the burning rate of homogeneous double-base propellants involves possible penetration of crossflow-induced turbulence into the fizz zone with resultant increase in heat feedback from the fizz zone reaction region to the propellant surface. However, due to the observed gas/liquid froth structure of this zone, it is not totally clear how effectively crossflow-induced turbulence

will penetrate through this zone toward the propellant surface. Accordingly, two limiting-case analyses have been developed and are presented below: (1) no turbulence penetration into the fizz zone, with the outer edge of the fizz zone being considered to be an effective surface as regards the flow field analysis; and, (2) treatment of the fizz zone as a pure gas, with the flow field analysis beginning at the actual propellant surface.

MODEL DEVELOPMENT

The model development was carried out in two phases. First, several fairly closely related models were developed for the combustion of homogeneous double-base propellants in the absence of crossflow. These models were tested against a data base developed by Miller, et al⁽¹⁵⁾, and one was selected for extension to treatment of crossflow effects. As mentioned above, two separate erosive burning models, representing limiting cases as regards penetration of crossflow-induced turbulence into the fizz zone, were then developed.

As indicated earlier, in the pressure range of practical interest, the final flame zone is sufficiently far from the propellant surface that under no-crossflow conditions it does not affect the propellant burning rate, with heat feedback from it to the fizz zone being negligible and the temperature gradient at the inner edge of dark zone being zero.

In the first variant of the no-crossflow model, the fizz reaction zone is assumed to be infinitesimally thin (flame sheet) with its distance from the surface being calculated as the product of the velocity of gas flow from the surface and a characteristic reaction time. Based on the work of Beckstead⁽¹⁶⁾, it is assumed that the burning mass flux and surface temperature are related by:

$$\dot{m} = A_s e^{-E_s/RT_s} \quad (1)$$

$$A_s = 5000 \text{ gm/cm}^2 \text{ sec}$$

$$E_s = 10000 \text{ calories/gm-mol}$$

Since there is no heat release between the surface and the fizz zone flame sheet (located at $X = L_{FZ}$), then between $X = 0$ and $X = L_{FZ}$:

$$\lambda \frac{d^2 T}{dX^2} - \dot{m} C_{PFZ} \frac{dT}{dX} = 0 \quad (2)$$

At $X = L_{FZ}$, with application of an energy balance and use of the fact that the temperature gradient is zero at the inner edge of the dark zone:

$$T = T_{DZ} \quad (3)$$

$$\lambda \left. \frac{dT}{dX} \right|_{X = L_{FZ}} = \dot{m} Q_{gas} \quad (4)$$

where T_{DZ} is the dark zone temperature and Q_{gas} is the heat release per unit mass in the fizz zone flame sheet. Application of an overall energy balance (with zero feedback from the final flame) yields:

$$Q_{gas} = C_{PFZ} (T_{DZ} - T_S) + C_{PS} (T_S - T_0) - Q_L \quad (5)$$

where T_0 is the propellant conditioning temperature and Q_L is the net surface/subsurface heat release per unit mass of propellant. Integration of Eqn. 2, application of the boundary conditions given by Eqns. 3 and 4, and substitution of Eqn. 5 yields:

$$T_S = T_{DZ} - \left[(T_{DZ} - T_S) + \frac{C_{PS}}{C_{PFZ}} (T_S - T_0) - \frac{Q_L}{C_{PFZ}} \right] \left(1 - e^{-\dot{m} C_{PFZ} L_{FZ} / \lambda} \right) \quad (6)$$

At this point, expressions for T_{DZ} , Q_L , and L_{FZ} are needed for closure of the problem.

Aoki and Kubota⁽¹⁴⁾ have recently published results of experimental determination of dark zone temperature as a function of pressure and formulation heat of explosion (H_{EX}): their data may be fit reasonably well by:

$$T_{DZ} = a + b H_{EX} \quad (7)$$

$$b = 0.425$$

$$a = 720 + 125 \ln(P), \quad P \leq 20 \text{ atm}$$

$$a = 855 + 80 \ln(P), \quad P > 20 \text{ atm}$$

Two expressions for Q_L were examined in the course of this study. The first of these, taken from the work of Beckstead⁽¹⁶⁾, relates Q_L to H_{EX} alone:

$$Q_L = 65.7 + 0.013 H_{EX} \quad (8a)$$

$$H_{EX}, Q_L \text{ in calories/gram}$$

As will be discussed later, this expression yielded excellent agreement between burning rate predictions and data at high pressures but led to a pressure exponent of zero at low pressures, in conflict with the data, due to lack of pressure

dependency of Q_L . (At sufficiently low pressures, less than approximately 10-20 atmospheres, depending on the value of H_{EX} , the burning becomes driven by the surface/subsurface heat release, with gas-phase feedback from the fizz zone going to zero.) Accordingly a modified expression, allowing for dependence of Q_L on pressure, was utilized to provide better agreement between low pressure burning rate data and predictions:

$$Q_L = (65.7 + 0.013 H_{EX}) (P/6)^{0.08} \quad (8b)$$

P in atmospheres

(Interestingly enough, subsequent to development of this model, the author found a report by Kubota, Ohlemiller, Caveny, and Summerfield⁽²⁰⁾ in which thermocouple measurements of temperature profiles in burning double-base propellants were used in combination with surface heat balances for estimation of surface heat release as a function of burning rate. Combining their data for uncatalyzed formulations with burning rate versus pressure data for the same formulations (Figs. 10, 19, and 52 of Ref. 20) yields a plot of Q_L versus pressure which indicates that Q_L is approximately proportional to pressure to the 0.10 power over a range of 1 to 100 atmospheres, quite close to the pressure dependency expressed in Eqn. 8b.)

Finally, the distance from the propellant surface to the fizz zone flame sheet (L_{FZ}) was calculated as the product of the average gas velocity across the fizz zone and a characteristic reaction time, given by the following equations:

$$v = \frac{\dot{m} R (T_{DZ} + T_S)}{2 P (MW)} \quad (9)$$

$$\tau_{FZRX} = \frac{K_{FZRX} e^{E_{FZ}/RT_{DZ}}}{T_{DZ} P^{(\nu-1)}} \quad (10)$$

Based on the work of Aoki and Kubota⁽¹⁴⁾ and Beckstead⁽¹⁶⁾, E_{FZ} was set equal to 40000 and the reaction order, ν , was chosen to be unity. With these substitutions, Eqns. 9 and 10 may be combined to yield:

$$L_{FZ} = \frac{\dot{m} R K_{FZRX} (T_{DZ} + T_S) e^{40000/RT_{DZ}}}{2 P (MW) T_{DZ}} \quad (11)$$

where K_{FZRK} is the fizz zone global reaction rate pre-exponential, which is determined by fitting one data point out of the Miller⁽¹⁵⁾ burning rate data base for NC(12.6% N)/NG/Secondary Plasticizer double-base formulations. (Since burning rate is observed to depend on the degree of nitration of nitrocellulose, this constant would probably change for formulations containing NC with different levels of nitration, such as JPN with its 13.5% N nitrocellulose.)

Substitution of Eqns. 7 and 8 into Eqns 6 and 11 reduces the problem to three equations (1, 6 and 11) three unknowns (\dot{m} , L_{FZ} , and T_S) which are simply solved (though care must be taken in low pressure cases where the gas-phase heat feedback becomes negligible), to give burning rate as a function of pressure and formulation heat of explosion.

In a second approach to the analysis of no-crossflow double base propellant combustion, it was assumed that the volumetric heat release is distributed uniformly across the entire fizz zone. In this case, Eqn. 2 is replaced by:

$$\lambda \frac{d^2 T}{dx^2} - \dot{m} C_{PFZ} \frac{dT}{dx} + \dot{Q} = 0 \quad (12)$$

where:

$$\dot{Q} = \frac{\dot{m}}{L_{FZ}} \left[C_{PFZ} (T_{DZ} - T_S) + C_{PS} (T_S - T_0) - Q_L \right] \quad (13)$$

and the boundary condition given by Eqn. 4 is replaced by:

$$\left. \frac{dT}{dx} \right|_{X=L_{FZ}} = 0 \quad (14)$$

Integration of Eqn. 12 followed by application of the boundary conditions given by Eqns. 3 and 14 yields:

$$T_S = T_0 + \frac{Q_L}{C_{PS}} + \frac{\lambda}{\dot{m} C_{PS} L_{FZ}} \left[(T_{DZ} - T_S) + \frac{C_{PS}}{C_{PFZ}} (T_S - T_0) - \frac{Q_L}{C_{PFZ}} \right] \left(1 - e^{-\dot{m} C_{PFZ} L_{FZ} / \lambda} \right) \quad (15)$$

as a replacement for Equation 6. The remainder of the analysis is identical with that of the first model variant.

The third model variant examined employed the Zeldovich approach to flame-speed calculations, with division of the fizz zone into a conductive-convective

region with no reaction and a conductive-reactive region in which convection is neglected. Details of this type of analysis are presented in a text by Glassman⁽¹⁷⁾ and will not be repeated here. For a first order gas-phase reaction, this analysis results in the following relationship between burning mass flux, dark zone temperature, surface temperature, and surface/subsurface heat release:

$$\dot{m} = \sqrt{\frac{2 K_{FZRZ} \lambda T_{DZ}^2 (e^{-40000/R T_{DZ}})_P}{C_{PFZ}(T_{DZ} - T_S) + C_{PS}(T_S - T_0) - Q_L}} \quad (16)$$

which may be combined with Eqns. 1, 7, and 8 for calculation of burning rate as a function of pressure and formulation heat of explosion. (It should be noted that Eqn. 16 becomes invalid if the surface temperature drops below a value given by $C_{PS}(T_S - T_0) = Q_L$: in this case, condensed-phase heat release controls and the burning rate is found by setting $T_S = Q_L/C_{PS} + T_0$ and substituting this value of T_S into Eqn. 1.)

Finally, a fourth no-crossflow model variant using an eigen-value problem approach as described below was developed. In this approach, the fizz zone reactions were assumed to be represented by a single global first order Arrhenius kinetics reaction. As before, Eqn. 1 was employed to relate the mass burning flux to surface temperature, and Eqns. 5, 7, and 8 were used for calculation of T_{DZ} , Q_L , and finally Q_{gas} as a function of surface temperature. Energy and species mass balances within the fizz zone yield:

$$\lambda \frac{d^2 T}{dx^2} - \dot{m} C_{PFZ} \frac{dT}{dx} + \dot{q} = 0 \quad (17)$$

$$\mathcal{D}_p \frac{d^2 y_R}{dx^2} - \dot{m} \frac{dy_R}{dx} - \dot{w}_R = 0 \quad (18)$$

where:

y_R = Mass Fraction of Reactant R

\dot{w}_R = Volumetric Rate of Depletion of Reactant R

\dot{q} = volumetric heat release rate

The Shvab-Zeldovich⁽¹⁸⁾ approach was then used to develop a relationship between $y_R(X)$ and $T(X)$:

$$y_R = \frac{C_{PFZ} y_{Rinit}}{Q_{gas}} [T_{DZ} - T] \quad (19)$$

where y_{Rinit} is the mass fraction of material leaving the surface which is reactant R. With the assumption of first order kinetics, the volumetric heat release rate may be expressed as:

$$\dot{q} = A_g Q_{gas} e^{-E_g/RT} P y_R/T \quad (20)$$

Combining Eqns. 17, 19, and 20, using $E_g = 40000$ cal/mole (again based on the work of Aoki and Kubota⁽¹⁴⁾ and Beckstead⁽¹⁶⁾), and lumping the product of A_g and $y_{R, init}$ into one constant to be evaluated by fitting one data point, one obtains:

$$\lambda \frac{d^2 T}{dX^2} - \dot{m} C_{PFZ} \frac{dT}{dX} + \frac{A_g' P C_{PFZ} e^{-40000/RT} (T_{DZ} - T)}{T} = 0 \quad (21)$$

with boundary conditions:

$$\dot{m} [C_{PFZ} (T_S - T_0) - Q_L] = \lambda \left. \frac{dT}{dX} \right|_{X=0} \quad (22)$$

$$T = T_{DZ} \text{ at } X \rightarrow \infty \quad (23)$$

For a given pressure and formulation heat of explosion, the following procedure is used to calculate a predicted burning mass flux. First, a value of surface temperature is guessed and Eqns. 5, 7, 8, and 22 are used to calculate \dot{m} , Q_{gas} , T_{DZ} , Q_L , and dT/dX at $X = 0$. Equation 21 is then integrated, using the $X = 0$ values of T and dT/dX , by a Runge-Kutta procedure out toward $X = \infty$. If T climbs above T_{DZ} , the calculation is terminated and a lower value of surface temperature guessed, while if the temperature derivative turns negative before T_{DZ} is reached, the calculation is terminated and a higher value of surface temperature is guessed, this procedure being repeated until the surface temperature is bracketed within 0.5°K (corresponding to an error band of approximately one percent on burning rate).

As will be discussed in the next section, all four zero-crossflow model variants have been found to give comparable predictions of the Miller⁽¹⁵⁾ data base for burning rate as a function of pressure and heat of explosion. Accordingly, the first variant (with pressure-dependent Q_L) was selected on the basis of its relative simplicity for extension to the case of nonzero crossflow. As mentioned earlier, two crossflow models have been developed: in the first,

the fizz zone is assumed to be structurally rigid, with no penetration of turbulence into it; while in the second, the fizz zone has been treated as a gas in terms of its fluid dynamic behavior.

A sketch of the postulated flame structure for the first (rigid fizz zone) model is presented as Figure 2. For convenience in applying a boundary layer analysis computer code previously developed for modeling of composite propellant erosive burning⁽²⁻⁴⁾, the coordinate system is chosen such that the origin ($X=0$) is at the interface of the dark zone and the fizz zone since in this model this interface is the "surface" of the propellant as regards the flow analysis. As may be seen, there are three distinct infinitesimally thin (flame sheet) heat release zones separated by regions of negligible heat release. As in the zero-crossflow case, mass burning flux is related to the surface ($X = -L_{FZ}$) temperature through Eqn. 1. In addition, it may be shown that the heat release at the fizz zone flame sheet is given by:

$$Q_{\text{gas}} = C_{\text{PFZ}} (a+b H_{\text{EX}} - T_S) + C_{\text{PS}} (T_S - T_0) - Q_L \quad (24)$$

with Q_L given by Eqn. 8b. Integration of the Fourier equation with no heat release between $X = -L_{FZ}$ and $X = 0$, followed by application of boundary conditions at $X = 0$:

$$T = T_{\text{FZ-DZ}} \text{ at } X = 0 \quad (25)$$

$$\lambda \left. \frac{dT}{dX} \right|_{X=0^-} = \dot{m} Q_{\text{gas}} + \lambda \left. \frac{dT}{dX} \right|_{X=0^+} \quad (26)$$

leads to:

$$T_S = T_{\text{FZ-DZ}} - \left[\frac{Q_{\text{gas}}}{C_{\text{PFZ}}} + \frac{\lambda}{\dot{m} C_{\text{PFZ}}} \left. \frac{dT}{dX} \right|_{X=0^+} \right] \left(1 - e^{-\dot{m} C_{\text{PFZ}} L_{\text{FZ}}/\lambda} \right) \quad (27)$$

(It should be noted that $T_{\text{FZ-DZ}}$ is not the same as T_{DZ} used previously in the no-crossflow analysis, due to heat feedback from the final flame causing an increase in this temperature.) L_{FZ} is calculated using the same equation form as Eqn. 11, with $T_{\text{FZ-DZ}}$ replacing T_{DZ} :

$$L_{\text{FZ}} = \frac{\dot{m} R K_{\text{FZR}} (T_{\text{FZ-DZ}} + T_S) e^{40000/RT_{\text{FZ-DZ}}}}{2 P (\text{MW}) T_{\text{FZ-DZ}}} \quad (28)$$

Data presented by Aoki and Kubota⁽¹⁴⁾ regarding dark zone dimensions were used to develop the following expression for the dark zone thickness:

$$\Delta L_{FF} = \frac{252}{p^{2.1}} \left(\frac{\dot{m}}{\dot{m}_{\text{no crossflow}}} \right) \quad (29)$$

where pressure is in atmospheres and ΔL_{FF} in centimeters. An overall energy balance is used to develop an expression for the final flame heat release:

$$Q_{FF} = C_{PDZ} (T_f - a - b H_{EX}) \quad (30)$$

where the flame temperature, T_f , is calculated from thermodynamic equilibrium considerations. For closure of the problem, expressions for T_{FZ-DZ} and $(dT/dX)|_{X=0^+}$ are required. Due to turbulence in the dark zone induced by crossflow, the effective (turbulent plus molecular) thermal conductivity varies strongly across this zone. Accordingly, the transport of energy across this zone is best calculated by breaking the zone up into many segments, over each of which effective thermal conductivity is nearly constant, solving the Fourier equation for each segment and applying boundary condition matching conditions at each segment interface. This procedure results in:

$$T_{FZ-DZ} = T_{Flame} - \frac{Q_{FF}}{C_{PDZ}} \left[1 - \prod_{N=1}^{N=NTOT} e^{-\dot{m} C_{PDZ} [X(N) - X(N-1)] / \lambda_t(N)} \right] \quad (31)$$

$$\left. \frac{dT}{dX} \right|_{X=0^+} = \frac{\dot{m} Q_{FF}}{\lambda_t(N=1)} \left[\prod_{N=1}^{N=NTOT} e^{-\dot{m} C_{PDZ} [X(N) - X(N-1)] / \lambda_t(N)} \right] \quad (32)$$

($N = 1$ at $X = 0$, $N = NTOT$ at $X = \Delta L_{FF}$)

where the values of effective thermal conductivity, λ_t , are calculated as a function of position using a turbulent boundary layer analysis procedure described in Ref. 2 - 4, and briefly outlined in Appendix A.

The following procedure is used to solve the above equations for burning mass flux at a given pressure, crossflow velocity, and formulation heat of explosion. First, the no-crossflow analysis is used to calculate the base burning mass flux for the given pressure and heat of explosion values. A value of \dot{m} is then guessed and Eqn. 29 is used to calculate ΔL_{FF} . Eqn. 30 is then used to calculate Q_{FF} and the flow profile analysis together with Eqns. 31 and 32 are used to evaluate T_{FZDZ} and $(dT/dX)|_{X=0^+}$. Eqn. 1 is next solved for T_G , and 24 for Q_{gas} , after which Eqns. 27 and 28 are solved

simultaneously for L_{FZ} and \dot{m} . The calculated \dot{m} is then checked against the previous value, a new value is guessed, and the procedure is repeated to convergence.

A sketch of the postulated flame structure defining the coordinate system for the second (gaseous fizz zone) erosive burning model is presented as Figure 3. Here, because the boundary layer analysis must begin at the propellant surface, the coordinate system is redefined so that the origin is at the actual propellant surface. The equation development for the model is essentially the same as for the rigid fizz zone model, except that in this case allowance must also be made for variation in effective thermal conductivity across the fizz zone as well as across the dark zone. This change results in replacement of Eqn. 27 by:

$$T_S = T_{FZ-DZ} - \left[\frac{Q_{gas}}{C_{PFZ}} + \frac{\lambda_{t, X=L_{FZ}}}{\dot{m} C_{PFZ}} \frac{dT}{dX} \Big|_{X=L_{FZ}^+} \right] \left(1 - \prod_{M=1}^{M=MTOT} e^{-\dot{m} C_{PFZ} [X(M) - X(M-1)] / \lambda_t(M)} \right) \quad (33)$$

($M=1$ at $X=0$, $M=MTOT$ at $X=L_{FZ}$)

and Eqns. 31 and 32 by:

$$T_{FZ-DZ} = T_{flame} - \frac{Q_{FF}}{C_{PDZ}} \left[1 - \prod_{N=1}^{NTOT} e^{-\dot{m} C_{PDZ} [X(N) - X(N-1)] / \lambda_t(N)} \right] \quad (34)$$

$$\frac{dT}{dX} \Big|_{X=L_{FZ}^+} = \frac{\dot{m} Q_{FF}}{\lambda_t(N=1)} \left[\prod_{N=1}^{NTOT} e^{-\dot{m} C_{PDZ} [X(N) - X(N-1)] / \lambda_t(N)} \right] \quad (35)$$

($N=1$ at $X=L_{FZ}$, $N=NTOT$ at $X=L_{FZ} + \Delta L_{FF}$).

The equation solution procedure is basically unchanged.

RESULTS AND DISCUSSION

As mentioned earlier, Miller⁽¹⁵⁾ has generated a systematic data base for burning rate of Nitrocellulose (12.6 N)/Nitroglycerine/Secondary Plasticizer double-base formulations as a function of pressure and heat of explosion, without crossflow. Each of the no-crossflow model variants described in the previous section has been used to predict the dependence of burn rate on pressure and H_{EX} for these formulations, with one point of the data base

being used to fix the one unknown constant, the fizz zone reaction rate pre-exponential, in each variant. For the flame sheet, uniformly distributed heat release, and Zeldovich approach variants, the base point used was at $P = 35$ atmospheres, $H_{EX} = 950$ calories/gram, while for the eigen-value approach, it was at $P = 49$ atmospheres, $H_{EX} = 950$ calories/gram. Predicted and measured burning mass fluxes are presented in Figures 4 - 8. In the first three of these figures, the surface/subsurface heat release parameter was assumed to be pressure-independent, while in the latter two figures it was allowed to depend on pressure in accordance with Eqn. 8b. As may be seen from Figures 4 - 6, three of the model variants, with pressure independent surface heat release, give reasonably good predictions of data for the higher pressure end of the data bank, but deviate somewhat at low pressure. The pressure at which the deviation occurs appears to increase with decreasing propellant heat of explosion. On the whole, the flame sheet and eigenvalue variants appear to do better than the Zeldovich - type model, while the uniform heat release approach (results not presented) does slightly worse. The explanation for the relatively poor agreement between theory and data at low pressure lies in the fact that at these lower pressures the burning begins to be driven totally by the surface/subsurface heat release, the offset distance of the fizz zone flame being so large as to provide negligible heat feedback to the surface. Since the surface/subsurface heat release was assumed to be pressure-independent this of course leads to a predicted burning rate pressure exponent of zero in these low pressure regions, at variance with experimental observations.

Accordingly, revised versions of the flame sheet and eigen-value model variants, with allowance for pressure-dependent surface heat release (in accordance with Eqn. 8b) were developed and tested against the Miller data base. Results of these calculations are presented in Figures 7 and 8. As may be seen, agreement between predicted and experimental burning rates is excellent with either model.

In Figure 9, predictions made with the flame sheet model, with allowance for pressure-dependent surface/subsurface heat release in accordance with Eqn. 8b are compared against data obtained by Aoki and Kubota for two propellants with much higher NC/NG ratios than those tested by Miller. No constants

were adjusted in making these predictions. As may be seen, at the higher pressures the agreement between data and predictions is excellent. However, at the low end of the pressure range examined, particularly for the lower energy formulation, theory and data diverge somewhat, with the model predicting higher burning rates than observed. The break between data and theory occurs at a burning mass flux of about $0.3 \text{ gm/cm}^2 \text{ sec}$ for each formulation. Examination of intermediate output from the model indicates that it is in this region that the condensed phase processes begin to control the burning rate, the gas phase flame moving so far away from the surface as to have no effect on burning rate at lower pressures. Thus, it appears that for improvement of the no-crossflow model in the low pressure regime, effort will have to be concentrated on better modeling of the condensed phase processes.

The two erosive burning models developed (one assuming essentially a rigid fizz zone structure with no turbulent transport property augmentation in this region, the other assuming that the fizz zone acts like a gas in terms of penetration of turbulence) have been tested against data obtained for two NG/NC propellants by Burick and Osborn⁽¹⁹⁾. These formulations, designated as BUU and BDI have heats of explosion of approximately 1050 cal/gm and 920 cal/gm, respectively. Predicted and observed burning mass fluxes are presented in Figures 10 - 13. As may be seen from Figure 10, the no-crossflow predictions of burning rate versus pressure for BUU are excellent. In addition, the erosive burning predictions made assuming full turbulence penetration through the fizz zone are quite good, while the rigid structure fizz zone model results in drastic underprediction of the effects of crossflow. This is more clearly shown in Fig. 11, where the burning mass flux (predicted and observed) is plotted against crossflow velocity at constant pressure. As may be seen, the effects of crossflow predicted assuming turbulent boundary layer development starting at the interface of the unburned propellant and the fizz zone agree quite well with data, while the alternative assumption regarding turbulence penetration into the fizz zone fails badly. Similar results for the BDI formulation appear in Figures 12 and 13.

SUMMARY

Several variants of a model for prediction of burning rate of uncatalyzed homogeneous double-base propellants as a function of pressure and heat of

explosion, in the absence of crossflow, have been developed and shown to give reasonable agreement with data, particularly for burn rates in excess of approximately $0.5 \text{ gm/cm}^2 \text{ sec}$. Allowance for pressure dependence of exothermic surface/subsurface reactions extends the region of good agreement between data and theory down to mass burning fluxes of approximately $0.3 \text{ gm/cm}^2 \text{ sec}$ (0.2 cm/sec). One of the model variants developed, a flame-sheet model, has been extended to allow for the effects of crossflow. Two variants of a crossflow model have been developed. In one of these, it is assumed that crossflow-induced turbulence does not penetrate the fizz zone and that the only mechanism leading to increased burning in the presence of crossflow is turbulence augmentation of transport properties in the dark zone resulting in significant heat feedback from the final flame, which does not come into play in the absence of crossflow. In the other variant, it is assumed that the fizz zone acts like a gas in terms of its fluid dynamic behavior, with crossflow-induced turbulence not only bringing the final flame into play but also increasing the effective transport properties across the fizz zone. The latter variant is found to result in good agreement between predictions and data, while the former variant results in marked underprediction of the effects of crossflow on double-base propellant burning rate.

NOMENCLATURE

A_S	Pre-exponential in Arrhenius expression relating mass burning flux to surface temperature
b	Blowing Parameter, defined by Eqn. A2
C_f	Skin friction coefficient, with blowing
C_{fo}	Non-blowing skin friction coefficient
C_{PDZ}	Heat capacity in dark zone
C_{PFZ}	Heat capacity in fizz zone
C_{PS}	Condensed-phase propellant heat capacity
E_{FZ}	Fizz zone reaction activation energy
E_S	Surface reaction activation energy
h	Flow channel half-height
H_{EX}	Propellant heat of explosion
K_{FZR}	Fizz zone reaction constant, defined by Eqn. 10
L_{FZ}	Fizz zone thickness
M	Crossflow Mach Number
MW	Molecular Weight of propellant ablation products

\dot{m}	Propellant burning mass flux
P	Pressure
Q_{FF}	Heat release per unit mass in final flame
Q_{gas}	Heat release per unit mass in fizz zone flame
Q_L	Net surface/subsurface heat release per unit mass
R	Gas law constant
T	Temperature
T_O	Propellant conditioning temperature
T_{flame}	Propellant adiabatic flame temperature
T_S	Propellant surface temperature
T_{DZ}	Dark zone temperature in absence of final flame influence
T_{FZ-DZ}	Temperature at Fizz Zone-Dark Zone Interface
u	Crossflow velocity
U_{fs}	Free stream crossflow velocity
X	Distance coordinate normal to propellant surface (Fig. 2 and 3)
ΔL_{FF}	Dark zone thickness
ϵ	Eddy viscosity
λ, λ_L	Molecular thermal conductivity of ablation products
λ_t	Total (molecular plus turbulent) thermal conductivity
μ	Molecular viscosity
ρ	Gas density
τ	Local shear stress
τ_{FZRX}	Fizz zone reaction time
τ_{wall}	Wall shear stress
v	Reaction order for Fizz zone reaction

REFERENCES

1. King, M.K., "A Model of Erosive Burning of Composite Propellants", J. Spacecraft and Rockets, 15, 3, pp 139-146 (1978)
2. King, M.K., "A Model of the Effects of Pressure and Crossflow Velocity on Composite Propellant Burning Rate," AIAA Paper 79-1171, AIAA/SAE/ASME 15th Joint Propulsion Conference, June, 1979.
3. King, M.K., "Experimental and Theoretical Study of the Effects of Pressure and Crossflow Velocity on Composite Propellant Burning Rate," 18th Symposium (International) on Combustion, Waterloo, Canada, 1980. To be printed in Meeting Proceedings.

4. King, M.K., "Predicted and Measured Effects of Pressure and Crossflow Velocity on Composite Propellant Burning Rate," 17th JANNAF Combustion Meeting, Langley, VA, 1980. To be included in CPIA Publication of Meeting Proceedings.
5. Renie, J.P., Condon, J.A., and Osborn, J.R., "Oxidizer Size Distribution Effects on Propellant Combustion," AIAA Paper 78-981, AIAA/SAE 14th Joint Propulsion Conference, July, 1978.
6. Parkinson, R.C., "Erosive Burning as a Boundary Layer Phenomenon in Rocket Motors," AIAA Paper 80-1208, AIAA/SAE/ASME 16th Joint Propulsion Conference, 1980.
7. Mukunda, H.S., "A Comprehensive Theory of Erosive Burning in Solid Rocket Propellants," Comb. Sci. and Technology, 18, pp 105-18 (1978).
8. Ben Reuven, M., and Caveny, L.H., "Erosive Burning Theory for Propellants With Extended Flame Zones," AIAA Paper 80-0142, AIAA 18th Aerospace Sciences Meeting, 1980.
9. Razdan, M.K., and Kuo, K.K., "Erosive Burning Study of Composite Solid Propellants by Turbulent Boundary Layer Approach," AIAA J, 17, pp 1225-1233 (1979)
10. Beddini, R.A., "A Reacting Turbulent Boundary Layer Approach to Solid Propellant Erosive Burning," AIAA J, 16, pp 898-905 (1978).
11. Beddini, R.A., "Aerothermochemical Analysis of Erosive Burning in a Laboratory Solid-Rocket Motor," AIAA J, 18, pp 1346-1353 (1980).
12. Lengelle, G., "Model Describing the Erosive Combustion and Velocity Response of Composite Propellants," AIAA J, 13, pp 315-322 (1975).
13. Rice, O.K., and Ginnell, R., "Theory of Burning of Double-Base Rocket Powders," J. Phys Chem., 54, pp 885-917, (1950).
14. Aoki, I., and Kubota, N., "Combustion Wave Structures of High and Low Energy Double-Base Propellants," AIAA Paper 80-1165, AIAA/SAE/ASME 16th Joint Propulsion Conference, July, 1980.
15. Miller, R.R. and Foster, R.L., Personal Communication, Hercules/ABL, August 1978. Data generated under Contract F04611-78-C-0005.
16. Beckstead, M.W., "A Model For Double Base Propellant Combustion," AIAA Paper 80-1164, AIAA/SAE/ASME 16th Joint Propulsion Conference, July, 1980.
17. Glassman, I., Combustion, Academic Press, NY, 1977.
18. Williams, F.A., Combustion Theory, Addison-Wesley Publ. Co., Reading,

19. Burick, R.J., and Osborn, J.R., "Erosive Combustion of Double-Base Solid Rocket Propellants," 4th ICRPG Combustion Conference, CPIA Publication 162, Vol. II, pp. 57-69, December, 1967.
20. Kubota, N., Ohlemiller, T.J., Caveny, L., and Summerfield, M., "The Mechanism of Super-Rate Burning of Catalyzed Double Base Propellants," Princeton Univ. Aerospace and Mechanical Sciences Report No. 1087, March, 1973.

APPENDIX A

BOUNDARY LAYER ANALYSIS FOR DETERMINATION OF EFFECTIVE THERMAL CONDUCTIVITY DISTRIBUTION

Details of the boundary layer analysis employed to determine distribution of total (molecular plus turbulent) thermal conductivity through the zones of interest are described in detail in Ref. 2-4: a brief outline and summary is presented below.

First the non-blowing skin friction coefficient is calculated as a function of crossflow Reynolds number from a smooth-wall equation:

$$C_{fo} = .00140 + .125 Re^{-0.32} \quad (A1)$$

(Options for treatment of a rough surface are also included in the analysis but were not invoked in this study.) The estimated mass burning flux (or value obtained in the previous calculation loop) is then used to generate the value of the blowing parameter, b :

$$b = \frac{2 \dot{m}}{(\rho U_{FS})_{\text{Crossflow}} C_{fo}} \quad (A2)$$

which is then used in calculation of the actual skin friction coefficient in the presence of blowing. Several optional equations for this parameter are included in the program: the one employed in the calculations presented herein (selected on the basis of success with prediction of composite propellant erosive burning) is:

$$C_f = C_{fo} \left[1 - \frac{b}{10} \right]^2 / \left[1 + \frac{b}{10} \right]^{0.4} \quad (A3)$$

This value was then used to calculate a shear stress at the surface via:

$$\tau_{\text{wall}} = (C_f/2) \rho_{fs} U_{fs}^2 \quad (A4)$$

Application of a momentum integral analysis for a two-dimensional channel yields the following expression for local shear stress as a function of distance from the propellant surface and the local crossflow velocity:

$$\tau = \tau_{\text{wall}} + \dot{m} u - Kx \quad (\text{A5})$$

$$K = 0.9 \dot{m} \bar{U} \left[2 + \frac{(\gamma + 1) M^2}{1 - M^2} \right] / h \quad (\text{A6})$$

In addition, the local shear stress is related to the local crossflow velocity gradient by:

$$\tau = (\mu + \rho \epsilon) du/dx \quad (\text{A7})$$

A Prandtl mixing length expression for eddy viscosity:

$$\epsilon = .168 y^2 (\text{DF})^2 du/dx \quad (\text{A8})$$

and equations of state relating ρ and μ to temperature were employed along with the approximation of a linear temperature gradient across the zone of interest to close the analysis. (In the calculations presented in this paper, the dumping factor was set equal to unity)

With these relationships, Equations A5 - A8 may be combined and integrated from the wall (with $u = 0$ at $X = 0$ as a starting boundary condition) to yield among other things, the variation of eddy viscosity (ϵ) with X . The total (molecular plus turbulent) thermal conductivity may then be calculated as a function of X from

$$\frac{\lambda_t}{\lambda_L} = 1 + \frac{\rho \epsilon}{\mu} = f(x) \quad (\text{A9})$$

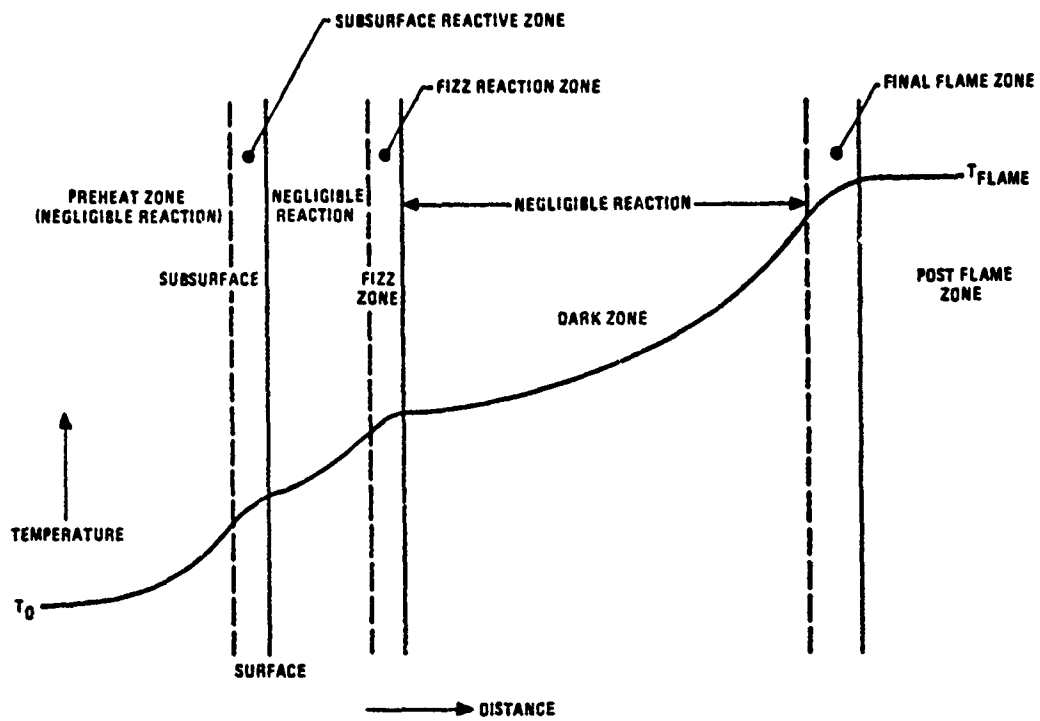


Figure 1. Postulated Double-Base Propellant Flame Structure.

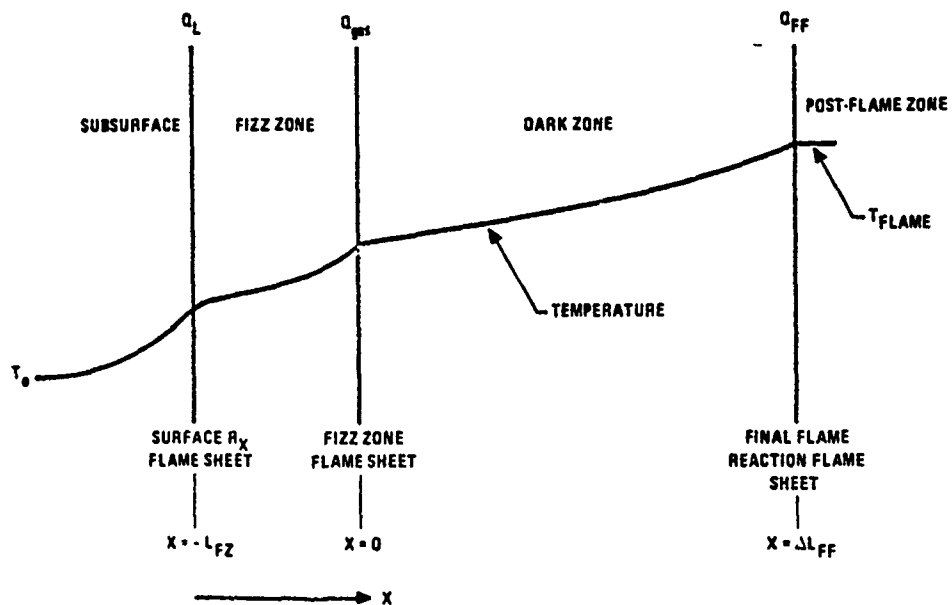


Figure 2. Rigid Fizz Zone Double-Base Propellant Erosive Burning Model.

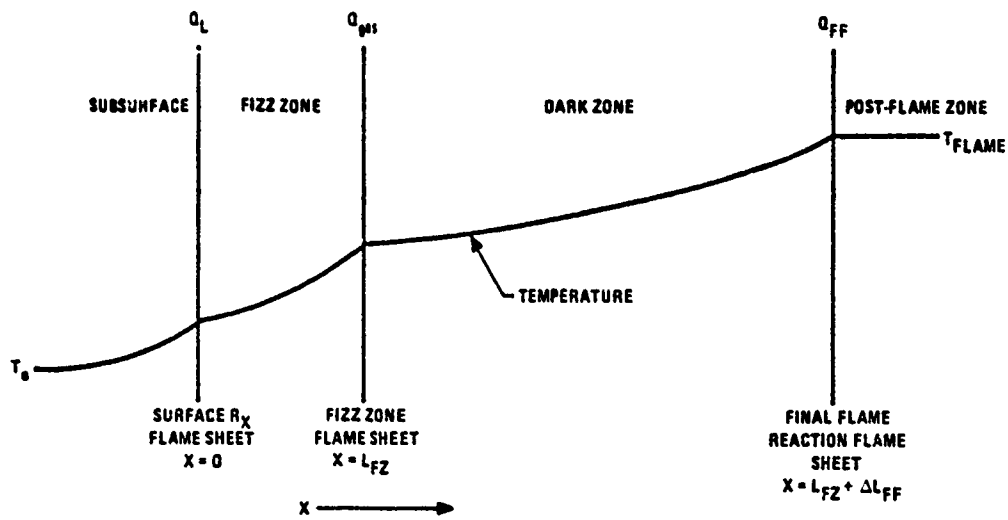


Figure 3. Gas Fizz Zone Double-Base Propellant Erosive Burning Model.

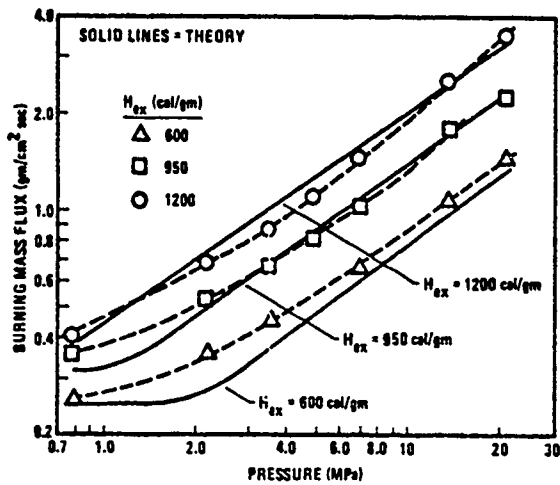


Figure 4. Comparison of Predicted Burning Rates Using a Flame Sheet Model with Miller Data (Surface/Subsurface Heat Release Independent of Pressure).

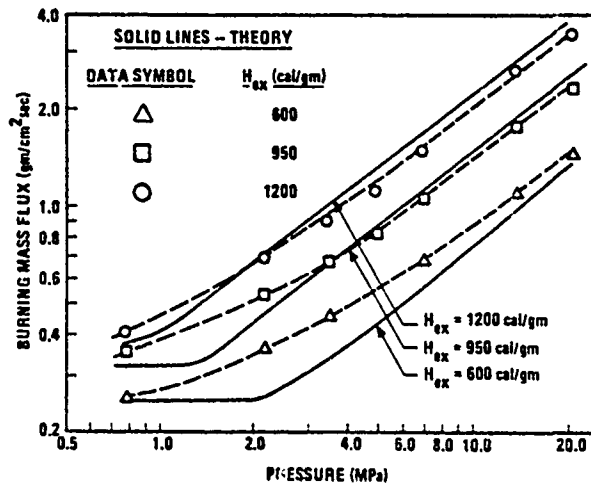


Figure 5. Comparison of Predicted Burning Rates using a Zeldovich Flame Model with Miller Data. (Surface/Subsurface Heat Release Independent of Pressure).

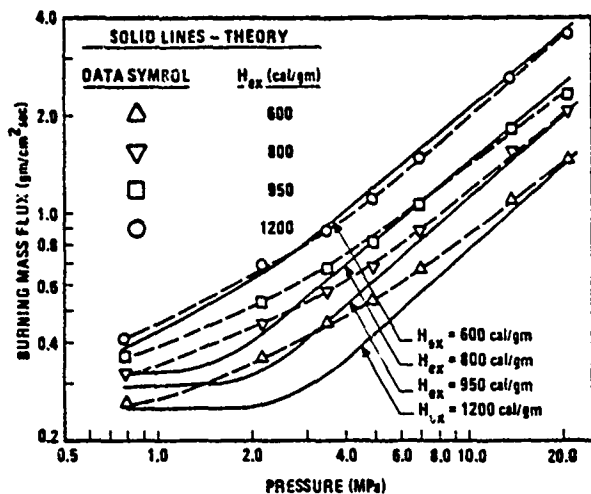


Figure 6. Comparison of Predicted Burning Rates Using an Eigen-Value Flame Model with Miller Data. [Surface/Subsurface Heat Release Independent of Pressure]

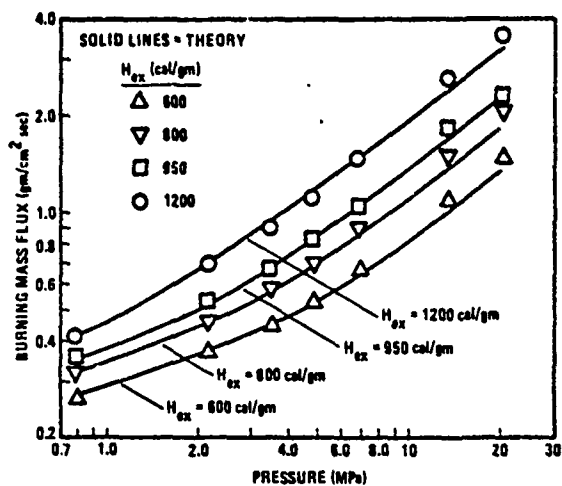


Figure 7. Comparison of Predicted Burning Rates Using a Flame-Sheet Model with Miller Data (Pressure-Dependent Surface/Subsurface Heat Release).

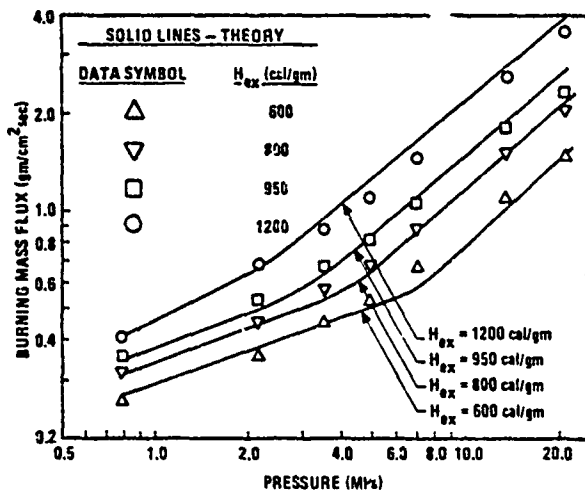


Figure 8. Comparison of Predicted Burning Rates Using an Eigen-Value Flame Model with Miller Data. [Pressure-Dependent Surface/Subsurface Heat Release]

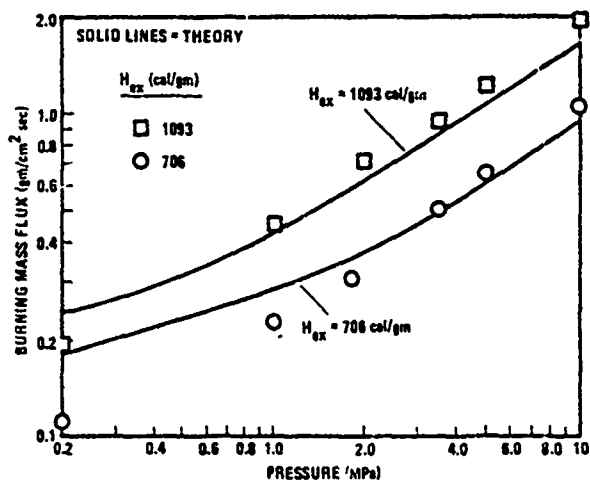


Figure 9. Comparison of Predicted Burning Rates Using a Flame-Sheet Model with Data of Aoki and Kubota (Pressure-Dependent Surface/Subsurface Heat Release).

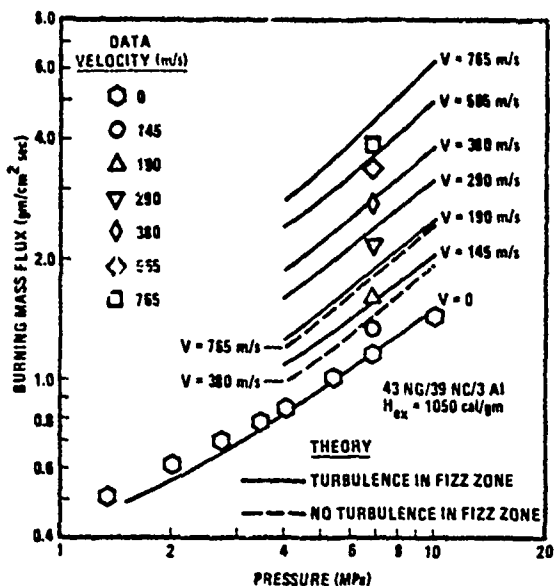


Figure 10. Predicted and Observed Burning Mass Fluxes for BUU Propellant.

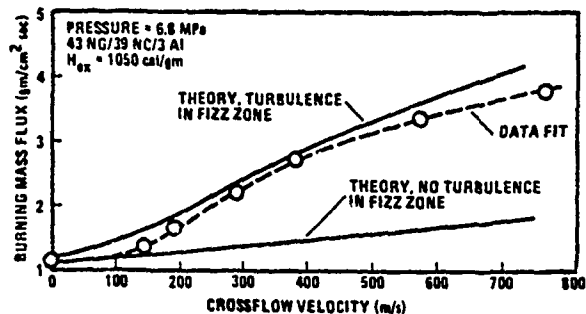


Figure 11. Predicted and Observed Effects of Crossflow Velocity on Burning Rate of BUU Propellant.

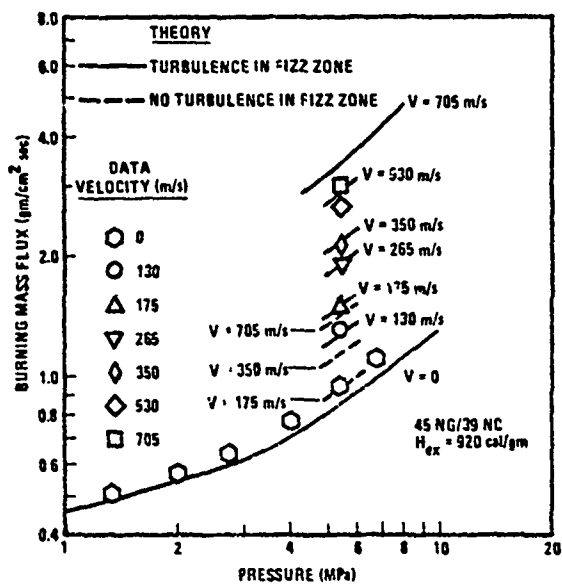


Figure 12. Predicted and Observed Burning Mass Fluxes for BDI Propellant.

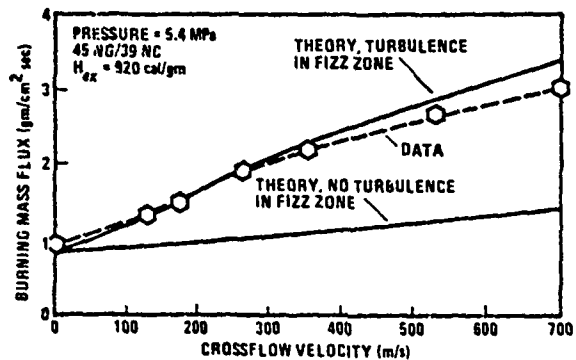


Figure 13. Predicted and Observed Effects of Crossflow on Burning Rate of BDI Propellant.

APPENDIX E

Technical Papers Summarizing
Experimental and Modeling Efforts at
Penn State on Erosive Burning
of Composite Propellants



AIAA 78-978R

**Erosive Burning Study of Composite Solid
Propellants by Turbulent Boundary-Layer
Approach**

M. K. Razdan and K. K. Kuo

Reprinted from

AIAA Journal

Volume 17, Number 11, November 1979, Page 1225
Copyright American Institute of Aeronautics and Astronautics, Inc., 1978. All rights reserved

Erosive Burning Study of Composite Solid Propellants by Turbulent Boundary-Layer Approach

M. K. Razdan* and K. K. Kuo†

The Pennsylvania State University, University Park, Pa.

Erosive burning of composite solid propellants is investigated by analyzing a steady, two-dimensional, chemically reacting, turbulent boundary layer over a propellant surface. Predicted erosive burning rates agree closely with experimental data. The erosive burning rate augmentation is found to be caused by the increase in heat feedback introduced by the increase in transport coefficients, and the turbulence enhanced mixing and reaction of the oxidizer and fuel gases. The increase in freestream gas velocity brings the location of the peak turbulence intensity and the heat release zone closer to the propellant surface, thereby increasing the burning rate of a propellant.

Nomenclature

a	= reaction time parameter in Summerfield's burning rate law, psia/in./s	k	= Von Karman's constant
A_e	= Arrhenius frequency factor in gaseous reactions, $(m^3)^{n-1} s^{-1} (kmole)^{1-n}$	K	$\equiv u_i u_i' / 2$, turbulent kinetic energy, m^2/s^2
A_s	= Arrhenius frequency factor in propellant surface decomposition, m/s	n	= order of chemical reaction
A^+	= damping constant in van Driest's hypothesis	p	= pressure, N/m ²
b	= diffusion time parameter in Summerfield's burning rate law, psia ^{1/3} /in./s	Pr	$\equiv C_p \mu / \lambda$, Prandtl number based upon the molecular properties of the fluid
$C_1 - C_4, C_\mu, C_\rho, C_\omega$	= constants in turbulence models	Pr_t	= Prandtl number for turbulent flow defined in Eq. (8)
C_p	$\equiv \sum_k Y_k C_{pk}$, average heat capacity of the reacting gases, kcal/kg-K	\dot{Q}_t	$\equiv \sum_k (\nu_k W_k \Delta h_{f,k}^0 \dot{\omega}_k) / (\nu_F W_F)$, rate of heat generation in gas phase, kcal/m ³ -s
C_{pk}	= heat capacity of the k th species, kcal/kg-K	Q_s	= heat of reaction defined in Eq. (22), kcal/kg
C_s	= heat capacity of solid propellant, kcal/kg-K	r_b	= total burning rate of a solid propellant, m/s
D	= diffusion coefficient in Fick's Law, m ² /s	r_{bo}	= strand burning rate of a solid propellant, m/s
D	= damping coefficient defined in Eq. (26)	Re_x	$\equiv \rho_\infty U_\infty x / \mu_\infty$, Reynolds number based on x
E_{ag}, E_{as}	= activation energies in the gas phase reaction and propellant surface decomposition, kcal/mole	R_N	= roughness height, m
g_F	$\equiv Y_F'^2$, mean square of fuel mass-fraction fluctuations	R_u	= universal gas constant, N-m/kmole K
$\Delta h_{f,k}^0$	= heat of formation of the k th species, kcal/kg	Sc	$\equiv \mu / \bar{\rho} D$, Schmidt number based upon molecular properties of the fluid
h_k	$\equiv \Delta h_{f,k}^0 + \int_T^T C_{pk} dT$, enthalpy of the k th species, kcal/kg	Sc_t	= Schmidt number for turbulent flow defined in Eq. (8)
H	$\equiv \sum_k Y_k h_k + u_i u_i' / 2$, stagnation enthalpy of gases, kcal/kg	T	= temperature, K
		T°	= reference temperature, 298.14 K
		T_p	= propellant temperature, K
		T_{pi}	= propellant initial temperature, K
		T_{ps}	= propellant surface temperature, K
		T_{ps}	= reference surface temperature of the propellant, K
		u	= gas velocity in x direction, m/s
		U_∞	= freestream velocity, m/s
		u_*	$\equiv \sqrt{\tau_w / \rho_\infty}$, friction velocity, m/s
		v	= gas velocity in y direction, m/s
		W	$\equiv (\sum_k \nu_k / W_k)^{-1}$, average molecular weight of gases, kg/kmole
		W_k	= molecular weight of the k th species, kg/kmole
		x	= coordinate along the propellant surface, m
		y	= coordinate normal to the propellant surface, m
		Y_k	= mass fraction of the k th species
		Y_{FS}	= mass fraction of fuel in a composite solid propellant
		Y_{OS}	= mass fraction of oxidizer in a composite solid propellant

Presented as Paper 78-978 at the AIAA/SAE 14th Joint Propulsion Conference, Las Vegas, Nev., July 25-27, 1978; submitted Oct. 6, 1978; revision received May 18, 1979. Copyright © American Institute of Aeronautics and Astronautics, Inc., 1978. All rights reserved. Reprints of this article may be ordered from AIAA Special Publications, 1290 Avenue of the Americas, New York, N.Y. 10019. Order by Article No. at top of page. Member price \$2.00 each, nonmember, \$3.00 each. Remittance must accompany order.

Index categories: Solid and Hybrid Rocket Engines; Reactive Flows; Boundary Layers and Convective Heat Transfer—Turbulent.

*Assistant Professor, Dept. of Mechanical Engineering. Member AIAA.

†Associate Professor, Dept. of Mechanical Engineering. Member AIAA.

(\quad)	= time-averaged quantity
$(\quad)'$	= fluctuating quantity
$(\quad)_{,i}$	= partial differentiation of the quantity in (\quad) with respect to x_i , $(\quad)/m$
δ	= boundary-layer thickness, m
ϵ	$\equiv \mu \nu'_{i,j} \mu'_{i,j} / \rho$, turbulent dissipation, m^2/s^3
λ	= thermal conductivity of the gas, kcal/m-s-K
λ_s	= thermal conductivity of the solid propellant, kcal/m-s-K
μ	= gas viscosity, kg/m-s
μ_{eff}	$\equiv \mu + \mu_t$, effective viscosity, kg/m-s
μ_t	= turbulent viscosity defined in Eq. (11), kg/m-s
$(\mu/Pr)_{eff}$	$\equiv (\mu/Pr) + (\mu_t/Pr_t)$, kg/m-s
$(\mu/Sc)_{eff}$	$\equiv (\mu/Sc) + (\mu_t/Sc_t)$, kg/m-s
ν_k	= number of kmoles of the k th species
ρ	= gas density, kg/m^3
ρ_s	= solid propellant density, kg/m^3
τ	$\equiv \mu_{eff} \partial \bar{u} / \partial y$, local shear stress, N/m^2
$\dot{\omega}_k$	= rate of production of species k due to chemical reactions, kg/m^3 -s

Subscripts

k	= species index representing fuel gas [F], oxidizer gas [O], and product gas [P]
∞	= freestream condition
w	= wall (propellant surface) condition

I. Introduction

EROSIIVE burning is a common phenomenon experienced in solid-propellant rocket motors, and generally represents an increase in propellant burning rate due to high-velocity combustion gases flowing parallel to the propellant surface. The ability to predict the burning rate is of prime importance in the design of a rocket motor, because both the thrust level and the burning time depend on the burning rate. Erosive burning is a serious problem in high-performance rockets and missiles with high-thrust, short-burning, solid-propellant motors. Nozzleless rocket motors recently have attracted considerable interest because they offer significant economic advantage over more conventional motors. Nozzleless rocket motors have low port-to-throat area ratios in which the gas velocity reaches sonic and supersonic speeds over the propellant surfaces, leading to the extremely serious problem of erosive burning.

In the past, the problem of erosive burning has been investigated by various methods, as reported in literature reviews by Kuo and Razdan,¹ and King.² Existing theories on erosive burning, in general, can be divided into three distinct classes, depending upon whether the theory is based on 1) a phenomenological heat-transfer theory that does not take into account chemical reactions and/or flame structure, 2) a flame theory based on a description of combustion mechanisms and/or flame structure, or 3) an aerothermochemical analysis that includes the consideration of heat, mass, and momentum transfer in a chemically reacting boundary layer.

Among phenomenological heat-transfer theories, the Lenoir-Robillard theory³ is referred to most often. The essence of this theory is that erosive burning rate is proportional to the forced convective heat-transfer coefficient. Representative work on erosive burning based on flame theory has been reported by Vandekerckhove,⁴ who considered the flame structure and the mechanism of solid phase decomposition in a double-based solid propellant. King⁵ has developed a model for the erosive burning of composite propellant, based on the assumption that the crossflow of gases bends the diffusion flame, thus bringing the heat release zone closer to the propellant surface.

The erosive burning theory based on the boundary-layer approach was first reported in the early work of Corner,⁶

who used the Prandtl-Karman boundary-layer theory to describe the flowfield. Tsuji,⁷ Razdan,⁸ and Schuyler and Torda⁹ analyzed the problem by considering a laminar boundary layer over the propellant surface. However, it must be noted that the flow in an erosive burning situation is normally turbulent. Lengelle¹⁰ used the integral solutions of turbulent boundary-layer equations in combination with a diffusion flame theory to develop his model. Beddini¹¹ has used a multiequation turbulence closure model to solve the boundary-layer problem. He considered the combustion of homogeneous propellants.

Although there are differing emphases in various approaches to solving the problem of erosive burning, the most realistic analysis must consider the interaction between flame zone structure and the flowfield. In this paper, such an interaction is considered through an aerothermochemical analysis of the problem, which includes the consideration of heat, mass, and momentum transfer in a chemically reacting turbulent boundary layer. The development of the current model is based on the combustion of the most commonly used ammonium perchlorate (AP) composite propellants and is, therefore, limited to these types of heterogeneous propellants.

Most of the successful strand-burning models^{12,13} of composite solid propellants consider the dominant effect of oxidizer-fuel (O/F) diffusion flame on the burning rate of the propellant. At normal rocket pressures (in the order of 100 atm), the pressure dependence of the burning rate of a composite propellant, as pointed out by Steinz et al.,¹² is brought about through the diffusion flame. Steinz et al. also note that the scale of unmixedness, as it affects the diffusion flame, is an important aspect of the burning process. In the presence of a flowfield, it is this diffusion flame that interacts with the turbulent crossflow of gases and, therefore, affects the heat flux to the propellant surface and the burning rate. Figure 1 clearly illustrates this point. The plot is based on the experimental data of Refs. 5 and 14. The erosive-burning data for various freestream velocities was taken from King's work.⁵ With known blowing rates and freestream velocities, the corresponding friction coefficient was obtained from Simpson and MacQuaid's data reported in Ref. 14. The data on friction coefficient are also available from earlier work by Micklely and Davis.¹⁵ However, the crossflow velocities in their work were quite low (about 18 m/s) and their data are correlated with (v_x/U_∞) , rather than the conventional mass blowing parameter $(\rho v_x)/(\rho U_\infty)$. Figure 1 shows that the domain of turbulence is very close to the propellant surface and that it interacts with the diffusional reaction zone, which is about 20-100 μm from the propellant surface. Makunda's¹⁶ calculations also show that the flame zone is in the turbulence region of the flowfield. With increasing crossflow velocities, the domain of turbulence comes closer to the propellant surface (see Fig. 1). It is clear that the diffusion flame is in a region where the turbulence cannot be ignored.

The objectives of the present study are: 1) to formulate a theoretical model, based on an aerothermochemical analysis of the erosive burning problem of composite solid propellants, which considers the heat, mass, and momentum transfer in a chemically reacting turbulent boundary layer; 2) to solve the theoretical model and to study the effects of gas velocity, pressure, and propellant physicochemical characteristics on the erosive burning rate of a composite solid propellant; and 3) to test the validity of the theoretical model by comparing the predicted erosive burning rates with experimental data.

II. Analysis

A. Description of the Physical Model

The physical model considered in the theoretical analysis consists of a flat plate with a fixed leading edge as shown in Fig. 2. A two-dimensional propellant slab glued to the

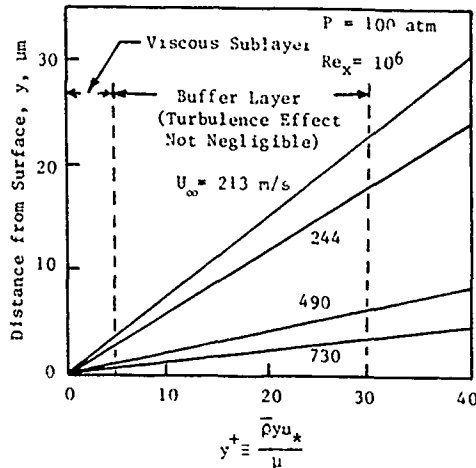


Fig. 1 Effect of freestream velocity on the domain of turbulence near a propellant surface.

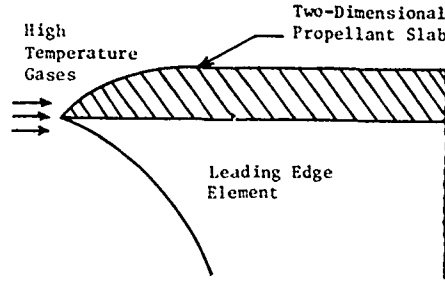


Fig. 2 Physical model considered in the theoretical formulation.

leading-edge element is ignited by the hot combustion gas in the freestream, which forms a turbulent boundary layer over the burning surface of the propellant. The boundary layer is considered to be quasisteady, two-dimensional, and chemically reacting.

B. Conservation Equations

To formulate the theoretical model, one begins with the general conservation equations for a reacting compressible fluid flow. In these equations, each instantaneous variable is replaced by its mean and fluctuating part (this is the well-known Reynolds' decomposition procedure), and all equations are time averaged.¹⁷ The following assumptions are then introduced into these equations: 1) the averaged flow properties are steady; 2) the mean flow is two dimensional; 3) for a flow of Mach number of order one,

$$\overline{\mu'(\partial u' / \partial y)} \ll \overline{\mu(\partial \bar{u} / \partial y)} \text{ and } \overline{\rho' u' v'} \ll \overline{\rho u' v'}$$

(according to Laufer¹⁸ the density fluctuations have a kinematic rather than a dynamic effect on the turbulence); 4) there is no reaction-generated turbulence¹⁹; 5) the Lewis number is unity; and 6) Fick's law of binary diffusion is valid.

Following the regular procedure for order-of-magnitude analysis, dominant terms in the time-averaged equations are retained to give the final form of the two-dimensional, steady-state, boundary-layer equations for a reactive turbulent compressible flow (see Ref. 17 for details). These equations for the conservation of mass, momentum, species and enthalpy, and the equation of state are:

$$\frac{\partial}{\partial x} (\bar{\rho} \bar{u}) + \frac{\partial}{\partial y} (\bar{\rho} \bar{v}) = 0 \tag{1}$$

where $\bar{\rho} \bar{v} = \bar{\rho} \bar{v} + \overline{\rho' v'}$.

$$\bar{\rho} \bar{u} \frac{\partial \bar{u}}{\partial x} + \bar{\rho} \bar{v} \frac{\partial \bar{u}}{\partial y} = \frac{\partial}{\partial y} \left[\mu_{\text{eff}} \frac{\partial \bar{u}}{\partial y} - \bar{v} \frac{\mu_t}{C_p \bar{\rho}} \frac{\partial \bar{p}}{\partial x} \right] \tag{2}$$

$$\bar{\rho} \bar{u} \frac{\partial \bar{Y}_k}{\partial x} + \bar{\rho} \bar{v} \frac{\partial \bar{Y}_k}{\partial y} = \frac{\partial}{\partial y} \left[\left(\frac{\mu}{Sc} \right)_{\text{eff}} \frac{\partial \bar{Y}_k}{\partial y} \right] + \bar{\omega}_k \tag{3}$$

$$\bar{\rho} \bar{u} \frac{\partial \bar{H}}{\partial x} + \bar{\rho} \bar{v} \frac{\partial \bar{H}}{\partial y} = \frac{\partial}{\partial y} \left\{ \left(\frac{\mu}{Pr} \right)_{\text{eff}} \frac{\partial \bar{H}}{\partial y} + \left[\mu_{\text{eff}} - \left(\frac{\mu}{Pr} \right)_{\text{eff}} \right] \frac{\partial \bar{u}^2 / 2}{\partial y} \right\} \tag{4}$$

$$\bar{p} = \bar{\rho} R_u \bar{T} / W \tag{5}$$

In arriving at Eqs. (2-4), we have used the following models for various correlations:

1) Reynolds stress $u'v'$ is related to eddy viscosity by the following equation²⁰:

$$-\overline{\rho u' v'} = \mu_t \frac{\partial \bar{u}}{\partial y} \tag{6}$$

2) Velocity density correlation has been modeled using Boussinesq approximation²⁰ as:

$$\overline{\rho' u'} = \frac{\mu_t}{C_p \bar{\rho}} \frac{\partial \bar{p}}{\partial x} \tag{7}$$

Mass transfer by turbulent diffusion $(\rho v)' Y'_k$, and heat transfer by turbulent diffusion $(\rho v)' h'_k$, are modeled by using Reynolds' analogy:

$$-\overline{(\rho v)' Y'_k} = \frac{\mu_t}{Sc_t} \frac{\partial \bar{Y}_k}{\partial y}, \quad -\overline{(\rho v)' h'_k} = \frac{\mu_t}{Pr_t} \frac{\partial \bar{h}_k}{\partial y} \tag{8}$$

A two-equation turbulence model,²⁰ in which the turbulence is assumed to be characterized by its kinetic energy K and its dissipation rate ϵ , has been employed for the closure of the present problem. In addition to the governing equations, Eqs. (1-5), two additional equations for K and ϵ are required. The K equation¹⁷ for a steady, two-dimensional, boundary-layer flow is:

$$\bar{\rho} \bar{u} \frac{\partial K}{\partial x} + \bar{\rho} \bar{v} \frac{\partial K}{\partial y} = \frac{\partial}{\partial y} \left[\left(\mu + \frac{\mu_t}{C_1} \right) \frac{\partial K}{\partial y} \right] + \mu_t \left[\left(\frac{\partial \bar{u}}{\partial y} \right)^2 - \frac{\bar{v}}{C_p \bar{\rho}} \frac{\partial \bar{p}}{\partial x} \frac{\partial \bar{u}}{\partial y} \right] - \bar{\rho} \epsilon \tag{9}$$

The exact form of the ϵ equation for a reacting flow is very difficult to model, because of the appearance of correlations involving fluctuating velocity gradients and density fluctuations. We use the form of ϵ equation as applicable to uniform property flow.²⁰ However, we modify it by retaining the full expression for production of K , which comprises the second term in square brackets on the right-hand side of Eq. (9). This practice has been followed with good success in reacting flows.²¹⁻²⁴ The ϵ equation¹⁷ for a steady, two-dimensional, boundary-layer flow is:

$$\bar{\rho} \bar{u} \frac{\partial \epsilon}{\partial x} + \bar{\rho} \bar{v} \frac{\partial \epsilon}{\partial y} = \frac{\partial}{\partial y} \left[\left(\mu + \frac{\mu_t}{C_2} \right) \frac{\partial \epsilon}{\partial y} \right] + C_3 \mu_t \left[\left(\frac{\partial \bar{u}}{\partial y} \right)^2 - \frac{\bar{v}}{C_p \bar{\rho}} \frac{\partial \bar{p}}{\partial x} \frac{\partial \bar{u}}{\partial y} \right] \frac{\epsilon}{K} - C_4 \bar{\rho} \frac{\epsilon^2}{K} \tag{10}$$

The turbulent viscosity μ_t is related to K and ϵ :

$$\mu_t = C_\mu \frac{\bar{\rho} K^2}{\epsilon} \quad (11)$$

where C_μ is a constant. The model of Eq. (11) has been used widely with considerable success.²⁰⁻²⁴

C. Modeling of Gas-Phase Chemical Reactions

The set of equations (1-5) and (9) and (10), with appropriate boundary conditions, can be solved, provided $\bar{\omega}_k$ in Eq. (3) is known. When a composite solid propellant burns, solid fuel and oxidizer particles transform into gases. The gases may react in several steps. However, in the present work, the following global single-step-forward chemical reaction is assumed:



where O and F represent the oxidizer and the fuel gases, respectively, and P represents the product gases.

The possible expression for the instantaneous global reaction rate is:

$$\omega_k = -W_k k_s \Pi_k (\rho Y_k / W_k) \nu_k \quad (13)$$

($k = O, F$, and specific reaction rate constant k_s is given by the Arrhenius law $k_s = A_s \exp[-E_{a_s}/R_u T]$). The time averaging of Eq. (13) represents one of the central difficulties of combustion modeling. One can replace the exponential term by its series expansion, thereby introducing correlations such as $\bar{Y}_O \bar{Y}_F$, $\bar{Y}_F \bar{T}'$, $\bar{Y}_O \bar{T}'$, \bar{T}'^2 , etc. Additional conservation equations must be solved for these correlations; this procedure, however, reduces the economy significantly and introduces more empiricism into the model.

One other approach, first proposed by Spalding,²⁵ is the eddy-breakup (EBU) model. In this model it is proposed that the gases in a turbulent flame, at high Reynolds numbers, should be considered as lumps or eddies of unburned and fully burned gas. Spalding assumed that the rate of burning depended upon the rate at which fragments of unburned gas (eddies) were broken into still smaller fragments by the action of turbulence, and that this rate was considered to be proportional to the rate of decay of turbulence energy. Spalding's initial version of the EBU model was based on the mixing-length hypothesis,²⁵ and Mason and Spalding²⁴ introduced the EBU model based on the two-equation model of turbulence to solve the problem of confined turbulent flames. The use of the EBU model for diffusion flames has been discussed by Lockwood²⁶; Magnussen and Hjertager²⁷ have used the EBU model for predicting soot formation in a diffusion flame. The EBU concept can be used to model the gas-phase reaction rate for the erosive-burning problem, in which the fuel and oxidizer gases are unmixed as they emerge from the propellant surface. The presence of the high-lateral shear in the boundary layer forms the turbulent eddies. It is reasonable to assume that these eddies engulf fuel and oxidizer gases, giving rise to oxidizer and fuel eddies. Further justification for assuming the existence of fuel eddies comes from the GDF theory,¹² according to which the gaseous fuel emerges as pockets (eddies) from the burning composite propellant surface.

We might then follow the EBU concept and also the arguments of Lockwood²⁶: in a diffusion controlled reaction, the rate of consumption of fuel is proportional to the rate of dissipation of the fuel-containing eddies, as characterized by the rate of diminution of the energy of the fluctuations, $g_F = \bar{Y}'_F^2$. This rate can be equated to the rate of supply of energy from the large-scale motion, which can be taken as proportional to the quantity of energy involved and to

reciprocal of the eddy time scale characterized by ϵ/K .

$$\bar{\omega}_F \propto -\bar{\rho} \sqrt{g_F} (\epsilon/K) \quad (14)$$

Equation (14) can be used, provided g_F is known. The conservation equation for g_F can be solved; however, we have simplified the analysis by assuming the production and dissipation terms of the g_F equation to be dominant. This assumption is particularly good in the near-wall region, which in the current problem is the important region in which most of the chemical reactions take place. Therefore, when equating the production and dissipation terms of the g_F equation (see Ref. 20), we arrive at

$$g_F \propto \frac{\mu_t}{\bar{\rho}} \frac{K}{\epsilon} \left(\frac{\partial \bar{Y}_F}{\partial y} \right)^2 \quad (15)$$

From Eqs. (11), (14), and (15), we finally get

$$\bar{\omega}_F = -C_\omega \bar{\rho} \sqrt{K} \left| \frac{\partial \bar{Y}_F}{\partial y} \right| \quad (16)$$

where C_ω is a constant. Equation (16) is used along with Eq. (3) to solve species distribution in the gas phase. It should be recognized that the reaction rate represented by Eq. (16) has some limitations. First, it is assumed that the rate of chemical kinetics is very fast, i.e., the reaction is diffusion limited. This assumption is particularly valid for gaseous reactions taking place under high pressures, such as those which exist in actual rocket situations. Second, the use of Eq. (16) is limited to turbulent boundary-layer flows. The primary reason for limiting the current study of erosive burning to turbulent boundary-layer flows is that the flowfield developed over most of the solid propellant grain in a practical rocket motor is turbulent.^{16,28} It is believed that the limitations of the current analyses to actual rocket motor situations are far less severe than those analyses which have been limited to laminar boundary-layer flows.^{7,9} Further, the application of Eq. (16) to a turbulent boundary-layer flow is more appropriate than the Arrhenius reaction rate law [Eq. (13)], which uses the average temperature and neglects various turbulence correlations. When various turbulence correlations in the Arrhenius reaction rate law are neglected, significant errors may appear in the calculations of reaction rates, as noted by Lockwood.²⁶

It may be noted that the species conservation equations are solved for \bar{Y}_F and $\bar{Y}_{OF} \equiv [\bar{Y}_O - (\nu_O W_O / \nu_F W_F) \bar{Y}_F]$. The choice of the latter variable, with the assumption of Eq. (12), eliminates the nonlinear source term in the equation for this variable. No separate conservation equation is needed for \bar{Y}_P , which is defined as $(1 - \bar{Y}_O - \bar{Y}_F)$.

D. Heat Conduction Equation in the Solid Phase

It is assumed that the heat conduction into the solid propellant is dominant in a direction normal to the burning surface. In a coordinate system attached to the burning surface, the temperature distribution in the solid propellant, at a given x location along the surface, is governed by:

$$\lambda_s \frac{\partial^2 T_p}{\partial y^2} = \rho_s C_p r_b \frac{\partial T_p}{\partial y} \quad -\infty < y \leq 0 \quad (17)$$

E. Burning Rate Equation

Burning rate of a solid propellant is a function of the surface temperature, and can be expressed by the Arrhenius law of surface pyrolysis:

$$r_b = A_s \exp\left(-\frac{E_{a_s}}{R_u T_{ps}}\right) \quad (18)$$

It is the surface temperature T_{ps} which provides the link between the burning rate and the gas dynamics. The surface temperature depends on the heat flux from gas to solid phase, and the heat flux is evaluated by solving the gas-phase conservation equations.

F. Boundary Conditions

To complete the formulation of the theoretical model, boundary conditions must be specified at the solid-gas interface as well as at the freestream. The interface mass and energy balance are obtained by considering the flux balance at the solid-gas interface. The mass balance equations can be written as:

$$(\bar{\rho} \bar{v} \bar{Y}_O)_w - \rho_s r_b Y_{OS} - \left(\bar{\rho} D \frac{\partial \bar{Y}_O}{\partial y} \right)_w = 0 \quad (19)$$

$$(\bar{\rho} \bar{v} \bar{Y}_F)_w - \rho_s r_b Y_{FS} - \left(\bar{\rho} D \frac{\partial \bar{Y}_F}{\partial y} \right)_w = 0 \quad (20)$$

First and second terms of the preceding equations represent, respectively, the component k ($= O$ or F) transported away from the interface by the normal velocity in the gas phase and in the vaporizing solid phase. The third term represents the component k transported from the gas to the solid by diffusion. The energy balance equation is written as:

$$\lambda_s \left. \frac{\partial T_p}{\partial y} \right|_w = \lambda \left. \frac{\partial \bar{T}}{\partial y} \right|_w + \rho_s r_b (h_{w-} - h_{w+}) \quad (21)$$

In Eq. (21), the term on the left-hand side represents the net heat flux to the solid propellant; on the right-hand side, the first term represents the heat flux from the gas to solid surface, and the second term represents the net heat release at the surface. Subscripts ($-$) and ($+$) represent, respectively, the solid and gas side of the solid-gas interface.

Following Levine and Culick,²⁹ the net heat release at the surface, per unit mass (equal to the difference between the enthalpies of the gas and solid on their respective sides of the interface), can be expressed as

$$\bar{Q}_s(T_{ps}) = h_{w+} - h_{w-} = \bar{Q}_s + (C_p - C_s)(T_{ps} - \bar{T}_{ps}) \quad (22)$$

where \bar{Q}_s is the net surface heat release (negative for exothermic reactions) at a reference surface temperature \bar{T}_{ps} .

By integrating Eq. (17) from $y = -\infty$, where $T_p = T_{ps}$, and $\bar{y} = 0$, where $T_p = T_{ps}$, and using the result along with Eq. (22) in Eq. (21), we find

$$\lambda \left. \frac{\partial \bar{T}}{\partial y} \right|_w = \rho_s r_b [C_p T_{ps} - C_s T_{ps} + \bar{Q}_s + (C_s - C_p) \bar{T}_{ps}] \quad (23)$$

Boundary conditions for K and ϵ are applied near the wall rather than at the wall. Near a wall, production and dissipation terms in the K equation are equated (a reasonable approximation in this region); therefore,

$$\epsilon = \frac{\mu_t}{\bar{\rho}} \left(\frac{\partial \bar{u}}{\partial y} \right)^2 \quad (24)$$

Turbulent viscosity μ_t close to the wall is calculated from van Driest's formula.³⁰

$$\mu_t = \bar{\rho} (kDy)^2 \frac{\partial \bar{u}}{\partial y} \quad (25)$$

The damping coefficient D is given by

$$D = 1 - \exp\left(-\frac{y\sqrt{\bar{\rho}\tau}}{A^+ \mu}\right) + \exp\left(-\frac{60y}{A^+ R_h}\right) \quad (26)$$

where τ is the local stress, A^+ is a constant, and R_h is the average roughness height. Equation (25) is particularly useful to include the effects of surface roughness on erosive burning. From Eqs. (11), (24), and (25), we find expressions for K and ϵ , as

$$K = \frac{(kDy)^2}{\sqrt{C_\mu}} \left(\frac{\partial \bar{u}}{\partial y} \right)^2 \quad (27)$$

$$\epsilon = (kDy)^2 \left| \frac{\partial \bar{u}}{\partial y} \right|^3 \quad (28)$$

The primary reason for choosing this procedure for the boundary condition of K and ϵ is that the models of various turbulence correlations in the development of K and ϵ equations are inappropriate near a wall. This fact is widely recognized by researchers in the area of the field of turbulence,^{20,31} and there is no unique method to avoid this difficulty. Jones and Launder³² have proposed some modifications in the K and ϵ equations. However, the solutions of modified K and ϵ equations have not been tested widely with experimental data; consequently, the universality of the additional empirical constants introduced in modified K and ϵ equations has not been tested. The near-wall treatment of the K and ϵ equation presented in the current analysis is somewhat similar to that of Chambers and Wilcox.³¹ It may be noted that the boundary conditions, Eqs. (27) and (28), give the values of K and ϵ consistent with their distributions in the near-wall region; this becomes apparent when one uses the log law of the wall for velocity in these equations (see Refs. 20 and 31). It may also be noted that Omori,³¹ in his calculations of the boundary layer in a rocket motor, has also considered two separate regions of the boundary layer, viz., the viscous sublayer region close to the wall and the wake region. Omori used a K - ϵ model²⁰ in solving his problem, and in the near-wall region, he used the modified van Driest correlation to specify the eddy viscosity distribution.

Other boundary conditions which are considered in the model are:

At the wall:

$$\bar{u} = 0, \quad \bar{v} = \rho_s r_b / \rho_w, \quad \bar{T} = \bar{T}_{ps} \quad (29)$$

At the freestream:

$$\bar{u} = U_\infty, \quad \bar{T} = T_\infty, \quad \bar{Y}_F = \bar{Y}_O = 0, \quad \frac{\partial K}{\partial y} = \frac{\partial \epsilon}{\partial y} = 0 \quad (30)$$

Governing Eqs. (1-5), (9), and (10), with boundary conditions, Eqs. (18-20), (23), and (27-30) complete the theoretical formulation. The system of partial differential equations is parabolic in nature and is solved numerically.

III. Numerical Procedure and Results

A. Numerical Procedure

A number of numerical techniques exist in literature to solve parabolic partial-differential equations. Several researchers²¹⁻²⁴ have used the numerical technique proposed by Patankar and Spalding²⁴; the same numerical procedure is followed in this study (see Ref. 17 for details).

About half of the 100 cross-stream intervals employed were distributed within 10% of the boundary-layer thickness, where the dependable variables change rapidly. The forward step size along the x direction is variable and was set at 0.3 times the boundary-layer thickness. Iterations of the boundary-layer solutions were found necessary to obtain a good convergence on the surface temperature. The maximum allowable percentage error in the convergence of the surface temperature was set equal to 0.01.

Table 1 Properties used in theoretical calculations

Property (dimensions)	Propellant type	
	AP, 75% PBAA/EPON, 25%	AP, 65% Polysulfide, 35%
a (psia/in./s)	230	0
A_s (m/s)	26174 @ $p = 100$ atm	25289 @ $p = 100$ atm
A^+ —	26 (Ref. 30)	26
b (psia ^{1/3} /in./s)	34.5	41.85
c_s (kcal/kg-K)	0.38	0.38
C_p (kcal/kg-K)	0.3	0.3
E_{as} (kcal/mole)	30	30
$\Delta h_{f,F}^0$ (kcal/kg)	55.93	-0.42
$\Delta h_{f,O}^0$ (kcal/kg)	-942.0	-936.6
$\Delta h_{f,P}^0$ (kcal/kg)	-1137.3	-1310.5
k —	0.41	0.41
P_r —	(Svehla's eq.) ³⁵ $\gamma/(1.77\gamma - 0.45)$	same eq.
P_{r1} —	0.9 (Ref. 36)	0.9
\dot{Q}_s (kcal/kg)	-166 (Ref. 12)	-240 (Ref. 35)
Sc —	0.7078	0.7078
Sc_i —	0.9	0.9
Tb_i (K)	298	298
\dot{T}_{ps} (K)	800	800
W_F (kg/kmole)	30	30
W_O (kg/kmole)	2 : 893	27.949
W_P (kg/mole)	20.381	25.69
Y_{FS} —	0.25	0.35
Y_{OS} —	0.75	0.65
γ —	1.26	1.26
λ (kcal/m-s-K)	$C_p \mu / Pr$	same eq.
μ_A (kg/m-s)	$8.7 \times 10^{-8} \sqrt{W_A} T^{0.65}$ (Ref. 35)	same eq.
ν_F (kmole)	1	1
ν_O (kmole)	3.2266	1.9935
ν_P (kmole)	5.888	3.3366
ρ_s (kg/m ³)	1600	1660

Table 2 Constants used in turbulence modeling

Constants	C_1	C_2	C_3	C_4	C_w	C_μ	C_p
Values	1.0	1.3	1.57	2.0	0.18	0.09	1.0
Reference source	20-22	20-22	21	22	24	20-22	21

B. Results and Discussion

Solutions were obtained for two types of composite propellant compositions: 1) ammonium perchlorate (75%) and PBAA/EPON (25%), and 2) ammonium perchlorate (65%) and polysulfide (35%). The various physical properties used in the calculations are given in Table 1, and the values of the constants used in the turbulence modeling are given in Table 2.

It is worthwhile to draw attention to the procedures followed in obtaining some of the properties used in Table 1, especially in the case of those parameters associated with the global single-step-forward reaction. The products generated from the AP primary flame (A/PA flame) due to the chemical reaction between NH_3 and HClO_4 are considered to form the equivalent oxidizer gas represented by the symbol [O] in the global reaction. The primary flame is assumed to be collapsed on the propellant surface. The calculations of Steinz et al.¹² demonstrate that in the burning of a composite propellant at

normal rocket pressures, the A/P flame is so thin ($\sim 1 \mu\text{m}$) compared to the oxidizer particle size and the O/F flame thickness that it may be considered to occur at the regressing propellant surface, merely depositing its heat there as gasification takes place. The GDF model¹² considers the effect of A/PA flame on the burning rate of a composite solid propellant when pressure is less than 10 atm. However, under normal rocket-motor pressure ranges (a typical rocket-motor pressure is around 100 atm), the dependence of the burning rate on pressure comes from the O/F diffusion flame of the AP composite propellant. Because the current erosive-burning model is not designed for unrealistically low pressures, the assumption of collapsed A/PA flame is therefore a reasonable one. The exothermic heat of formation of the equivalent oxidizer gas is obtained from the thermochemistry calculation using the CEC72 program.³⁷ The inputs necessary for this calculation are the heat of formation of the solid AP and the gas pressure. This calculation also gives the average value of the molecular weight of the equivalent oxidizer gas.

It is assumed that the equivalent gaseous fuel, represented by the symbol [F], is formed by the ablation of the solid fuel-binder due to random scission/systematic unzipping of the polymer chain, as discussed in Ref. 12. The heat of formation of the equivalent fuel gas was calculated from the difference between the heat of formation of the solid fuel binder and the heat of decomposition. The heat of formation of the equivalent product gases, represented by symbol [P], is obtained from the overall thermochemistry calculation of AP and fuel-binder combustion. The average molecular weight of the product gases is also determined from this calculation. The stoichiometric coefficient ν_O , ν_F , and ν_P are determined from the mass balance of the global reaction for a given propellant of known initial oxidizer-to-fuel ratio.

The procedure used to calculate the pre-exponential factor in the Arrhenius law of surface pyrolysis A_s is as follows: For a particular propellant, the strand burning-rate law is assumed to be known. Using this law, the value of r_{b0} at a pressure of 30 psi can be determined. At this pressure, the measured surface temperature is known^{12,38}; therefore, with known r_{b0} , T_{ps} , and E_{as} , Eq. (18) is used to evaluate A_s .

Figure 3 shows the calculated distributions of turbulent kinetic energy, Reynolds stress, and velocity in the chemically reacting turbulent boundary layer considered over the propellant surface. The peak turbulent kinetic energy is located farther from the wall than that in a conventional flat-plate turbulent boundary, due to the strong surface blowing rates caused by the burning of the solid propellant. Calculated

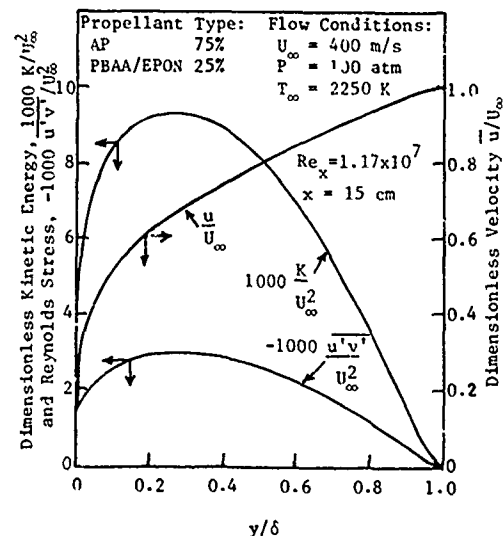


Fig. 3 Calculated distributions of turbulent kinetic energy, Reynolds stress and velocity.

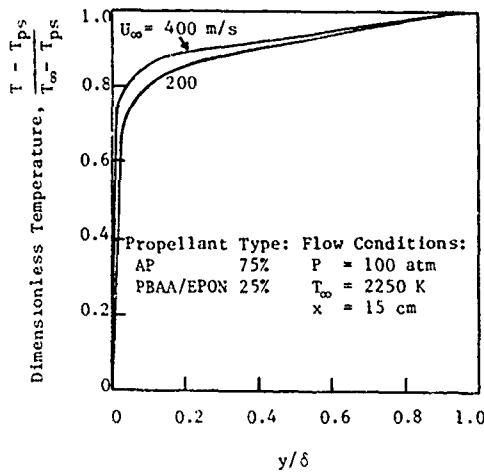


Fig. 4 Calculated temperature distributions for different freestream velocities.

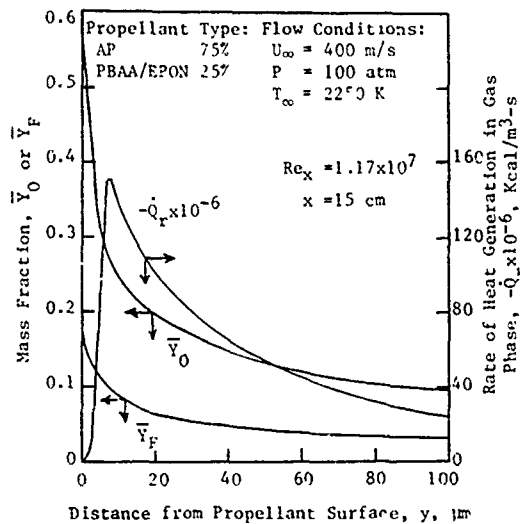


Fig. 5 Calculated distribution of oxidizer and fuel mass fractions, and the rate of heat generation in the gas phase close to the propellant surface.

temperature distributions for different freestream velocities are shown in Fig. 4. The temperature rises rapidly from its value at the propellant surface and gradually approaches the freestream gas temperature at the edge of the boundary layer. The rapid rise from the surface is caused by the chemical reactions occurring in the gas-phase region close to the propellant surface as illustrated in Fig. 5, which shows the calculated distribution of the rate of heat generation in the gas phase. Figure 5 also shows the distributions of the oxidizer and fuel mass fractions which drop to very small values in a region close to the propellant surface, due to the higher rate of reaction of this region.

The temperature gradient becomes steeper (higher gas-to-solid heat flux) at the surface as the freestream velocity increases (see Fig. 4). This is expected because the higher the level of turbulent intensity, the higher the chemical reactions in the gas phase. This effect can be seen from the results plotted in Figs. 6 and 7. The results of Fig. 6 show that the increase in freestream velocity brings the location of the peak turbulent intensity closer to the propellant surface. This has a significant effect on the flowfield near the propellant surface. The closeness of the peak turbulence intensity to propellant surface means that the turbulent eddies with high frequencies also come closer to the propellant surface. This causes an

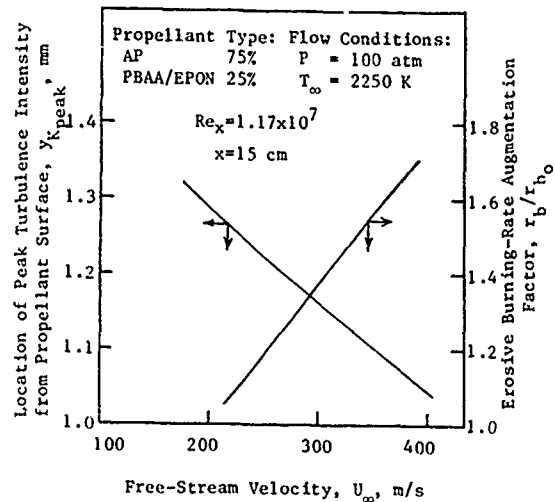


Fig. 6 Effect of freestream velocity on the location of the peak turbulent intensity from propellant surface and the subsequent effect on erosive burning rate.

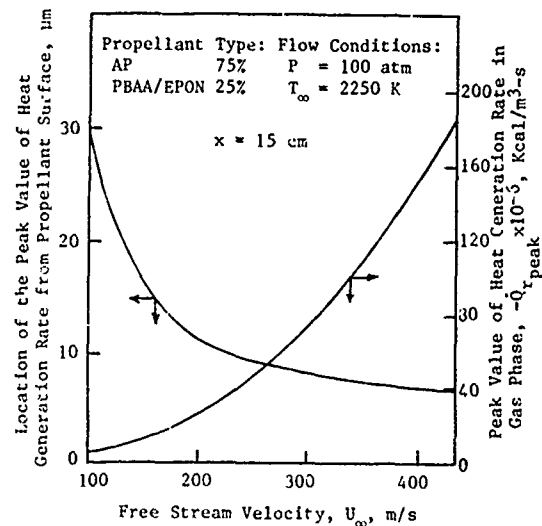


Fig. 7 Effect of freestream velocity on the peak value of heat generation rate in gas phase and its location from propellant surface.

increase in the mixing rate of oxidizer and fuel species, therefore increasing the gas-phase reaction rate and bringing it closer to the propellant surface. The results plotted in Fig. 7 show that the peak value of the heat generation rate in the gas phase, due to chemical reactions, increases with increasing velocity, and the location of this peak comes closer to the propellant surface. Therefore, the increased heat flux eventually increases the erosive burning augmentation factor (r_b/r_{b0}), as shown in Fig. 6.

It may be noted that for any U_∞ , the location of the peak value of K (Fig. 6) is farther away from the propellant surface than the location of the maximum value of Q_r (Fig. 7). This, however, does not mean that the turbulence has negligible influence in the gaseous reactions in a region where the reaction rate is maximum (corresponding to maximum Q_r). For example, present calculations (for $U_\infty = 400$ m/s) show that μ_t in this region is more than 10 times the value of μ . Therefore, there is a strong effect of turbulence in this region, even though the peak value of K is away from this region. It is clear from Eq. (16) that the reaction rate is influenced not only by the level of K , but also by the gradient \dot{Y}_F which is steeper near the propellant surface. Thus the maximum

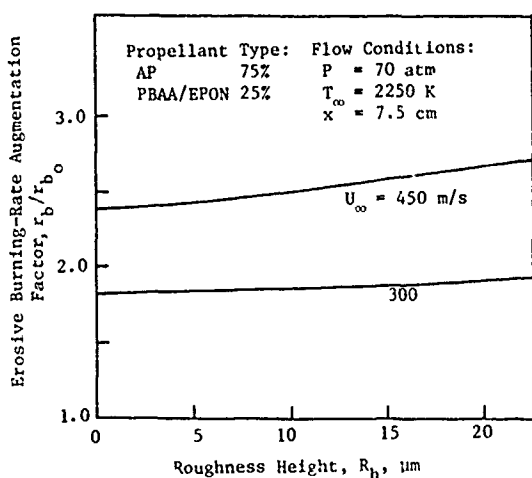


Fig. 8 Comput. erosive burning rate augmentation factor showing the effect of propellant-surface roughness height at different freestream velocities.

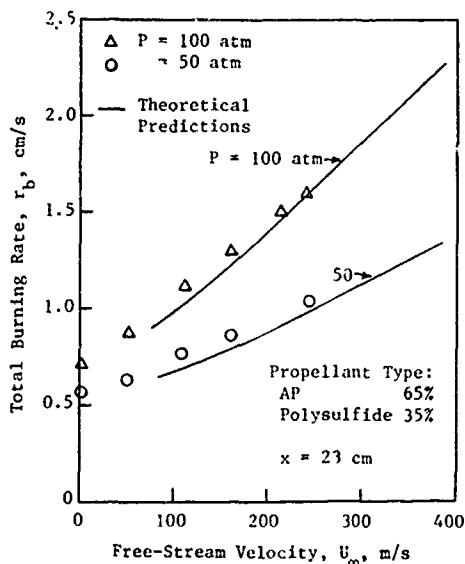


Fig. 9 Comparison of the predicted erosive burning rates with the experimental data of Marklund and Lake.³⁹

reaction rate region is much closer to the propellant surface than the location of peak turbulence intensity.

The turbulent nature of the flowfield over the propellant surface contributes in two important ways to the erosive burning situation. First, it enhances the diffusional mixing of the fuel and oxidizer gases, bringing the gas-phase reaction zone and the heat-release zone closer to the propellant surface as the freestream velocity increases. Second, the rate of heat transfer to the propellant surface is increased because the turbulence increases transport coefficients of the gas phase. The overall effect of turbulence, therefore, is to enhance heat feedback which, in turn, increases the burning rate of a propellant as shown in Fig. 6.

Figure 8 demonstrates the effect of surface roughness on the augmentation factor for different freestream velocities. As the roughness height increases, the augmentation factor also increases. This is to be expected since roughness aids the fuel and oxidizer mixing process, because of increased turbulent activity closer to the propellant surface. However, the effect of roughness diminishes for lower freestream velocities. This is because the viscous sublayer thickness increases at low velocities, submerging the roughness elements in the sublayer

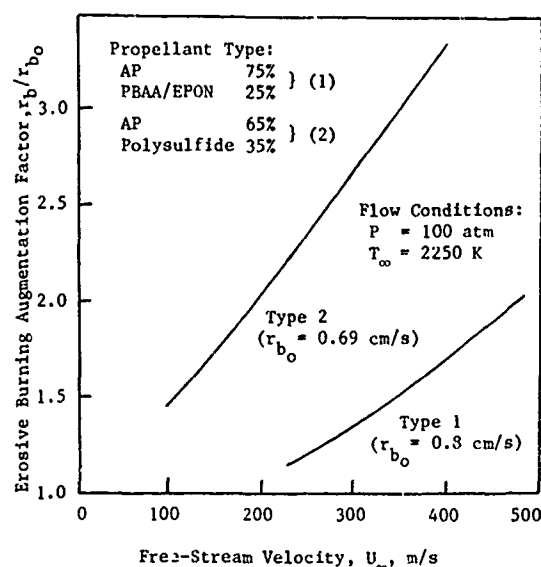


Fig. 10 Effect of normal burning rate on the erosive burning rate augmentation factor.

and, therefore, lessening their effect on the erosive burning process.

Figure 9 shows the predicted erosive burning rates for AP/polysulfide propellant, and the results are compared with the experimental data of Marklund and Lake.³⁹ The results were computed at the same Reynolds number as in the experiments described in Ref. 39. The effect of freestream velocity on total burning rate is compared at two pressures of 100 and 50 atm. Total burning rate increases with an increase in either pressure or velocity. The figure indicates that the agreement between the theoretical and experimental results is very close. It may be pointed out that the present computations are not carried out for very low freestream velocities (< 80 m/s), because then the ratio $\rho_s r_b / \rho_\infty U_\infty$ is no longer small and the boundary-layer approximation used in the current model will be violated.

Figure 10 shows the effect of normal burning rate on the erosive burning rate augmentation factor. The AP/polysulfide propellant (type 2), with a lower value of normal burning rate, is found to be more sensitive to erosive burning than that of the propellant (type 1) which has a higher value of normal burning rate. This observation is consistent with the experimental observation of Marklund and Lake.³⁹

IV. Summary and Conclusions

1) The erosive burning problem of composite solid propellants has been modeled by considering a two-dimensional, chemically reacting, turbulent boundary layer over a propellant surface. The theoretical model has been solved numerically, and the predicted erosive burning rates showed a close agreement with the experimental data of Marklund and Lake.³⁹

2) The predicted results also show that propellants with lower normal burning rates are more sensitive to erosive burning than those with higher normal burning rates; and, the surface roughness of a propellant augments the erosive burning rate of a composite solid propellant.

3) The basic mechanism for the erosive burning effect is believed to be the increased heat feedback to propellant surface introduced by the increase in transport coefficients, and the turbulence-enhanced mixing and reaction of the oxidizer and fuel gases. In addition, the increase in freestream gas velocity brings the location of the peak turbulence intensity and the reaction zone closer to the propellant surface. Thus, more heat is released near the surface, thereby in-

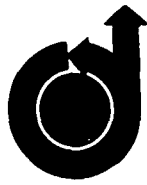
creasing the heat feedback to the propellant surface and the burning rate of a solid propellant.

Acknowledgment

A part of this work was performed under the sponsorship of the Air Force Office of Scientific Research, (AFOSR), Bolling Air Force Base, Washington, D.C., under Contract No. AFOSR-76-2914. Currently, the work is being done under a subcontract from the Atlantic Research Corporation, which is the prime contractor for AFOSR under the management of R. F. Sperlein, Contract No. F49620-78-C-0016.

References

- ¹Kuo, K. K. and Razdan, M. K., "Review of Erosive Burning of Solid Propellants," *12th JANNAF Combustion Meeting*, CPIA Publication 273, Vol. II, 1975, pp. 323-338.
- ²King, M. K., "Review of Erosive Burning Models," *JANNAF Workshop on Erosive Burning/Velocity Coupling*, Lancaster, Calif., March 1977.
- ³Lenoir, J. M. and Robillard, G., "A Mathematical Method To Predict the Effects of Erosive Burning in Solid-Propellant Rockets," *Sixth Symposium (International) on Combustion*, Reinhold, New York, 1957, pp. 663-667.
- ⁴Vandenkerckhove, J. A., "Erosive Burning of a Colloidal Solid Propellant," *Jet Propulsion*, Vol. 28, Sept. 1958, pp. 599-603.
- ⁵King, M. K., "An Analytical and Experimental Study of the Erosive Burning of Composite Propellants," AFOSR-TR-78-0060, Final Report to U.S. Air Force Office of Scientific Research, Nov. 1977.
- ⁶Corner, J., *Theory of Interior Ballistics of Guns*, John Wiley and Sons, New York, 1950, pp. 73-81.
- ⁷Tsuji, H., "An Aerothermochemical Analysis of Erosive Burning of Solid Propellant," *Ninth Symposium (International) on Combustion*, Williams & Wilkins, Baltimore, Md., 1963, pp. 384-393.
- ⁸Razdan, M. K., "Theoretical Studies on the Erosive Burning of Double-Base Solid Propellants," Master of Technology Thesis, Indian Institute of Technology, Kanpur (1974).
- ⁹Schuyler, F. L. and Torda, T. P., "An Aerothermochemical Analysis of Solid Propellant Combustion," *AIAA Journal*, Vol. 4, Dec. 1966, pp. 2171-2177.
- ¹⁰Lengelle, G., "Model Describing the Erosive Combustion and Velocity Response of Composite Propellants," *AIAA Journal*, Vol. 13, March 1975, pp. 315-322.
- ¹¹Beddini, R., "Reacting Turbulent Boundary-Layer Approach to Solid Propellant Erosive Burning," *AIAA Journal*, Vol. 16, Sept. 1978, pp. 898-905.
- ¹²Steinz, J. A., Stang, P. L., and Summerfield, M., "The Burning Mechanism of Ammonium Perchlorate-Based Composite Solid Propellants," AIAA Paper 68-658, 1968.
- ¹³Beckstead, M. W., Derr, R. L., and Price, C. F., "A Model of Composite Solid Propellant Combustion Based on Multiple Flames," *AIAA Journal*, Vol. 8, Dec. 1970, pp. 2200-2207.
- ¹⁴Squire, L. C., "The Constant Property Turbulent Boundary Layer with Injection, A Reanalysis of Some Experimental Results," *International Journal of Heat Mass Transfer*, Vol. 13, May 1970, pp. 939-942.
- ¹⁵Mickley, H. S. and Davis, R. S., "Momentum Transfer for Flow over a Flat Plate with Blowing," NACA TN 4017, Nov. 1957.
- ¹⁶Makunda, H. S., "A Comprehensive Theory of Erosive Burning in Solid Rocket Propellants," *Combustion Science and Technology*, Vol. 18, Nos. 3 and 4, 1978, pp. 105-118.
- ¹⁷Razdan, M. K. and Kuo, K. K., "Erosive Burning Studies of Composite Solid Propellants by the Reacting Turbulent Boundary-Layer Approach, AFOSR-TR-78-0035, Tech. Rept. to U.S. Air Force Office of Scientific Research, Nov. 1977.
- ¹⁸Laufer, J., "Thought on Compressible Turbulent Boundary Layers," NASA SP-216, Dec. 1968.
- ¹⁹Kulgein, N. G., "Transport Processes in a Compressible Turbulent Boundary Layer," *Journal of Fluid Mechanics*, Vol. 12, March 1962, pp. 417-437.
- ²⁰Launder, B. E. and Spalding, D. B., *Mathematical Models of Turbulence*, Academic Press, New York, 1972, p. 9.
- ²¹Lockwood, F. C. and Naguib, A. S., "The Prediction of the Fluctuations in the Properties of Free, Round-Jet, Turbulent, Diffusion Flames," *Combustion and Flame*, Vol. 24, No. 1, 1975, pp. 109-124.
- ²²Gosman, A. D., Lockwood, F. C., and Syed, S. A., "Prediction of a Horizontal Free Turbulent Diffusion Flame," *Sixteenth Symposium (International) on Combustion*, Combustion Institute, 1976, pp. 1543-1555.
- ²³Elghobashi, S. E. and Pun, W. M., "A Theoretical and Experimental Study of Turbulent Diffusion Flames in Cylindrical Furnaces," *Fifteenth Symposium (International) on Combustion*, Combustion Institute, 1974, pp. 1353-1365.
- ²⁴Mason, H. B. and Spalding, D. B., "Prediction of Reaction Rates in Turbulent Pre-Mixed Boundary Layer Flows," *Combustion Institute, First European Symposium*, 1973, pp. 601-606.
- ²⁵Spalding, D. B., "Mixing and Chemical Reaction in Steady Confined Turbulent Flames," *Thirteenth Symposium (International) on Combustion*, Combustion Institute, 1971, pp. 649-657.
- ²⁶Lockwood, F. C., "The Modeling of Turbulent Premixed and Diffusion Combustion in the Computation of Engineering Flows," *Combustion and Flame*, Vol. 29, No. 2, 1977, pp. 111-122.
- ²⁷Magnussen, B. F. and Hjertager, B. H., "On Prediction of Soot Formation and Combustion in Turbulent Flames with Special Reference to a Free-Jet C₂H₂ Diffusion Flame," *Combustion Institute, 2nd European Symposium*, Vol. 1, 1975, pp. 385-390.
- ²⁸Williams, F. A., Berrieré, M., and Haung, N. C., "Fundamental Aspects of Solid Propellant Rockets," AGARDograph-116, Technivision, 1969, p. 438.
- ²⁹Levine, J. N. and Culick, F.E.C., "Nonlinear Analysis of Solid Rocket Combustion Instability," AFRPL-TR-74-45 Final Rept., Vol. 1, 1974.
- ³⁰van Driest, E. R., "On Turbulent Flow Near a Wall," *Journal of the Aeronautical Sciences*, Vol. 23, Nov. 1956, pp. 1007-1011.
- ³¹Chambers, T. L. and Wilcox, D. C., "Critical Examination of Two-Equation Turbulence Closure Models for Boundary Layers," *AIAA Journal*, Vol. 15, June 1977, pp. 821-828.
- ³²Jones, W. P. and Launder, B. E., "The Calculation of Low-Reynolds-Number Phenomena with a Two-Equation Model of Turbulence," *International Journal of Heat Mass Transfer*, Vol. 16, June 1973, pp. 1119-1129.
- ³³Omori, S., "Eddy Viscosity Calculation Along the Chemical Rocket Thrust Chamber Wall Using Turbulent Kinetic Energy," *Combustion Science and Technology*, Vol. 7, No. 6, 1973, pp. 229-240.
- ³⁴Patankar, S. V. and Spalding, D. B., *Heat and Mass Transfer in Boundary Layers*, Inter-text Books, London, 1970.
- ³⁵Peretz, A., Kuo, K. K., Caveny, L. H., and Summerfield, M., "Starting Transient of Solid Propellant Rocket Motors with High Internal Gas Velocities," *AIAA Journal*, Vol. 11, Dec. 1973, pp. 1719-1727.
- ³⁶Kays, W. M., "Heat Transfer to the Transpired Turbulent Boundary Layer," *International Journal of Heat Mass Transfer*, Vol. 15, May 1972, pp. 1023-1044.
- ³⁷Gordon, S. and McBride, B. J., "Computer Program for Calculation of Chemical Equilibrium Compositions, Rocket Performance, Incident and Reflected Shocks, and Chapman-Jouquet Detonations," NASA SP-273, 1971.
- ³⁸Sabadell, A. J., Wenograd, J., and Summerfield, M., "Measurement of Temperature Profiles Through Solid Propellant Flames Using Fine Thermocouples," *AIAA Journal*, Vol. 3, Sept. 1965, pp. 1580-1584.
- ³⁹Marklund, T. and Lake, A., "Experimental Investigation of Propellant Erosion," *ARS Journal*, Vol. 3, Feb. 1960, pp. 173-178.



AIAA 79-1172R

**Measurements and Model Validation for
Composite Propellants Burning under
Cross Flow of Gases**

M. K. Razdan and K. K. Kuo

Reprinted from

AIAA Journal

Volume 18, Number 6, June 1980, Page 669

Copyright American Institute of Aeronautics and Astronautics, Inc., 1979. All rights reserved

Measurements and Model Validation for Composite Propellants Burning under Cross Flow of Gases

Mohan K. Razdan* and Kenneth K. Kuo†
The Pennsylvania State University, University Park, Pa.

Erosive burning rates of three types of ammonium perchlorate-based composite propellant formulations were measured by using the high-speed motion picture method. Experiments were conducted in a test rig designed to develop a well-defined, turbulent boundary layer with a distinct leading edge by the flow of combustion gases over two-dimensional propellant samples. Erosive burning rate correlations which relate the burning rate to freestream velocity and pressure were developed. The comparison of experimental data and theoretical results obtained from the erosive burning model, based upon the turbulent boundary-layer approach developed by the authors, showed a close agreement.

Nomenclature

a	= pre-exponent in strand burning rate law, (cm/s) (MPa) ⁻ⁿ
A_{ih}	= throat area of exit nozzle, m ²
A_{is}	= cross-sectional flow area in test section, m ²
d_{AP}	= average size of AP particles, μm
h_{is}	= height of flow channel above propellant surface, m
H	= height of test section without propellant sample, m
K	= constant in erosive burning rate correlation, (MPa) ^{-n_p} (m/s) ^{-n_u}
n_u	= velocity exponent in erosive burning rate correlation
M_{is}	= Mach number in test section
n	= pressure exponent in strand burning rate law
n_p	= pressure exponent in erosive burning rate correlation
p	= pressure, MPa
r_b	= $r_{b0} + r_{be}$, total burning rate, cm/s
r_{be}	= erosive burning rate, cm/s
r_{b0}	= strand burning rate, cm/s
R	= gas constant, 437.6 N-m/kg-K
t	= time, s
T_0	= stagnation temperature, 2258 K
T_∞	= freestream gas temperature, K
U_{ih}	= threshold velocity, m/s
U_{is}	= average velocity in test section, m/s
U_∞	= freestream velocity in test section, m/s
x	= distance from leading edge along propellant surface, cm
y	= location of burning propellant surface, cm
α_1	= constant in erosive burning rate correlation, (cm/s) ^{n_u} (MPa) ⁻ⁿ
δ	= boundary layer thickness, m
η	= exponent in boundary layer velocity profile
γ	= ratio of constant pressure and constant volume specific heats, 1.26
ω	= pressure exponent in Eq. (5)

Presented as Paper 79-1172 at the AIAA/SAE/ASME 15th Joint Propulsion Conference, Las Vegas, Nev., June 18-20, 1979; submitted Sept. 13, 1979; revision received Nov. 26, 1979. Copyright © American Institute of Aeronautics and Astronautics, Inc., 1979. All rights reserved. Reprints of this article may be ordered from AIAA Special Publications, 1290 Avenue of the Americas, New York, N.Y. 10019. Order by Article No. at top of page. Member price \$2.00 each, nonmember, \$3.00 each. Remittance must accompany order.

Index categories: Solid and Hybrid Rocket Engines; Boundary Layers and Convective Heat Transfer—Turbulent.

*Assistant Professor, Dept. of Mechanical Engineering. Member AIAA.

†Associate Professor, Dept. of Mechanical Engineering. Member AIAA.

I. Introduction

THE term "erosive burning" refers to the sensitivity of the solid-propellant burning rate to the velocity of the combustion gases flowing parallel to the propellant surface. The burning rate generally increases with an increase in gas velocity. A high-velocity gas flow usually occurs in the central port of a propellant grain used in a rocket motor. In designing rocket motors, it is essential to be able to predict the burning rate under high cross-flow velocities, since both the thrust level and the web burnout time depend on the burning rate. Erosive burning effect is particularly important in the design of high-thrust, short-burning-time solid-propellant motors for high-acceleration rockets and missiles. Gases in a nozzleless rocket motor choke somewhere within the port, and the gas velocity reaches sonic and supersonic speeds over some portions of the propellant surfaces, leading to high erosive burning rates. In order to have high performance, it is necessary to achieve high-loading fractions (ratio of propellant weight to combustion chamber volume) in a solid-propellant rocket motor. However, with high-loading fractions, erosive burning often results in high-pressure peaks, unequal propellant-web burnout, and extended heat exposure of the chamber wall. Chamber failure may even occur due to overpressurization immediately after ignition, when combustion gas velocity is at maximum. An understanding of the erosive burning characteristics of a solid propellant can lead to the elimination of these problems through proper modifications in the motor and/or grain design.

The literature reviews by Kuo and Razdan¹ and by King² indicate that the erosive burning behavior of solid propellants has been investigated in the past by both experimental and theoretical methods. Over the years, a number of models for a possible erosive burning mechanism have been developed to predict the burning rates of solid propellants. These models include: 1) the work of Lenoir and Robillard,³ based on a heat-transfer theory; 2) Vandekerckhove's work,⁴ based on a flame theory; 3) the flame-bending model of King;⁵ and 4) the boundary layer models of Razdan and Kuo,⁶ Beddini,⁷ and Lengellé.⁸ Although there are various approaches to attacking the problem of erosive burning, a realistic approach must consider the burning of the solid propellant under the influence of a boundary layer (mostly turbulent) developed over the propellant surface by the flow of combustion gases.

Experimental studies on erosive burning are important for comparing theoretical predictions and measured erosive burning rates. Erosive burning has been studied experimentally in various ways. The methods used include, for example, partial or interrupted-burner techniques,⁹⁻¹¹

cineradiography technique,¹⁰ X-ray flash and pressure pick-up methods,¹² conductivity probe technique,¹³ and high-speed photography technique.^{5,14} None of these experimental studies were designed to be compatible for a boundary layer type of theoretical analysis. Moreover, in most of the previous experimental work, the freestream velocities were limited to low values. In the wake of the recent developments of theoretical models⁶⁻⁸ based on turbulent boundary-layer approaches, there is a need for erosive burning data for propellants over which turbulent boundary layers are formed. The present experimental approach is unique in that the experiments were conducted in a test rig designed to develop a turbulent boundary layer with a distinct leading edge by the flow of gases over a propellant sample. There is no previous report of erosive burning data under such conditions.

The objectives of the present study were to: 1) conduct erosive burning tests at various pressures and freestream velocities on two-dimensional flat ammonium perchlorate-based composite solid propellant slabs; 2) establish a data base for erosive burning rate as a function of gas velocity, pressure, and propellant physico-chemical characteristics; 3) correlate the erosive burning rate data in terms of freestream velocity and pressure; and 4) use the experimental data for the verification of the theoretical model developed by the authors at the Pennsylvania State University.

II. Experimental Apparatus

A. Erosive Burning Test Rig

The present experiments were designed for verification purposes, so that erosive burning rates measured at various freestream velocities and pressures can be compared with theoretical calculations. Consistent with the theoretical model,⁶ the propellant samples in all tests were of flat geometry.

In the design consideration, two requirements were imposed on the structure of the experimental apparatus: 1) experiments should be compatible with the theoretical model;⁶ and 2) combustion product gas temperature, pressure, and freestream velocity for burning of a propellant should be similar to that surrounding combustion of a typical solid propellant motor. Therefore, a turbulent boundary layer should be formed over a flat test propellant surface by the flow of a high-velocity gas, and the propellant should burn at typical rocket pressures of 25-100 atm. Various materials and dimensions of the test rig were selected on the basis of a computer-aided design and parametric study, and the requirements of high-pressure and high-temperature gas flow (see Ref. 15 for details). A schematic diagram of the test is shown in Fig. 1. Description and function of each important component is given in the following.

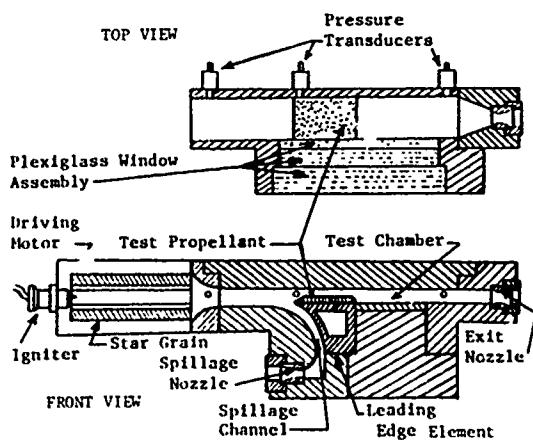


Fig. 1 Schematic diagram of erosive burning test rig.

Driving Motor

A high-pressure, high-velocity, hot combustion gas flow needed to simulate actual rocket conditions was generated in the driving motor by burning a 30-cm long and 11.96-cm outer diameter, 8-point star-shaped N-4 solid-propellant grain. It may be noted here that the flame temperature of the driver propellant grain is different from that of the test propellant samples. Consequently, the freestream temperature in the present experiments was different from the flame temperature of a test propellant. However, this is not believed to affect the results, because the erosive burning rate in previous studies^{5,12} was found to be independent of the freestream gas temperature. The neutral burning characteristics of the driver propellant grain helped to maintain a steady-state pressure in the test chamber after a short ignition transient interval. The driving motor was constructed of 304 stainless steel, with a length of 30 cm, an inner diameter of 12 cm, and an outer diameter of 17.8 cm.

Igniter System

To ignite the propellant charge in the driving motor, a pyrotechnic igniter (MK 125 MOD 5) was used. The igniter was held in a stainless steel igniter holder threaded into a flange attached at the head end of the driving motor. The igniter was set off by a remotely controlled ignition circuit, and the power supply was carried to the igniter through an insulated electrode gland feedthrough [Nanmac Corp., Model A-501-Cu(ss)].

Following ignition of the propellant grain, the product gases flow out of the driving motor into the test chamber through a nozzle. This nozzle, constructed of 304 stainless steel, was designed to converge from a square cross section (42.3 cm²) at the end of the driving motor to a rectangular cross section (17.8 cm²) at the entrance of a test chamber.

Test Chamber

Several important elements were designed to form the 39-cm long test chamber made of 304 stainless steel with a rectangular cross section 7 cm × 2.54 cm:

1) The test chamber was equipped with a transparent plexiglass window assembly composed of an inner sacrificial plexiglass window (25.4 cm × 3.81 cm × 1.27 cm), a middle window (25.4 cm × 3.81 cm × 2.54 cm), and a top window (27.94 cm × 6.35 cm × 3.81 cm). Rubber O-rings between the middle and top windows were used to insure a tight seal. A new sacrificial window was used in each test firing. The test-propellant sample was clearly visible through the plexiglass window assembly.

2) An interchangeable wedge-shaped stainless steel leading edge was provided, and a test-propellant sample was glued to the top flat surface of the leading edge. The length of the leading edge (10.8 cm) allowed the development of a turbulent boundary layer over a large portion of the propellant sample.

3) A spillage channel was provided. A small amount of the product gases flowed through the channel and out of the test chamber, enabling the boundary layer to develop from the beginning of the leading edge.

4) An interchangeable top plate was designed to vary the channel height in the test section to change gas velocity. Pressure gradient can also be controlled by using a tapered top plate.

5) Convergent-divergent interchangeable exit nozzles made of stainless steel were designed to control the pressure and gas velocity in the test chamber. Various nozzles, with throat diameters of 1.93 cm, 2.08 cm, and 2.42 cm, were used. The exit-nozzle assembly contained a burst diaphragm designed to rupture at a given critical pressure of 30 atm. A small nozzle with a throat diameter of 0.65 cm was used at the end of the spillage channel. To ensure that the spillage channel remained open during the test firing, the burst diaphragm was not used in the small nozzle assembly.

B. Burning Rate Measuring Technique

The high-speed motion picture method was used to determine the burning rate of a test-propellant sample. The burning test propellant was photographed by a 16-mm high-speed motion picture camera (400-ft capacity Hycam Model K20S4E-115). A telescopic lens (Elgeet Rochester Co., 6-in., $f/3.8$, ciné Navitar No. A2305) was also used with the camera. The framing rate of the camera during the experiments was set from 1000 to 1500 frames per second. The camera was equipped with two light-emitting diodes (LED), one for generating timing signals at a preselected frequency and the other for a common-time marker. During the filming of the burning propellant, time marks were recorded on the film, and a common-time mark was also recorded on the film at that time at which ignition was started in a test firing. At the same time, a voltage signal was recorded on a magnetic tape recording system which also recorded pressure-time data at various locations of the test rig. In this way, burning rate vs time data were coordinated with pressure vs time data. The light-emitting diodes were operated by a timing light generator (LED driver), which was fabricated by The Pennsylvania State University Electronics Services and has a frequency range of 10-10,000 Hz. The frequency in the present experiments was set at 100 Hz.

The film was analyzed frame by frame on a motion analyzer, by means of the Vanguard motion analyzer (M-16GD Serial No. 772 projection head, C-11D Serial No. 773 projection case). The motion analyzer projects a 4 \times -magnified picture on a screen. The screen has two crosshairs which can be moved in x and y directions. The distance moved by these crosshairs is obtained from two micrometer dials accurate to a thousandth of an inch. A frame counter is also provided to record the number of frames moved between readings. The readings taken from the analyzer were the y distances (propellant surface location) at a fixed x location, and the frame counter readings. Readings were taken approximately 100 frames apart. The time interval between each reading was calculated from the number of time marks on the film. To convert the y -dial readings recorded from the magnified image to the actual readings, each y -dial reading was multiplied by a scale factor. The scale factor is defined as the ratio between actual object thickness (measured propellant thickness before ignition in a test firing) to the projected image thickness (y -dial reading of the propellant).

C. Instrumentation

Pressure Measuring Equipment

The pressure measuring system consists of piezo-electric quartz transducers, charge amplifiers, and a recording system. Pressure was measured at three locations: 1) near the inlet to the rectangular convergent nozzle at the exit of the driving motor; 2) near the leading edge; and 3) near the exit nozzle. Three pressure transducers (Kistler Model 601B), with a pressure range up to 1000 atm, were used. These transducers were equipped with water-cooled adapters (Kistler Model 628C), which protected the transducers from excessive heating by the high temperature gases. A silicon-rubber insulation material was used to protect the transducer diaphragms from the hot gases. Transducers were not mounted flush with the inner surface of the test chamber, but were slightly recessed from it to provide additional thermal protection. The charge signal produced by a transducer is proportional to the pressure signal, and it was amplified through a charge amplifier (Kistler Model 504E) and recorded on a tape recorder. Calibrations of pressure measurements were made through the charge amplifiers by applying a DC voltage equal to the transducer sensitivity (picoCoulombs/ ft^2) applied by the manufacturer. The output of the charge amplifier, which represents the measured pressure in volts of voltage (volts/psi), was then recorded. This calibration procedure was checked periodically by measuring a known pressure (using

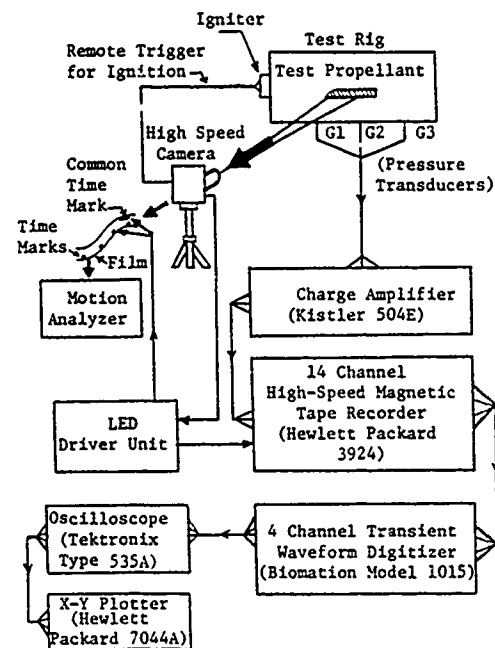


Fig. 2 Schematic diagram of data acquisition system.

high pressure nitrogen) with the same transducers as those used in the present experiments.

Data Acquisition System

Figure 2 illustrates the components of the data acquisition system used in the present erosive-burning experiments. It consists of pressure transducers, charge amplifiers, a 14-channel tape recorder (Hewlett Packard Model 3924 tape system), a 4-channel transient wave form digitizer (Biomation Model 1015), an oscilloscope (Tektronix type 535A), an x-y plotter (Hewlett-Packard 7044A), a high-speed movie camera, an LED driver unit, and a motion analyzer. A pressure transducer produces a small electric charge proportional to the pressure in the test chamber. This charge is carried by an insulated high impedance cable to the charge amplifier, which after amplification converts it into voltage output proportional to the pressure. The output of the charge amplifier is recorded on an FM channel of the tape recorder. Output of the tape recorder is connected to the Biomation digitizer, which converts the data from analog to digital form. The data can be displayed on an oscilloscope, or plotted on the x-y plotter for a hard copy. The burning rate data are obtained through the use of the high-speed motion picture camera and motion analyzer.

D. Procedure Used in Conducting Erosive Burning Test Firings

Before conducting erosive burning test firings, a series of cold flow tests was performed to check the uniformity of the flow out of the rectangular convergent nozzle. Measurements were made with pitotstatic probes at the exit plane of the convergent nozzle. The measured velocity distributions consistently indicated the uniformity of the flow within the potential core over the major portion of the nozzle exit plane. The data also indicated that the nozzle geometry is adequate for providing a two-dimensional flow. During the course of an erosive burning test firing, a number of safety precautions were taken because of the complexity of the test rig setup. A check list prescribing a systematic procedure for setting up each test firing was used. Some of the requisites for preparing a test firing are described below:

1) Internal surfaces of the driving-motor star grain were spread with an igniter paste composed of potassium perchlorate, boron, and titanium mixed in hexane. The ad-

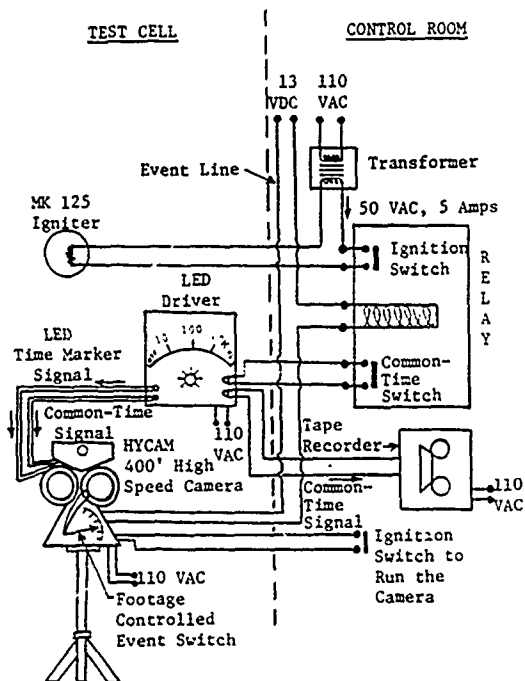


Fig. 3 Circuit diagram for remotely controlled ignition and high-speed photography system.

vantage of using igniter paste was its ability to spread the flame uniformly and rapidly, thus reducing the time interval of pressurization after ignition.

2) The test propellant was glued to the flat surface of the leading-edge element with an epoxy containing Epon 828 (90%) and diethylene triamine (10%). Normally, 24 h was required for the glue to dry and firmly hold the propellant on the leading edge. Typical test propellant dimensions were length, 10.7 cm; width, 7.3; and thickness, 1.75 cm. The leading-edge portion of the propellant was tapered to ensure smooth development of a boundary layer. The trailing-edge portion of the propellant was also tapered slightly to avoid any flow separation effect in the vicinity of the trailing edge. A little extra width beyond that of the leading-edge width was left for the test propellant sample in each experiment. This was necessary in order to ensure good compression between the sacrificial plexiglass window and the propellant. In this way, no combustion gases could penetrate between the propellant and the plexiglass window.

3) A thin layer of flame retardant (chlorofluorocarbon, Halocarbon 25-5S) was applied to the propellant's front and back surfaces, which were in contact with the plexiglass window and the test chamber wall, respectively. The propellant compression and the use of flame retardant are essential to the experiment in order to prevent flame spreading between the contact surfaces. Flame retardant was also used on the inner surface of the sacrificial plexiglass window to suppress the burning of the window. This helped to obtain a clear view of the burning test propellant sample. In a few of the earlier test firings, it was found that combustion gases generated a small crack in the propellant near the leading edge (stagnation region); eventually, the crack became larger as a result of crack propagation and rapid flame penetration into the crack. A small portion of the propellant leading edge was also covered with the flame retardant layer to avoid development of cracks.

4) The contact surfaces of various components of the test rig were sealed by applying a layer of rubber-based adhesive sealant (Permatex No. 6BR). This was found to be very effective in achieving a good seal.

5) A pre-ignition test was made just before each actual test firing. A fuse wire was used to simulate the igniter, the high-

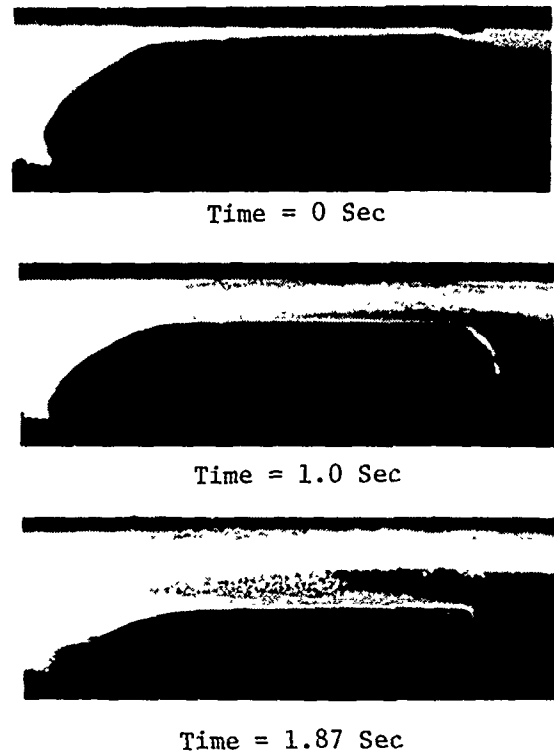


Fig. 4 Photographs showing location of test-propellant surface at various times during a test firing.

speed movie camera was loaded with a dummy film, and various control switches were then activated in the same sequence as in an actual test firing. If the setup was appropriate, the fuse wire would burn, thus confirming the proper function of the remotely controlled ignition circuit.

6) Four camera lights (two 1000 W and two 650 W) were used to illuminate the window and the propellant in the test chamber.

7) A 16-mm, 200-ft color film was used in each test firing. The film used was Kodak, Eastman Ektrachrome 7250 with ASA 400 (tungsten). The f-stop on the telescopic lens was set at 8.0 for all tests conducted.

Remotely Controlled Ignition System

A circuit diagram for the remotely controlled ignition and high-speed photography system is shown in Fig. 3. Basically, the MK 125 igniter is set off by an event switch built into the high-speed movie camera. When the ignition switch is activated, the camera takes some time to reach a steady preselected framing rate. Corresponding to this time is the length of film which the camera rolls before ignition. Film length is dependent on the selected framing rate (e.g., 30 ft for the present experiments, at about 1500 frames per second) and can be preset with a footage-controlled event switch built into the camera. After the camera runs through the initial film length, the event switch closes, activating a relay switch, and then setting off the igniter.

III. Data Reduction and Analysis

A. Calculation of Burning Rate from Experimental Data

Burning rate data were obtained from the photographic record of a test firing, as discussed in Sec. II.B. Three photographs showing the location of the test-propellant surface during a test firing at various times are shown in Fig. 4. For each y reading, the corresponding time t was computed from the number of time marks on the film. In order to permit accurate computation of first derivatives ($r_b = dy/dt$), a least-square polynomial fit through $y-t$ data was conducted

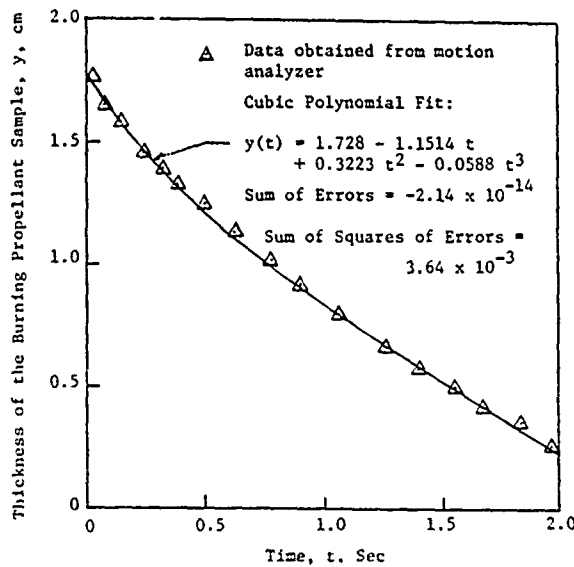


Fig. 5 Least-square polynomial fit to measured y vs t data.

to obtain an equation for $y(t)$. Polynomials from the second to the fifth degree were employed, and depending on the least square error, the best fitted polynomial was chosen to represent the data. A typical case is shown in Fig. 5. The sum of squares of errors for this fit was very small (3.64×10^{-3}). The burning rate was calculated by differentiating the polynomial equation with respect to time. In this way, burning rate vs burning time data were obtained from all the test firings. It may be pointed out that the accuracy of the measured burning rate depends on the accuracy of the measurement of the location of the burning propellant surface. Measurements were taken with a motion analyzer capable of measuring line resolution to within 0.001 in. and at an average time interval of 0.01 s. The error introduced in evaluating the burning rate is less than 3%. Because the time marks were put on the film at a precisely known frequency, no error is expected in the calculation of the time interval between film readings.

B. Calculation of Freestream Gas Velocity

Direct measurement of the velocity in the test section is very difficult because of the presence of high-temperature and high-pressure gases. Therefore, the freestream velocity is indirectly calculated from the one-dimensional gas dynamic relationships for flow through a nozzle. Using these relationships and the mass conservation, the average gas velocity in the test section, U_{ts} , was found from the following equation (see Ref. 16):

$$U_{ts} = \left(\frac{A_{th}}{A_{ts}} \right) \sqrt{T_0} \left\{ \gamma R \left(\frac{2}{\gamma+1} \right)^{\frac{\gamma+1}{\gamma-1}} \right\}^{\frac{1}{2}} \left\{ 1 + \frac{\gamma-1}{2} M_{ts}^2 \right\}^{1/(\gamma-1)} \quad (1)$$

where A_{ts} is the flow cross-sectional area over the propellant test sample, A_{th} is the throat area of the exit nozzle, and M_{ts} is the average Mach number of the combustion gases in the test section. The Mach number was calculated from the following equation (see Ref. 16):

$$M_{ts} = \left\{ \frac{2}{\gamma+1} + \frac{\gamma-1}{\gamma+1} M_{ts}^2 \right\}^{\frac{\gamma+1}{2(\gamma-1)}} \left(\frac{A_{th}}{A_{ts}} \right) \quad (2)$$

A_{ts} was computed from the product of the width and height h_{ts} of the flow channel above the surface of a test propellant in the test section. This height was obtained from the difference between the height of the test section without

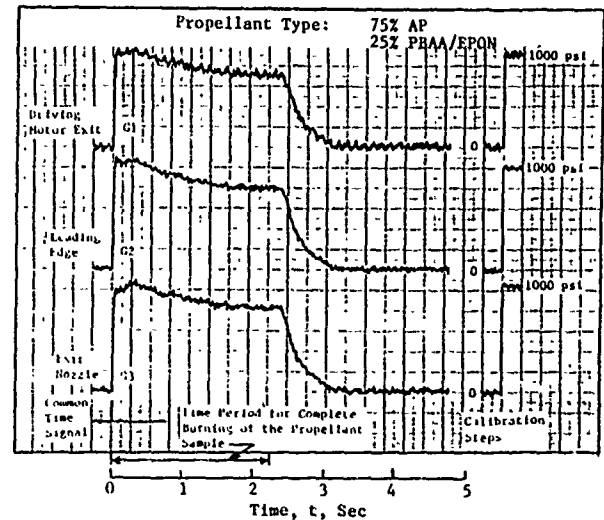


Fig. 6 Measured pressure-time traces in an erosive burning test firing with exit-nozzle throat diameter of 1.93 cm.

propellant sample, H , and the measured location y of the propellant surface. The Mach number in the test section is obtained from Eq. (2), and the average velocity is then calculated from Eq. (1). To obtain an expression for the freestream velocity, correction should be made in the average velocity to account for the boundary layer developed over the propellant surface and the top plate of the test chamber. The freestream velocity was obtained from the following equation:

$$U_{\infty} = U_{ts} \left[1 - \left(\frac{\eta}{1+\eta} \right) \frac{2\delta}{h_{ts}} \right] \quad (3)$$

where δ is the boundary-layer thickness and η is the exponent in a power-law velocity profile (η was taken as 1/7 in these calculations). Boundary-layer thickness was found from the functional relationship of δ in terms of Reynolds number for a turbulent boundary-layer flow. Equation (3) was developed from a boundary-layer analysis to account for viscous blockage effect in the test section.

C. Erosive-Burning Rate Correlations

Using the measured experimental data, correlations were developed between erosive burning rate augmentation factor (r_b/r_{b0}), freestream velocity, and pressure. The functional form of these correlations was obtained from the experimental data, as explained in the following. The burning rate at a particular pressure is seen to increase somewhat linearly with freestream velocity. An equation relating burning rate and velocity can be written as

$$r_b = r_{b0} + \alpha (U_{\infty} - U_{th})^n \quad (4)$$

where U_{th} represents the threshold velocity and α is a constant which must be a function of pressure, since the experimental data indicate that the slope of the r_b vs U_{∞} data changes with pressure. Therefore, the following relationship is assumed:

$$\alpha = \alpha_1 p^\omega \quad (5)$$

In this equation α_1 and ω are unknown constants. Although Eq. (4) contains the threshold velocity consideration, our experimental data for all three propellants tested showed no threshold effect. The threshold velocity is retained in Eq. (4) to maintain the generality of the form of the correlation.

From the graphical plot of experimental data for r_b vs U_{∞} at three different pressures, approximate values for the

Table 1 Propellant data

Propellant type	I (4525)	II (5051)	III
Composition	AP/HTPB	AP/HTPB	AP/PBAA-EPON
Average particle size, μm	20	200	76
Weight percent of oxidizer	73	73	75
Pre-exponent a in the strand burning rate law, (cm/s) $(\text{MPa})^{-n}$	0.305	0.2026	0.2452
Pressure exponent n in the strand burning rate law	0.5611	0.5427	0.41
Flame temperature of propellant gas, K	1667	1667	1920
Propellant density, kg/m^3	1492	1492	1600

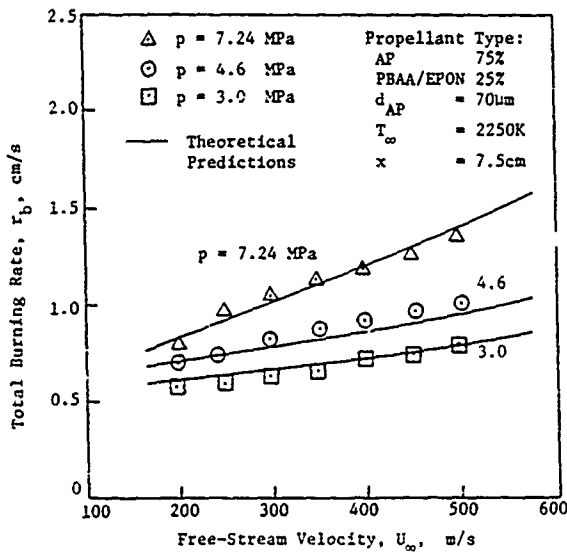


Fig. 7 Comparison of predicted burning rates with experimental data at various pressures and freestream velocities for propellant III.

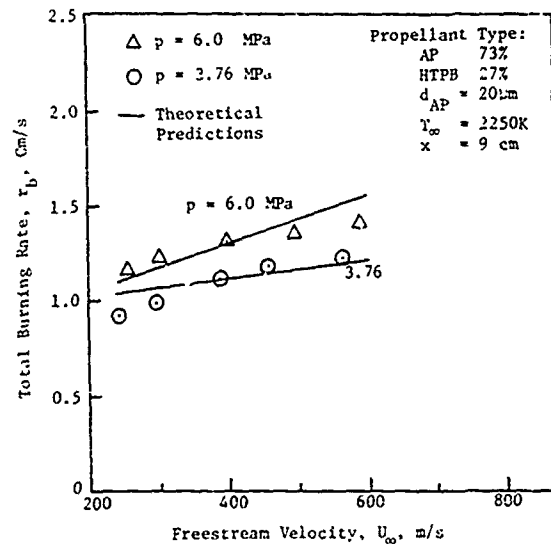


Fig. 8 Comparison of predicted burning rates with experimental data at various pressures and freestream velocities for propellant I.

constants α_f , ω , and n_u were obtained. The values of the approximate constants were then optimized by a regression analysis of the experimental data for the burning rate, freestream velocity, and pressure. The regression analysis was performed with the NLIN2 computer program¹⁷ of the Share Program Library. The model supplied to the NLIN2 program was represented by the following correlation:

$$r_{b_e} = \alpha_f p^\omega (U_\infty - U_{th})^{n_u} \quad (6)$$

This equation is obtained from Eqs. (4) and (5), while r_{b_e} is the erosive burning rate component of the total burning rate r_b of a solid propellant. Using the strand burning rate law ($r_{b_0} = ap^n$) and Eqs. (4) and (5), the correlation represented by Eq. (6) can be written in the following convenient form:

$$(r_b/r_{b_0}) = 1 + Kp^n p (U_\infty - U_{th})^{n_u} \quad (7)$$

The correlation given by Eq. (7) represents, within limits of available data, the effect of freestream velocity and pressure on the burning rate of the solid composite propellants studied. The correlation equation can be represented by a 45 deg line on a r_b/r_{b_0} vs $1 + Kp^n p (U_\infty - U_{th})^{n_u}$ plot. These plots are discussed in the following section.

IV. Results and Discussion

Figure 6 shows a typical pressure-time trace recorded during a test firing with an exit nozzle throat diameter of 1.93 cm. Several observations can be made from the pressure-time traces:

1) The pressure variation between the peak pressure and the start of the tail-off region is not significant, and the mean

flow in the boundary layer can be considered as quasi-steady at any particular time.

2) In all the erosive burning experiments conducted, the time period for a test propellant sample to consume completely was within the time interval during which the chamber was pressurized. The flame-spreading time for the star grain in the driving motor was very short, as can be seen from the sharp pressurization following immediately after the onset of ignition. Therefore, most of the burning time of the star grain was adequately utilized during the test run.

3) The common-time signal shown in Fig. 6 represents that instant at which remotely controlled ignition takes place. This time always coincides with the first discernible pressure rise in the test rig.

Erosive burning characteristics of three types of AP-based composite solid propellants were studied. These propellants and their data are listed in Table 1. Propellants designated by I and II are the same as those used by King⁵ in his study (propellant numbers 4525 and 5051 in Table 1 correspond to King's formulation numbers). While propellants I and II have the same binder (HTPB) and oxidizer-to-fuel ratio (73:27), their AP particle size is quite different: 20 μm for propellant I and 200 μm for propellant II. Pressure and velocity ranges covered in the present study were 2 to 7 MPa for pressure, and 200 to 700 m/s for freestream velocity.

Experimental results obtained for AP/PBAA-EPON propellant are plotted in Fig. 7, which shows the variation of total burning rate with freestream velocity at pressures of 7.24, 4.6 and 3.0 MPa. As expected, the burning rate increases with the increase in both pressure and freestream velocity. The slope of the burning rate vs velocity curves decreases with the decrease in pressure. At the same time, the

burning rate at lower pressure changes very slowly at low velocities (close to 200 m/s). Calculated results from the turbulent boundary layer model⁶ developed by authors are also plotted in Fig. 7. The agreement between the predicted and measured burning rates is quite close for all pressure considered.

For AP/HTPB propellants, Figs. 8 and 9 show the variation of the measured burning rate with freestream velocity at different pressures. The comparison between the results shown in Figs. 8 and 9 indicates a noticeable difference in the burning behavior of the two propellants with identical ingredients, but with different oxidizer particle sizes. The erosive effect is more pronounced for propellant II with larger particle size, since the gradient of r_b vs U_∞ in Fig. 9 is steeper

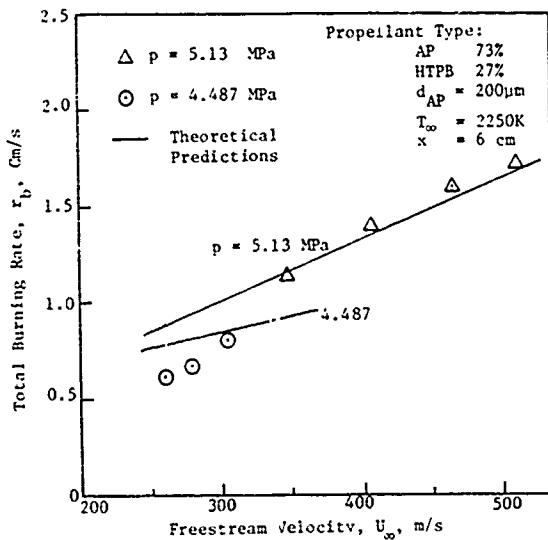


Fig. 9 Comparison of predicted burning rates with experimental data at various pressures and freestream velocities for propellant II.

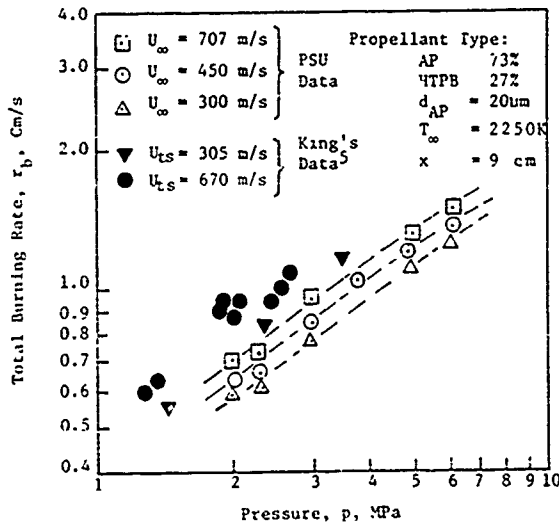


Fig. 10 Measured burning rate vs pressure data for different freestream velocities.

than that in Fig. 8. It is believed that the higher erosive burning rates for propellants with large particles is caused by the roughness effect of the propellant surface. The roughness increases the turbulence activity near a propellant surface, thereby increasing the gas-to-solid heat flux and the burning rate of a propellant. As the particle size increases, the height of the roughness also increases, as does the burning rate of a propellant. This phenomenon is in agreement with the predictions of the turbulent boundary-layer model⁶ developed at The Pennsylvania State University. The predictions for propellants I and II are shown as solid lines in Figs. 8 and 9, respectively. The agreement between the theoretical and experimental results is generally good. The surface roughness height of 35% of the AP particle size was used in theoretical calculations. This value of roughness height was obtained by systematically varying the roughness height until the predictions matched the measured burning rate of a propellant. At the same time, all other physical and chemical input data of the propellant were held constant in theoretical calculations. Because of the lack of experimental data for surface roughness, the above procedure of including the surface roughness effect in the theoretical calculations is believed to be reasonable.

It may be noted that the strand burning behavior of the two AP/HTPB propellants is also different as a result of differing particle sizes. Propellant I with 20 μ AP has a higher strand burning rate r_{b0} than propellant II with 200 μ AP. For example, at a pressure of 4 MPa, the strand burning rate of propellant I is 0.664 cm/s and that of propellant II is 0.43 cm/s. Previous studies^{5,9,12} have found that the strand burning rate of a propellant affects its erosive burning behavior. The present study shows that at a particular velocity, propellant II with lower strand burning rate is more sensitive to the erosive burning effect (see Fig. 9) than is propellant I, with higher strand burning rate. The higher erosive effect for propellant II compared to that of propellant I is believed to be caused by both the larger AP particle size and the lower strand burning rate of the propellant. The effect of strand burning rate on the erosive burning response of a propellant is also predicted by the turbulent boundary layer model.⁶

Measured burning rates for propellant I are plotted against pressure in Fig. 10. This plot was constructed so that a comparison could be made with King's data.⁵ King has represented most of his data on r_b vs p plots. A set of data points for different freestream velocities is shown in Fig. 10. The data points from King's work at an average test-section velocity of 305 m/s do not compare well with the data obtained from the present study at a freestream velocity of about 300 m/s. A possible reason for the discrepancy could be that the data reduction procedure used by King is quite different from that used in this study. It was found in our study that the error in reacing the instantaneous web thickness from the motion pictures could affect results significantly. Care was taken, with repeated film readings, to measure the web thickness with an accurate motion analyzer. Only a few data points are plotted in Fig. 10, owing to the difficulty of finding a larger number of data points for the burning rate at various pressures while at the same time keeping the freestream velocity constant.

Using the present erosive burning data, correlations similar to Eq. (7) were developed. The correlation coefficients for the three types of propellants investigated are listed in Table 2. It is noted that the functional form of Eq. (7) does not have the

Table 2 Correlation coefficients

Propellant type	I	II	III
$K, (\text{MPa})^{-n_p} (\text{m/s})^{-n_u}$	4.8×10^{-3}	3.167×10^{-4}	2×10^{-4}
n_p	0.35	1.463	0.705
n_u	0.69	1.42	1.252

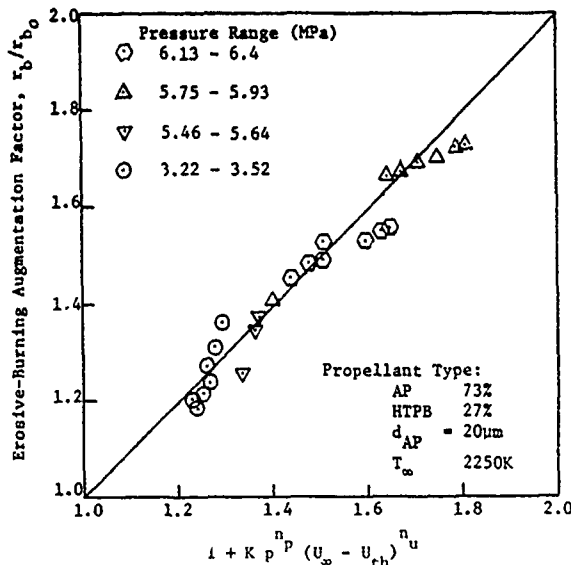


Fig. 11 Experimental data for erosive burning augmentation factor correlated with pressure and freestream velocity for propellant I.

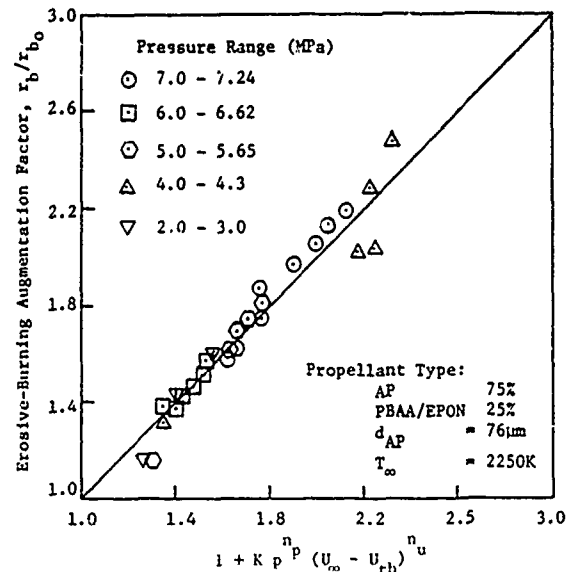


Fig. 13 Experimental data for erosive burning augmentation factor correlated with pressure and freestream velocity for propellant III.

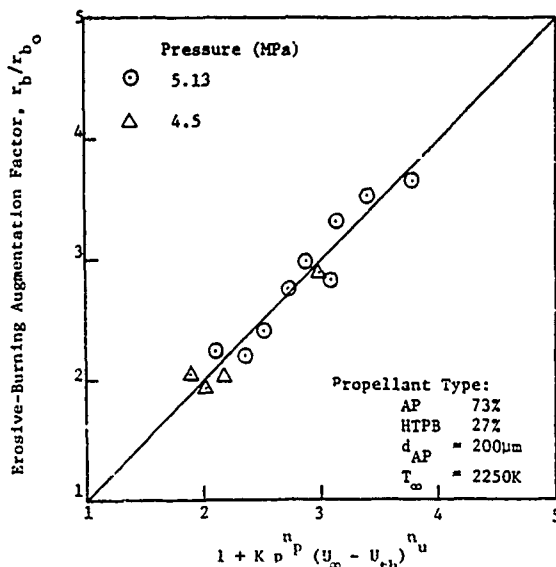


Fig. 12 Experimental data for erosive burning augmentation factor correlated with pressure and freestream velocity for propellant II.

dependence of erosive burning augmentation ratio r_b/r_{b0} on streamwise distance x . The burning rate was measured at three locations ($x = 3$ cm, 6 cm, and 9 cm) along the test propellant surface. A study of the data did not reveal any significant variation of the burning rate along the x direction. This observation was also made by viewing movies of the test firings in which the propellant surface remained horizontal as it burnt downwards. It is believed that the insignificant x -dependence of the burning rate is due to the fact that mass flow rate of gases over the test propellant samples in the experiments remained nearly constant. Contribution from a burning propellant sample mass flow rate was small in all experiments, typically about 6%. It is known from previous studies^{9,10} that the erosive burning rate of a solid propellant is strongly influenced by the mass flow rate of gases over the propellant surface. Therefore, with the gaseous mass flow rate nearly constant along the x coordinate, the change in burning rate is also insignificant.

The comparison of experimental data with erosive correlations for propellants I, II, and III are shown in Figs.

11-13, respectively. Most of the data points are very close to the 45 deg line on these plots. The results of Figs. 11-13 indicate that the correlation given in the form of Eq. (7) is suitable to represent the erosive burning rate data obtained for the three types of composite propellants studied. Such correlations can be used conveniently in the design considerations of a solid propellant rocket motor. The form of the correlations may serve as a guide for other types of composite propellants for which similar correlations can be developed.

V. Summary and Conclusions

An experimental apparatus for measuring the erosive burning rates of solid propellants under wide ranges of pressures and freestream velocities was designed and fabricated. The erosive burning behavior of three types of composite solid propellants was studied by burning test propellant slabs in turbulent boundary layers formed by the flow of hot combustion gases over the propellant samples. The burning rates at various pressures and freestream velocities were measured by a high-speed motion picture technique in which the burning propellant surface was photographed during test firing. The following observations and conclusions can be made from the present study:

- 1) The predicted results show that propellants with lower strand burning rates are more sensitive to erosive burning than those with higher strand burning rates.
- 2) The erosive burning effect becomes more pronounced when the oxidizer particle size of a composite propellant is increased.
- 3) The erosive burning rate correlates well with chamber pressure and freestream velocity. Correlations were developed from the measured burning rate data. Correlations of this type can be used in design considerations of a solid-propellant rocket motor.
- 4) The experimental data are in close agreement with predicted results obtained from the erosive burning model (based on the turbulent boundary layer approach) developed by the authors.

Acknowledgment

This report represents a part of the results of the research work performed under a subcontract from the Atlantic Research Corporation, the prime contractor for the Air Force Office of Scientific Research (Contract No. F49620-78-C-0016), under the management of Capt. R. F. Spelein. The

authors would like to acknowledge the processing of propellant samples arranged by D. George at AFRPL and by M. K. King at Atlantic Reserach Corporation. The assistance of R. L. Kovalcin, W. D. Jones, S. M. Kovacic, F. X. White, and J. G. Siefert of The Pennsylvania State University, is also acknowledged.

References

- ¹Kuo, K. K. and Razdan, M. K., "Review of Erosive Burning of Solid Propellants," *12th JANNAF Combustion Meeting*, CP1A Publication 273, Vol. 2, 1975, pp. 323-338.
- ²King, M. K., "Review of Erosive Burning Models," JANNAF Workshop on Erosive Burning/Velocity Coupling, Lancaster, Calif., March 7-8, 1977.
- ³Lenoir, J. M. and Robillard, G., "A Mathematical Method to Predict the Effects of Erosive Burning in Solid-Propellant Rockets," *Sixth Symposium (International) on Combustion*, Reinhold, New York, 1957, pp. 663-667.
- ⁴Vandenkerckhove, J. A., "Erosive Burning of a Colloidal Solid Propellant," *Jet Propulsion*, Vol. 28, Sept. 1958, p. 599-603.
- ⁵King, M. K., "Erosive Burning of Composite Solid Propellants: Experimental and Modeling Studies," *Journal of Spacecraft and Rockets*, Vol. 16, May-June 1979, pp. 154-162.
- ⁶Razdan, M. K. and Kuo, K. K., "Erosive Burning Study of Composite Solid Propellants by Turbulent Boundary-Layer Approach," *AIAA Journal*, Vol. 17, Nov. 1979, pp. 1225-1233.
- ⁷Beddini, R., "Reacting Turbulent Boundary-Layer Approach to Solid Propellant Erosive Burning," *AIAA Journal*, Vol. 16, Sept. 1978, pp. 896-895.
- ⁸Lengelle, J., "Model Describing the Erosive Combustion and Velocity Response of Composite Propellants," *AIAA Journal*, Vol. 13, March 1975, pp. 315-322.
- ⁹Green, L., Jr., "Erosive Burning of Some Composite Solid Propellants," *Jet Propulsion*, Vol. 24, Jan.-Feb. 1954, pp. 9-15.
- ¹⁰Kreidler, J. W., "Erosive Burning: New Experimental Techniques and Methods of Analysis," AIAA Paper 64-155, Palo Alto, Calif., Jan. 1964.
- ¹¹Peretz, A., "Investigation of the Erosive Burning of Solid-Propellant Grains with Variable Port Area by Means of Interrupted Burning Experiments," *AIAA Journal*, Vol. 6, May 1967, pp. 910-912.
- ¹²Marklund, T. and Lake, A., "Experimental Investigation of Propellant Erosion," *ARS Journal*, Vol. 3, Feb. 1960, pp. 173-178.
- ¹³Dickinson, L. A., Jackson, F., and Odgers, A. L., "Erosive Burning of Polyurethane Propellants in Rocket Engines," *Eighth Symposium (International) on Combustion*, Williams and Wilkins, Baltimore, 1962, pp. 754-759.
- ¹⁴Zucrow, M. J., Osborn, J. R., and Murphy, J. M., "An Experimental Investigation of the Erosive Burning Characteristics on a Non-Homogeneous Solid Propellant," AIAA Paper 64-107, Palo Alto, Calif., Jan. 29-31, 1964.
- ¹⁵Razdan, M. K., and Kuo, K. K., "Erosive Burning Studies of Composite Solid Propellants by the Reacting Turbulent Boundary-Layer Approach," AFOSR-TR-79-1155, Scientific Report to U.S. Air Force Office of Scientific Research, March 1979.
- ¹⁶Shapiro, A. H., *The Dynamics and Thermodynamics of Compressible Fluid Flow*, Vol. 1, Ronald Press, New York, 1953, pp. 83-95.
- ¹⁷Marquardt, D. W., "Least Square Estimation of Nonlinear Parameters," Engineering Dept., E. I. DuPont de Nemours and Co., Inc., Share Distribution No. 3094, 1965.

Sponsored By:

American Institute of Aeronautics and Astronautics (AIAA)

Society of Automotive Engineers (SAE)

American Society of Mechanical Engineers (ASME)

AIAA-80-1209
Turbulent-Flow Analysis and
Measurements of Erosive-
Burning Rates
of Composite Solid Propellants
M. K. Razdan and K. K. Kuo,
Pennsylvania State University,
University Park, Pa.

AIAA/SAE/ASME 16th
JOINT PROPULSION CONFERENCE

June 30-July 2, 1980/Hartford, Connecticut

TURBULENT-FLOW ANALYSIS AND MEASUREMENTS OF
EROSIVE-BURNING RATES OF
COMPOSITE SOLID PROPELLANTS

M. K. Razdan[§] and K. K. Kuo*
Department of Mechanical Engineering
The Pennsylvania State University
University Park, Pennsylvania

Abstract

An axisymmetric turbulent boundary layer was analyzed in order to investigate erosive burning in composite solid-propellant rocket motors. It was found that there is a strong interaction between the core-flow acceleration and turbulence level in the boundary layer. The increase of turbulence near the surface of the propellant plays an important role in the erosive-burning mechanism. Reducing the port diameter makes a rocket motor more sensitive to erosive burning. When the port diameter is uniform, the erosive-burning rate increases toward the aft end of a rocket motor. This trend is less pronounced or even reversed when the port diameter is divergent. Experimental measurements show that propellants at lower initial temperatures, and propellants with lower normal burning rates, are more sensitive to erosive burning.

I. Introduction

Interest in nozzleless and other high-performance rocket motors with low port-to-throat area ratios has stimulated the need for a better understanding of the erosive-burning characteristics of solid propellants. Crossflow gas velocity within these rocket motors can reach sonic and even supersonic speeds over some portions of the propellant surfaces, leading to high augmentation of the burning rate of a solid propellant. This augmentation, caused by the crossflow of gases, is referred to as the erosive-burning phenomenon.

Because previous studies on erosive burning, have been reviewed by Kuo and Razdan,¹ and King,² and a summary and classification of various erosive-burning theories has been presented by Razdan and Kuo,³ no literature review is given in this paper. A theoretical model, in which a chemically reacting two-dimensional turbulent boundary layer was analyzed to predict erosive-burning rates of composite solid propellants, was recently developed by the authors.³ Predicted results showed a close agreement with data obtained from the experimental study conducted by the authors.⁴ In the present work, the turbulent-flow analysis of the erosive-burning problem is performed for the axisymmetric flow of gases inside a cylindrical propellant grain. The analysis is limited to the combustion of commonly used ammonium perchlorate (AP) composite propellants burning in the turbulent boundary layer region of a rocket motor. It should be noted that the region of turbulent flow usually encompasses the major length of a rocket motor.

The objectives of the present study are: 1) to formulate a theoretical model for the erosive-burning problem of composite solid propellants by analyzing the flow in a cylindrical rocket motor; 2) to solve the theoretical model and to perform a parametric study of the effects of gas dynamic operating conditions on erosive burning; 3) to conduct erosive-burning tests on AP-based composite solid propellants; and 4) to correlate erosive-burning rate data in terms of flow variables.

II. Analysis

A. Description of Physical Model

The physical model considered in the theoretical analysis consists of an axisymmetric flow of gases inside a cylindrical solid propellant grain, as shown in Fig. 1. The gases form a turbulent boundary layer over the burning surface of the propellant. The analysis considers both developing and fully-developed regions of the flow which is assumed to be quasisteady and turbulent. The coordinate system used in the analysis is depicted in Fig. 1.

B. Conservation Equations

In the viscous flow region of the boundary layer, Reynolds' decomposition and time averaging procedure is used to develop conservation equations. A second-order two-equation K-ε turbulence model⁵ is used to achieve the closure of the turbulent flow problem. Major assumptions made in the analysis are: 1) averaged flow properties are steady; 2) mean flow is axisymmetric; 3) there is no reaction-generated turbulence; 4) the Lewis number is unity; and 5) Fick's law of diffusion is valid. Conservation equations of mass, momentum, species, enthalpy, turbulence kinetic energy, turbulence dissipation, and the equation of state are:

$$\frac{\partial}{\partial x} (\overline{r\rho u}) + \frac{\partial}{\partial r} (\overline{r\rho v}) = 0 \quad (1)$$

$$\text{where } \overline{\rho v} = \overline{\rho} \overline{v} + \overline{\rho'v'}$$

$$\overline{\rho} \overline{u} \frac{\partial \overline{u}}{\partial x} + \overline{\rho} \overline{v} \frac{\partial \overline{u}}{\partial r} = \frac{1}{r} \frac{\partial}{\partial r} [r \mu_{\text{eff}} \frac{\partial \overline{u}}{\partial r}] - \frac{d\overline{p}}{dx} \quad (2)$$

$$\overline{\rho} \overline{u} \frac{\partial \overline{y}_k}{\partial x} + \overline{\rho} \overline{v} \frac{\partial \overline{y}_k}{\partial r} = \frac{1}{r} \frac{\partial}{\partial r} [r (\frac{\mu}{Sc})_{\text{eff}} \frac{\partial \overline{y}_k}{\partial r}] + \overline{\omega}_k \quad (3)$$

[§]Assistant Professor, now employed as Research Engineer by Exxon Research and Engineering Co., Linden, N.J. Member AIAA.

*Associate Professor, Associate Fellow AIAA

$$\bar{\rho} \bar{u} \frac{\partial \bar{H}}{\partial x} + \bar{\rho} \bar{v} \frac{\partial \bar{H}}{\partial r} = \frac{1}{r} \frac{\partial}{\partial r} \left\{ r \left[\left(\frac{\mu}{Pr} \right)_{\text{eff}} \frac{\partial \bar{H}}{\partial r} + \left(\mu_{\text{eff}} - \left(\frac{\mu}{Pr} \right)_{\text{eff}} \right) \frac{\partial \bar{u}^2}{\partial r} \right] \right\} \quad (4)$$

$$\bar{\rho} \bar{u} \frac{\partial K}{\partial x} + \bar{\rho} \bar{v} \frac{\partial K}{\partial r} = \frac{1}{r} \frac{\partial}{\partial r} \left[r \left(\mu + \frac{\mu_t}{C_1} \right) \frac{\partial K}{\partial r} \right] + \mu_t \left(\frac{\partial \bar{u}}{\partial r} \right)^2 - \bar{\rho} \epsilon \quad (5)$$

$$\bar{\rho} \bar{u} \frac{\partial \epsilon}{\partial x} + \bar{\rho} \bar{v} \frac{\partial \epsilon}{\partial r} = \frac{1}{r} \frac{\partial}{\partial r} \left[r \left(\mu + \frac{\mu_t}{C_2} \right) \frac{\partial \epsilon}{\partial r} \right] + C_3 \mu_t \left(\frac{\partial \bar{u}}{\partial r} \right)^2 \frac{\epsilon}{K} - C_4 \bar{\rho} \frac{\epsilon^2}{K} \quad (6)$$

$$\bar{p} = \bar{\rho} R_u \bar{T} / W \quad (7)$$

Turbulent viscosity μ_t is expressed in terms of ϵ and ϵ as

$$\mu_t = C_\mu \bar{\rho} \frac{K^2}{\epsilon} \quad (8)$$

Various correlations have been modeled and replaced in Eqs. (2) - (5). These models were discussed by the authors in Ref. 3.

In the potential flow region of the developing flow, the following equations are considered for momentum and energy:

$$\rho_c U_c \frac{dU_c}{dx} = - \frac{d\bar{p}}{dx} \quad (9)$$

$$T_c = T_{tc} \left(1 + \frac{\gamma-1}{2} M_c^2 \right) \quad (10)$$

Equation (10) is a consequence of isentropic assumption. The centerline velocity U_c is calculated from Eq. (9), and the axial pressure gradient is calculated from the overall momentum balance, using the following equations:

$$- \frac{d\bar{p}}{dx} = \{ 2\pi R \tau_w + \frac{d}{dx} (\rho_b A U_b^2) \} / A \quad (11)$$

$$\frac{d}{dx} (\rho_b U_b A) = 2\pi R \rho_s r_b \quad (12)$$

Equation (12) is obtained from the overall mass balance inside a rocket motor. The pressure gradient expressed by Eq. (11) includes the effects of change in the flow area, and the change in bulk density ρ_b along x direction.

For chemical reactions in the gas phase, the following single-step forward reaction is assumed:



The reaction is assumed to be diffusion-controlled, and the reaction rate expression is based on the eddy-breakup model of Spalding.⁶⁻⁷ This expression, as discussed by the authors,³ can be written as

$$\bar{\omega}_F = - C_\omega \bar{\rho} \sqrt{K} \left| \frac{\partial \bar{Y}_F}{\partial r} \right| \quad (14)$$

The main restriction in using Eq. (14) is its applicability to a turbulent flow situation, which is the case in the present problem. With the assumption of Eq. (13), the species conservation equations are solved for \bar{Y}_F and $\bar{Y}_{OF} \equiv [\bar{Y}_O - (v_O W_O / v_F W_F) \bar{Y}_F]$. The introduction of the latter variable eliminates the nonlinear source term in the equation for \bar{Y}_{OF} .

C. Boundary Conditions

At the solid-gas interface, mass and energy balances lead to the following boundary conditions:

$$(\bar{\rho} \bar{v} \bar{Y}_O)_{r=R} - \rho_s r_b Y_{OS} + \left(\rho \mathcal{D} \frac{\partial \bar{Y}_O}{\partial r} \right)_{r=R} = 0 \quad (15)$$

$$(\bar{\rho} \bar{v} \bar{Y}_F)_{r=R} - \rho_s r_b Y_{FS} + \left(\rho \mathcal{D} \frac{\partial \bar{Y}_F}{\partial r} \right)_{r=R} = 0 \quad (16)$$

$$\lambda \left. \frac{\partial \bar{T}}{\partial r} \right|_{r=R} = \lambda_s \left. \frac{\partial T_p}{\partial r} \right|_{r=R} - \rho_s r_b [(C_p - C_s)(T_{ps} - \bar{T}_{ps}) + \bar{Q}_s] \quad (17)$$

where \bar{Q}_s , in Eq. (17), is defined (following Levine and Culick⁸) as the net surface heat release (negative for exothermic reactions) at a reference temperature \bar{T}_{ps} . The net heat flux to the solid propellant is obtained by integrating the heat conduction equation in the solid phase,

$$- \lambda_s \left. \frac{\partial T_p}{\partial r} \right|_{r=R} = (T_{ps} - T_{p1}) \rho_s C_s r_b \quad (18)$$

The burning rate of the solid propellant is expressed as a function of surface temperature through the use of the Arrhenius Law of surface pyrolysis:

$$r_b = A_s \exp \left(- \frac{E_{as}}{R_u T_{ps}} \right) \quad (19)$$

For K and ϵ equations, Eqs. (5) - (6), the following boundary conditions³ are applied:

$$K = \frac{(k \mathcal{D} y_w)^2}{\sqrt{C_\mu}} \left(\frac{\partial \bar{u}}{\partial r} \right)^2 \quad (20)$$

$$\epsilon = (k \mathcal{D} y_w)^2 \left| \frac{\partial \bar{u}}{\partial r} \right|^3 \quad (21)$$

These boundary conditions are applied near the propellant surface, rather than directly at the surface, to avoid the low turbulence-Reynolds-number region in which the application of K and ϵ equations is inappropriate (see Ref. 3). Turbulence viscosity μ_t close to the wall is calculated

from van Driest's formula as modified by Cebeci and Chang⁹ to include the effect of surface roughness:

$$\mu_t = \bar{\rho} (Dky_w)^2 \left| \frac{\partial u}{\partial r} \right| \quad (22)$$

$$\text{where } D \equiv 1 - \exp \left[- \frac{(y_w + \Delta y_w) \bar{\rho} u_*}{A^+ \mu} \frac{\tau}{\tau_w} \right] \quad (23)$$

$$\Delta y_w \equiv 0.9 \left(\frac{\mu}{\bar{\rho} u_*} \right) \left[\sqrt{R_h^+} - R_h^+ \exp(-R_h^+/6) \right] \quad (24)$$

$$R_h^+ \equiv \bar{\rho} u_* R_h / \mu \quad (25)$$

Other boundary conditions at the propellant surface ($r=R$) are

$$\bar{u} = 0, \bar{T} = \bar{T}_{ps}, \bar{v} = \rho_s r_b / \bar{\rho}(x, R) \quad (26)$$

and at the edge of the boundary layer ($y=0$) are

$$\bar{u} = U_c, \bar{T} = T_c, \bar{Y}_F = \bar{Y}_O = 0, \frac{\partial K}{\partial r} = \frac{\partial \epsilon}{\partial r} = 0 \quad (27)$$

D. Numerical Method

The coordinate transformation and numerical scheme proposed by Patankar and Spalding¹⁰ was used in this study. Solutions of the differential equations were obtained by numerically integrating the equations along the transverse direction, while marching forward along the x direction (see Ref. 11 for details). About half of the 100 cross-stream intervals employed were distributed within 10% of the boundary-layer thickness, where the dependable variables change rapidly. Because of strong interaction between the potential core and the viscous boundary layer caused by the axial pressure gradient, a small forward step was taken along the x direction, typically about 0.2 times the boundary layer thickness. The size of this step was reduced during the forward marching computation if changes in U_c and T_c calculations from Eqs. (9) - (10) exceeded specified limits. Iterations of the boundary-layer solutions were performed to obtain convergence on the surface temperature. The maximum allowable error in the convergence of the surface temperature was set at 0.01 percent.

III. Theoretical Results

A. Physical Properties Used in Calculations

Theoretical solutions were obtained for a composite propellant composed of 75% Ammonium Perchlorate and 25% PBAA/EPON by weight. Various physical properties used in the calculations, and the references from which some of the properties were taken, are listed in Table 1. The procedure followed in obtaining some of the parameters associated with the global single-step forward reaction has been discussed in detail in Ref. 3. Values of the constants used in the turbulence modeling are given in Table 2, and sources of the constants are given in Ref. 3.

Computations were started at a preselected downstream x location, and the starting profiles for velocity and turbulent kinetic energy and

dissipation were obtained by using the same equations used by Chambers and Wilcox.¹² The initial centerline velocity was varied for the parametric study.

Table 1. Properties Used in Theoretical Calculations

$a = 0.245 \text{ cm/s}/(\text{MPa})^n$	$A_s = 5.65 \text{ m/s}$
$A^+ = 26$ (Ref. 13)	$C_s = 0.3 \text{ kcal/kg-K}$
$C_p = 0.3 \text{ kcal/kg-K}$	$E_{as} = 15 \text{ kcal/mole}$
$\Delta h_{f,F}^\circ = 55.9 \text{ kcal/kg}$	$\Delta h_{f,0}^\circ = -942 \text{ kcal/kg}$
$\Delta h_{f,p}^\circ = -1137.3 \text{ kcal/kg}$	$k = 0.41$
$n = 0.41$	$Pr = \gamma/(1.77\gamma - 0.45)$ Svehla's eq. ¹⁴
$Pr_t = 0.9$ (Ref. 15)	$\bar{Q}_s = -250 \text{ kcal/kg}$
$Sc = Pr$	$Sc_t = 0.9$
$T_{pi} = 298\text{K}$	$\bar{T}_{ps} = 800\text{K}$
$W_F = 30 \text{ kg/kmole}$	$W_o = 27.9 \text{ kg/kmole}$
$W_p = 20.4 \text{ kg/kmole}$	$Y_{FS} = 0.25$
$Y_{OS} = 0.75$	$\gamma = 1.26$
$\lambda = C_p \mu / Pr \text{ kcal/m-s-K}$	$\mu_k = 8.7 \times 10^{-8} \sqrt{W_k} T^{0.65}$ (Ref. 13)
$v_F = 1 \text{ kmole}$	$v_o = 3.23 \text{ kmole}$
$v_p = 5.9 \text{ kmole}$	$\rho_s = 1600 \text{ kg/m}^3$

Table 2. Constants Used in Turbulence Modeling

Constants	C_1	C_2	C_3	C_4	C_w	C_μ
Values	1.0	1.3	1.57	2.0	0.18	0.09

B. Results and Discussion

Figure 2 shows the calculated distributions of velocity (nondimensionalized with initial centerline velocity) at various distance-to-diameter ratios, x/D . Velocity gradient increases with the downstream distance, since the flow inside the rocket motor is accelerating because of a strong favorable pressure gradient. At $x/D = 30$, the flow is within the fully-developed region. The kinetic energy and Reynolds' stress profiles at the corresponding x/D stations are shown in Fig. 3. Since the velocity gradient increases with distance x , a corresponding increase occurs in both K and $u'v'$ with increasing x . Figure 3 also shows that the distance between the peak turbulent kinetic energy and the propellant surface decreases as the flow accelerates in the downstream direction. This was also observed in the simulative study of erosive burning made by Yamada et al.¹⁶ Thus, with increasing distance x , more turbulence activity occurs closer to the propellant surface, enhancing the diffusion processes and the reaction rate, Eq. (14), near the surface.

The increased reaction rate effect is evident from the results plotted in Fig. 4, which shows the

IV. Experimental Study

A. Burning-Rate Measuring Technique

Although this paper deals with the analysis of the erosive burning of a cylindrical propellant grain, it is important to note the difficulty in measuring erosive burning rates in cylindrical propellant grains directly. Most of the literature available on erosive burning of cylindrical grains is based upon indirect data reduction procedures of measured pressure-time traces.

The purpose of the present erosive-burning experiments, which were conducted on flat AP-based composite propellant test samples, was to compare the erosive-burning predictions of a two-dimensional theoretical model⁵ with the experimental data obtained with propellants burning under two-dimensional flow situations. The details of the results obtained for a number of propellants can be found in Ref. 4. In this paper, experimental results obtain with a different composite propellant are reported.

Experiments were conducted in a test rig consisting of a driving motor and a test chamber. A star-shaped solid propellant grain was used to generate hot combustion gases which flow through a nozzle into the test chamber. The test chamber contains a stainless steel leading edge element to which a two-dimensional test propellant slab was glued. The test propellant was ignited by the hot combustion gases which formed a turbulent boundary layer over the burning surface of the propellant. The burning rate of the propellant was measured by a high-speed motion picture method. Using high-speed motion pictures (~1500 frames/sec) taken during a test firing, the burning process of a test propellant was observed through a plexiglass window. The film was analyzed, frame by frame, on a motion analyzer to calculate the distance burned in a known time interval. A regression analysis of the readings taken from the motion analyzer was made to evaluate the burning rate. Detailed description of the experimental setup, instrumentation, and data reduction procedure can be found in Ref. 4.

B. Experimental Results

Erosive-burning tests were conducted with a propellant designated by (IV), which has a composition of 72% AP, 26% HTPB, and 2% Fe_2O_3 by weight, with an average AP particle size of 20 μm . This propellant is the same as that used by King¹⁸ (propellant formulation designated by King as 4869). Propellant (IV) has a pre-exponent in the strand-burning-rate law equal to 0.725 $cm/s/(MPa)^n$, a pressure exponent equal to 0.385, a flame temperature equal to 1667K, and a propellant density equal to 1519.5 kg/m^3 .

Figure 10 shows the measured total burning rate plotted against freestream velocity at different pressures. Two sets of data are shown in Fig. 10, corresponding to tests conducted at two initial propellant temperatures, $T_{pi} = 7.8^\circ C$ and $14.4^\circ C$. The tests made under a low initial propellant temperature were conducted in cold weather conditions by allowing the test apparatus and the propellant sample to reach a thermal equilibrium with the surrounding atmosphere. Sufficient time (> 4 hours) was allowed for thermal equilibrium to be reached. Figure 10 shows that the erosive effect is stronger in the case of the low T_{pi} propellant. It should be noted that the data obtained in the two cases is not at the same pressure. The two sets of data differ in pressure by about 2 MPa, which corresponds

calculated distribution of fuel and oxidizer mass fractions, and the rate of heat generation in the gas phase near the propellant surface. With the increase in x/D , the peak value of the heat generation rate increases in magnitude and its location becomes closer to the propellant surface. This indicates a strong interaction between turbulence and the gas-phase reaction rate. Due to the higher reaction rate at $x/D = 30$, as compared to that at $x/D = 15$ in Fig. 4, the mass fractions of both fuel and oxidizer species decrease faster in the direction away from the propellant surface. The temperature gradient steepens as a consequence of the increase in the reaction rate; this can be seen from the calculated temperature distributions plotted near the propellant surface in Fig. 5 at various x/D values. Higher temperature gradient with increasing x/D means higher gas-to-solid heat flux, and, therefore, increased burning rate as x/D increases.

The erosive-burning augmentation factor, r_b/r_{b0} , is plotted as a function of x for different port diameters of a rocket motor in Fig. 6. It is seen that r_b/r_{b0} increases as x increases. Figure 6 also shows the variation of pressure and centerline velocity with distance x . With a favorable pressure gradient, the pressure decreases while the centerline velocity increases. The results given in Fig. 6 also indicate that decreasing the port diameter causes r_b/r_{b0} to increase. However, because this increase is caused by the changes in both port diameter and x location (centerline velocity), in order to emphasize the port diameter effect, results of r_b/r_{b0} are plotted in Fig. 7 as a function of port diameter for a number of fixed centerline velocities. In this way, the effect of x -variation of U_c on r_b/r_{b0} is eliminated, and the port diameter effect is isolated. The results again show that decrease in port diameter makes a rocket motor more sensitive to erosive burning. This conclusion is in agreement with the study conducted by Beddini.¹⁷

The effect of nonuniform diameter along x on the erosive-burning augmentation factor is shown in Fig. 8. The results have been plotted for $\tan \alpha = 0, 0.01, \text{ and } 0.015$, where α is the divergence angle of the rocket motor grain (see Fig. 1). As is well-known, the erosive-burning effect is usually strong in the initial burning phase of a rocket motor when the diameter is nearly uniform. This corresponds to $\tan \alpha = 0$ in Fig. 8 (D being constant along x); r_b/r_{b0} increases significantly as the flow accelerates in the x direction. However, when $\tan \alpha > 0$, r_b/r_{b0} behavior changes significantly along s , as depicted in Fig. 8. With $\tan \alpha = 0.01$, there is less acceleration and, therefore, the erosive-burning effect remains more or less constant as x increases. With $\tan \alpha = 0.015$, r_b/r_{b0} is seen to decrease as x increases; this is due to the effects of the thickening boundary layer. In sharp contrast to the effect of acceleration, the effect of thickening boundary layer is to reduce r_b/r_{b0} . Therefore, depending upon the grain geometry, the erosive-burning effect could either increase or decrease in the axial direction toward the aft end of a rocket motor.

Figure 9 shows the effect of propellant surface roughness on the erosive-burning augmentation factor. Increasing the height of the roughness increases the augmentation factor. This is consistent with the experimental study conducted by the authors,⁴ which showed a larger erosive-burning effect on a composite propellant with larger AP particle size and, therefore larger surface roughness.

to about a 14% difference in r_{b0} . However, total burning rates for the two sets of data under erosive-burning conditions (at $U_{\infty} = 350$ m/s) differ by about 26%. Thus, the additional erosive-burning contribution can be considered to be the result of lowering T_{pi} .

The effect of normal burning rate on the erosive-burning augmentation factor is shown in Fig. 11 for two similar propellants differing only in r_{b0} . Propellant (I) (AP/HTPB/73/27,20 μ MAP) has a lower normal burning rate of 0.687 cm/s at a pressure of 4.25 MPa, while propellant (IV) has a higher normal burning rate equal to 1.265 cm/s at the same pressure. The propellant (I) with lower r_{b0} is more sensitive to erosive-burning. Other researchers¹⁷⁻¹⁹ have reported similar findings.

Using the measured experimental data, correlation between the erosive-burning augmentation factor, freestream velocity, and pressure was developed. A nonlinear regression analysis of the data was used to obtain the correlation coefficients. Comparison of the experimental data with erosive-burning correlation is shown in Fig. 12. Most of the data are close to the 45° line. Values of the correlation coefficients are given in Fig. 12. Although a term for threshold velocity U_{th} is included in the correlation for generalization, no significant threshold velocity was observed in the present tests. It should also be noted that due to limited data as a function of T_{pi} , a suitable correlation could not be found to include the T_{pi} effect. The correlation represented in Fig. 12 is for $T_{pi} = 14.4^{\circ}\text{C}$. It is hoped that in the near future data will be obtained at a number of different initial temperatures, and that the T_{pi} effect can then be included in the erosive-burning correlation.

V. Summary and Conclusions

1. The problem of erosive burning of composite solid propellants was modeled by considering an axisymmetric turbulent boundary layer inside a rocket motor. The theoretical model was solved numerically, and a parametric study for the effect of a number of important variables was conducted.
2. The erosive-burning augmentation factor increases with the increase in axial distance when the port diameter of the rocket motor is uniform (representing an initial time period immediately following the ignition in a rocket motor). For a nonuniform (diverging) port diameter, the augmentation factor increases at a lesser rate, and even decreases with increasing x if divergence is large.
3. Rocket motors with a smaller port diameter are more sensitive to erosive burning than those with larger diameters.
4. Surface roughness increases the erosive-burning effect of a composite solid propellant.
5. Mechanism of erosive burning is believed to be caused by increased turbulence activity near the propellant surface as the axial velocity outside the boundary layer is increased. The increased turbulence activity increases both the diffusion process and the reaction rate with gas phase near the propellant surface.

6. Experimental measurements show a propellant with a lower initial temperature is more sensitive to erosive burning. Propellants with a lower normal burning rate are also more sensitive to erosive burning.

Acknowledgements

This work represents a part of the research performed under a subcontract from the Atlantic Research Corporation which is the prime contractor for the Air Force Office of Scientific Research, Contract No. F49620-78-C-0016, under the management of Dr. L. H. Caveny. The authors would like to acknowledge the arrangements made by Dr. D. George at AFRPL and Dr. M. K. King at Atlantic Research Corporation for propellant samples. The assistance of R. Arora, F. X. White, and J. G. Siefert of The Pennsylvania State University is acknowledged.

Nomenclature

a	Pre-exponent in strand-burning-rate law, (cm/s)/(MPa) ^{1/2}
A	Cross-section flow area
A _s	Arrhenius frequency factor in propellant surface decomposition, m/s
A ⁺	Damping constant in van Driest's hypothesis
C ₁ -C ₄ , C _μ , C _ω	Constants in turbulence models
C _p	$\equiv \sum_k Y_k C_{pk}$, average heat capacity of reacting gases, Kcal/Kg-K
C _{pk}	Heat capacity of k th species, Kcal/Kg-K
C _s	Heat capacity of solid propellant, Kcal/Kg-K
d _{AP}	Average diameter of Ammonium Perchlorate Particles, m
D	Port diameter of rocket motor
D	Diffusion coefficient in Fick's Law, m ² /s
D	Damping coefficient defined in Eq. (23)
E _{as}	Activation energy in propellant surface decomposition, Kcal/mole
Δh _{f,k} ^o	Heat of formation of k th species, Kcal/Kg
h _k	$\equiv \Delta h_{f,k}^o + \int_{T_0}^{T_c} C_{pk} dT$, static enthalpy of k th species, Kcal/Kg
H	$\equiv \sum_k Y_k h_k + u_1 u_1 / 2$, stagnation enthalpy of gases, Kcal/Kg
κ	Von Karman's constant
K	$\overline{u_1' u_1' / 2}$, Turbulent kinetic energy, m ² /s ²

Nomenclature (Con't)			
K_e	Constant in erosive-burning rate correlation, $(\text{MPa})^{-n_p} (\text{m/s})^{-n_u}$	v	Gas velocity in y-direction, m/s
M	Mach number	W	$\equiv (\sum_k Y_k / W_k)^{-1}$, average molecular weight of gases, Kg/Kmole
n	Exponent in strand-burning-rate law	W_k	Molecular weight of k^{th} species, Kg/Kmole
n_p	Pressure exponent in erosive burning-rate correlation	x	Coordinate in axial direction, m
n_u	Velocity exponent in erosive-burning-rate correlation	y	Coordinate normal to propellant surface, m
p	Pressure, N/m^2	y_w	$\equiv R-y$, coordinate with its origin on propellant surface, m
Pr	$\equiv C_p \mu / \lambda$, Prandtl number based upon molecular properties of fluid	Y_k	Mass fraction of k^{th} species
Pr_t	Prandtl number for turbulent flow	Y_{FS}	Mass fraction of fuel in a composite solid propellant
\dot{Q}_r	$\equiv \frac{1}{v_F W_F} \sum_k v_k W_k \Delta h_{f,k}^{\circ} \bar{\omega}_k$, Rate of heat generation in gas phase, $\text{Kcal/m}^3\text{-s}$	Y_{OS}	Mass fraction of oxidizer in a composite solid propellant
r	Coordinate in radial direction	$(\bar{\quad})$	Time averaged quantity
r_b	Total burning rate of a solid propellant, m/s	$(\quad)'$	Fluctuating quantity
r_{b_o}	Strand burning rate of a solid propellant, m/s	$(\quad)_{,i}$	Partial differentiation of quantity in (\quad) with respect to x_i , $(\quad)/m$
R	Port radius of rocket motor	<u>Greek Symbols</u>	
R_h	Roughness height, m	α	Angle of divergence of port radius
R_u	Universal gas constant, N-m/Kmole-K	δ	Boundary layer thickness, m
Sc	$\equiv \mu / \rho D$, Schmidt number based upon molecular properties of fluid	ϵ	$\equiv \mu \overline{u'_{i,j} u'_{i,j}} / \rho$, Turbulent dissipation, m^2/s^3
Sc_t	Schmidt number for turbulent flow	γ	Ratio of constant-pressure and constant-volume specific heats
T	Temperature, K	λ	Thermal conductivity of gas, Kcal/m-s-K
T_{ci}	Initial centerline temperature, K	λ_s	Thermal conductivity of solid propellant, Kcal/m-s-K
T°	Reference temperature, 298.14 K	μ	Gas viscosity, Kg/m-s
T_p	Propellant temperature, K	μ_{eff}	$\equiv \mu + \mu_t$, Effective viscosity, Kg/m-s
T_{pi}	Propellant initial temperature, K	μ_t	Turbulent viscosity defined in Eq. (8), Kg/m-s
T_{ps}	Propellant surface temperature, K	$(\frac{\mu}{Pr})_{\text{eff}}$	$\equiv \frac{\mu}{Pr} + \frac{\mu_t}{Pr_t}$, Kg/m-s
T_{ci}	Initial stagnation temperature, K	$(\frac{\mu}{Sc})_{\text{eff}}$	$\equiv \frac{\mu}{Sc} + \frac{\mu_t}{Sc_t}$, Kg/m-s
\bar{T}_{ps}	Reference surface temperature of propellant, K	v_k	Number of Kmoles of k^{th} species
u	Gas velocity in x-direction, m/s	ρ	Gas density, Kg/m^3
U	Axial velocity outside boundary layer, m/s	ρ_s	Solid propellant density, Kg/m^3
U_{ci}	Initial centerline velocity, m/s	τ	$\equiv \mu_{\text{eff}} \partial \bar{u} / \partial y$, Local shear stress, N/m^2
U_{th}	Threshold velocity, m/s	$\dot{\omega}_k$	Rate of Production of species k due to chemical reactions, $\text{Kg/m}^3\text{-s}$
u_*	$\equiv \sqrt{\tau_w / \rho_{\infty}}$, Friction velocity, m/s		

Subscripts

- b Bulk or averaged variable
- c Centerline condition
- k Species index representing fuel gas [F], oxidizer gas [O], and product gas [P]
- ∞ Freestream condition
- w Wall (propellant surface) condition

References

1. Kuo, K. K. and Razdan, M. K., "Review of Erosive Burning of Solid Propellants," 12th JANNAF Combustion Meeting, CPIA Publication 273, Vol. 11, 1975, pp. 323-338.
2. King, M. K., "Review of Erosive Burning Models," JANNAF Workshop on Erosive Burning/Velocity Coupling, Lancaster, CA, March 1977.
3. Razdan, M. K. and Kuo, K. K., "Erosive Burning Study of Composite Solid Propellants by Turbulent Boundary-Layer Approach," AIAA Journal, Vol. 17, Nov. 1979, pp. 1225-1233.
4. Razdan, M. K. and Kuo, K. K., "Experimental Measurements of Erosive Burning Rates of Composite Solid Propellants," AIAA Paper No. 79-1172, AIAA/SAE/ASME 15th Joint Propulsion Conference, June 18-20, 1979, Las Vegas, Nevada (accepted for publication in AIAA Journal).
5. Launder, B. E. and Spalding, D. B., Mathematical Models of Turbulence, Academic Press, New York, 1972, p. 9.
6. Spalding, D. B., "Mixing and Chemical Reaction in Steady Confined Turbulent Flames," Thirteenth Symposium (International) on Combustion, Combustion Institute, 1971, pp. 649-657.
7. Mason, H. B. and Spalding, D. B., "Prediction of Reaction Rates in Turbulent Pre-Mixed Boundary Layer Flows," Combustion Institute, First European Symposium, 1975, pp. 601-606.
8. Levine, J. N. and Culick, F. E. C., "Nonlinear Analysis of Solid Rocket Combustion Instability," AFRPL-TR-74-45, Final Report, Vol. I, 1974.
9. Cebeci, T. and Chang, K. C., "Calculation of Incompressible Rough-Wall Boundary-Layer Flows," AIAA Journal, Vol. 16, July 1978, pp. 730-735.
10. Pantankar, S. V. and Spalding, D. B., Heat and Mass Transfer in Boundary Layers, Inter-text Books, London, 1970.
11. Razdan, M. K. and Kuo, K. K., "Turbulent Boundary-Layer Analysis and Experimental Investigation of Erosive Burning Problem of Composite Solid Propellants," AFOSR-TR-79-1155, Scientific Report to U.S. Air Force Office of Scientific Research, March 1979.
12. Chambers, T. L., and Wilcox, D. C., "Critical Examination of Two-Equation Turbulence Closure Models for Boundary Layers," AIAA Journal, Vol. 15, June 1977, pp. 821-828.
13. Van Driest, E. R., "On Turbulent Flow Near a Wall," Journal of the Aeronautical Sciences, Vol. 23, pp. 1007-1011, 1956.
14. Peretz, A., Kuo, K. K., Caveny, L. H., and Summerfield, M., "Starting Transient of Solid Propellant Rocket Motors with High Internal Gas Velocities," AIAA Journal, Vol. 11, Dec. 1973, pp. 1719-1727.
15. Kays, W. M., "Heat Transfer to the Transpired Turbulent Boundary Layer," International Journal of Heat Mass Transfer, Vol. 15, May 1972, pp. 1023-1044.
16. Yamada, K., Goto, M., and Ishikawa, N., "Simulative Study on the Erosive Burning of Solid Rocket Motors," AIAA Journal, Vol. 14, Sept. 1976, pp. 1170-1177.
17. Beddini, R. A., "Reacting Turbulent Boundary-Layer Approach to Solid Propellant Erosive Burning," AIAA Journal, Vol. 16, Sept. 1978, pp. 898-905.
18. King, M. K., "Erosive Burning of Composite Solid Propellants: Experimental and Modeling Studies," Journal of Spacecraft and Rockets, Vol. 16, May-June, 1979, pp. 154-162.
19. Green, L., Jr., "Erosive Burning of Some Composite Solid Propellants," Jet Propulsion, Vol. 24, Jan.-Feb. 1954, pp. 9-15.
20. Marklund, T. and Lake, A., "Experimental Investigation of Propellant Erosion," ARS Journal, Vol. 3, Feb. 1960, pp. 173-178.

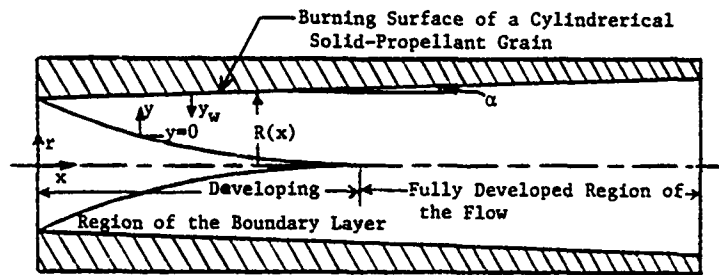


Fig. 1 Physical Model Considered in the Theoretical Formulation.

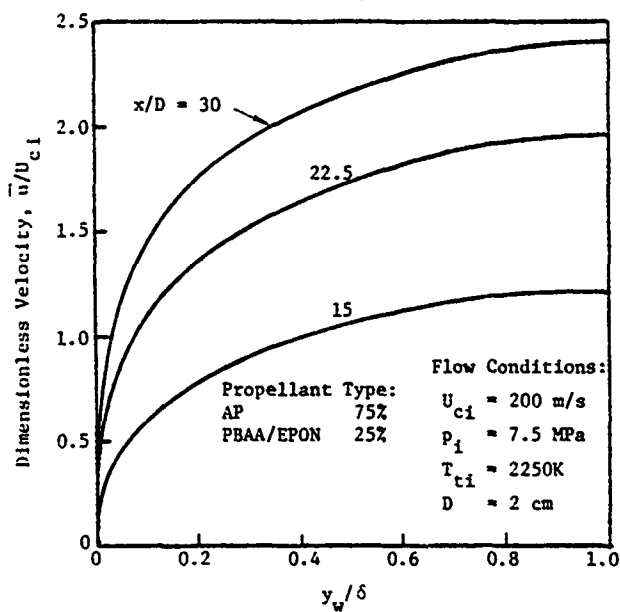


Fig. 2 Calculated Velocity Distributions in the Boundary Layer at Various Axial Locations

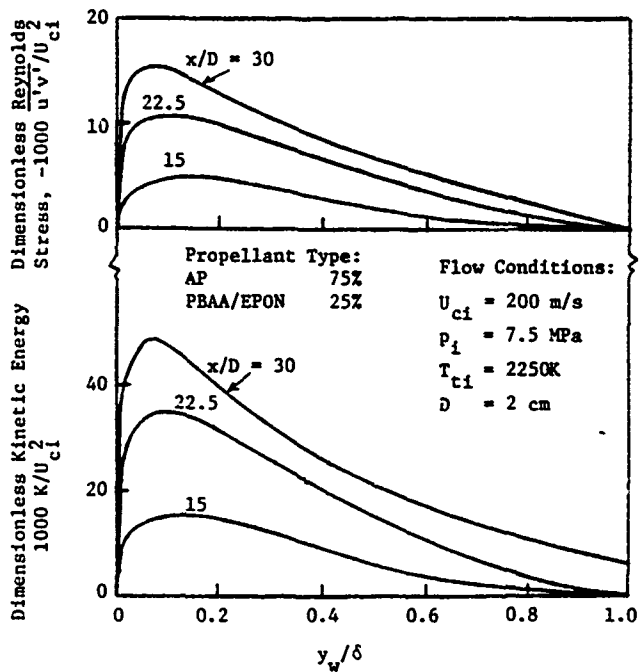


Fig. 3 Calculated Distributions of Turbulent Kinetic Energy and Reynolds Stress in the Boundary Layer at Various Axial Locations

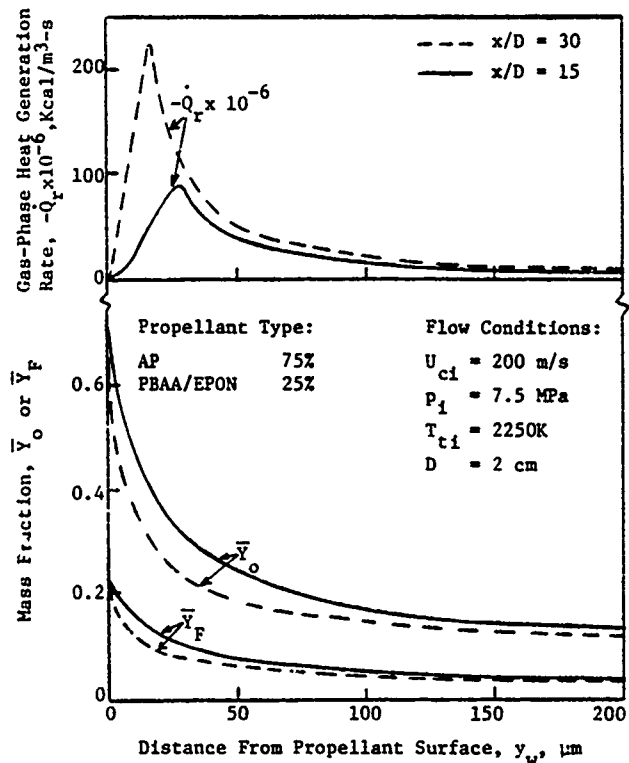


Fig. 4 Calculated Distribution of Oxidizer and Fuel Mass Fractions, and the Rate of Heat Generation in the Gas Phase Near the Propellant Surface

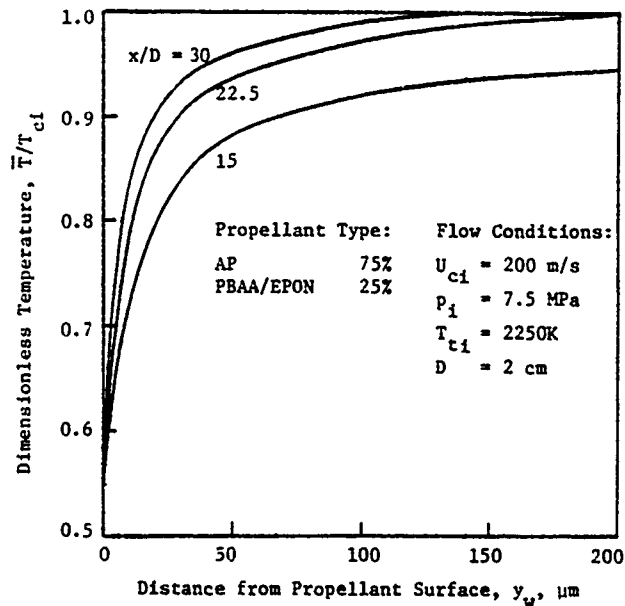


Fig. 5 Calculated Temperature Distributions Near the Propellant Surface at Different Axial Locations

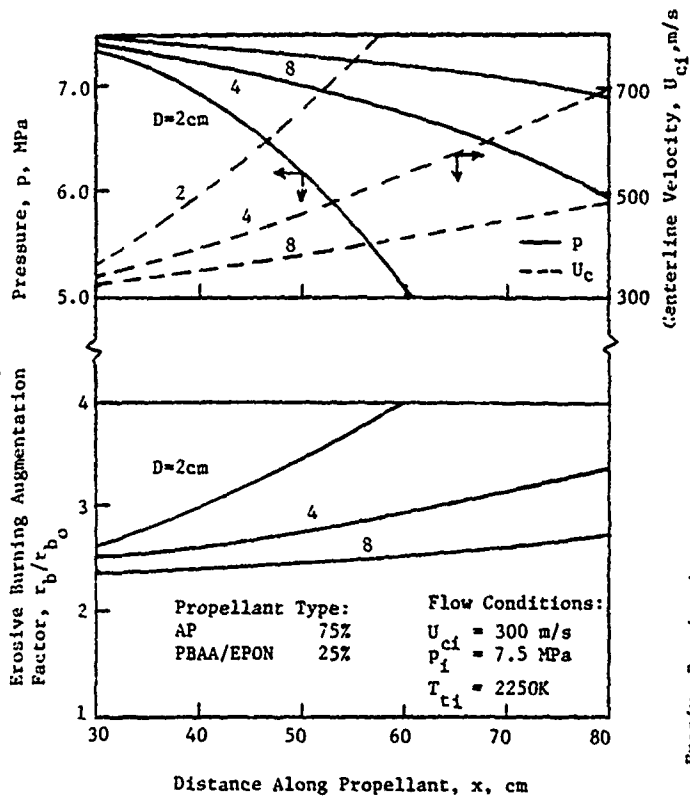


Fig. 6 Calculated Variations of Pressure, Centerline Velocity, and Erosive Burning Augmentation Factor Along Axial Direction for Different Port Diameters of Rocket Motors

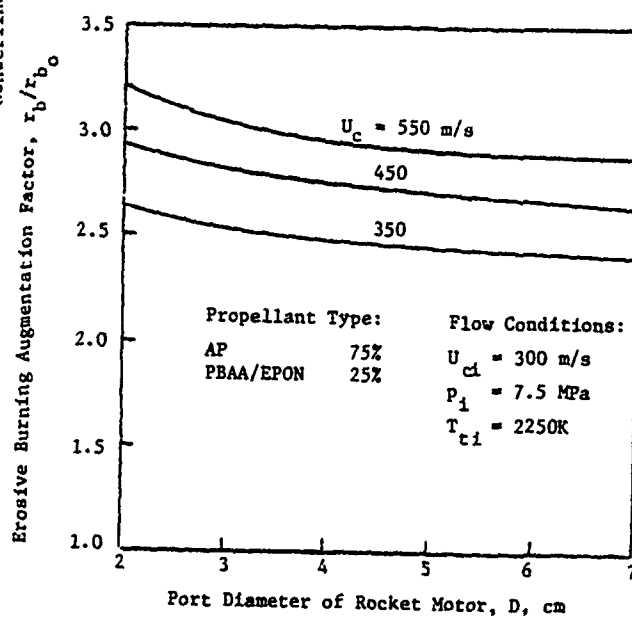


Fig. 7 Effect of Port Diameter on Erosive Burning Augmentation Factor at Different Centerline Velocities

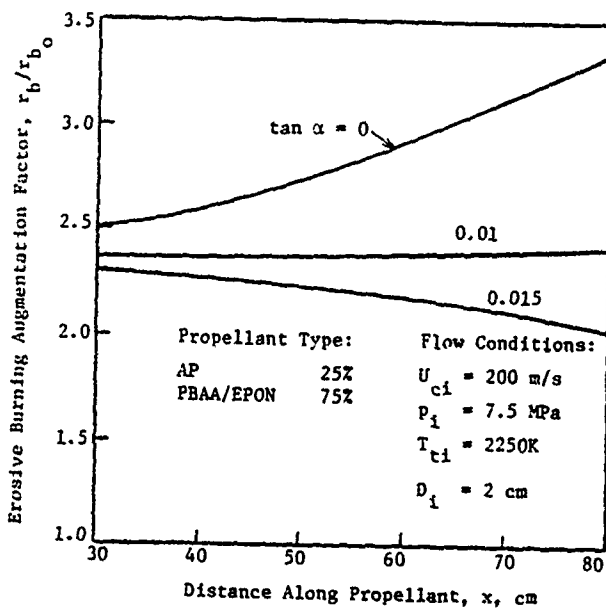


Fig. 8 Effect of Nonuniform Port Diameter on Erosive Burning Augmentation Factor

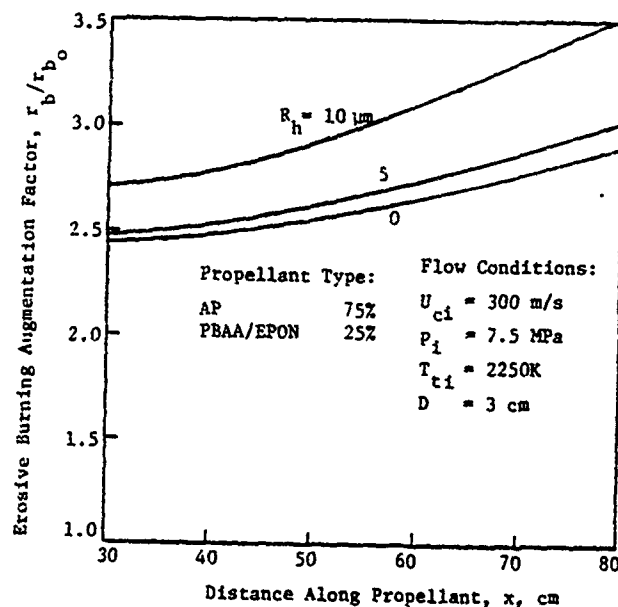


Fig. 9 Calculated Erosive Burning Augmentation Factor Showing the Effect of Propellant-Surface Roughness

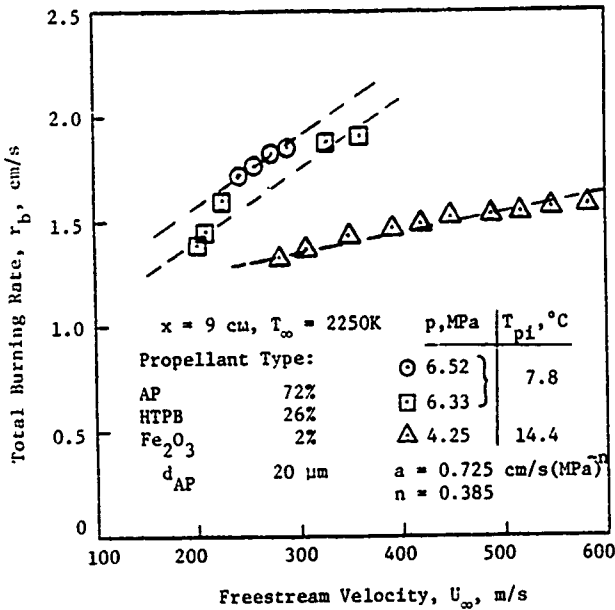


Fig. 10 Measured Burning Rates at Various Pressures and Freestream Velocities for Two Different Initial Temperatures of the Propellant (IV).

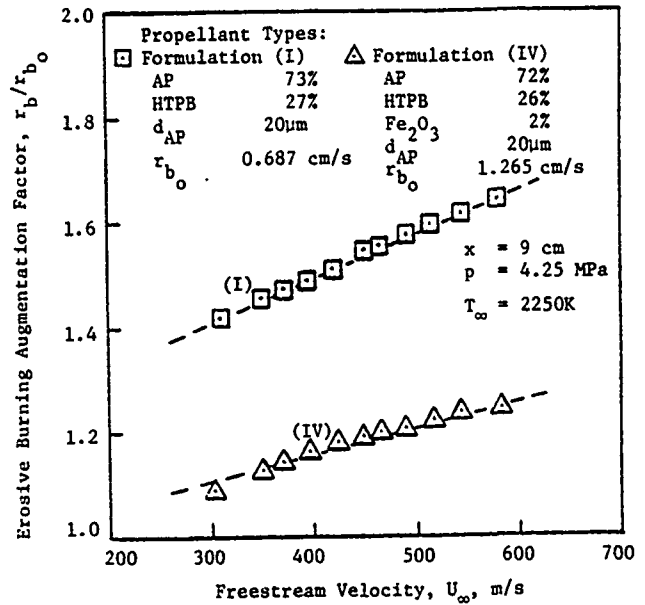


Fig. 11 Effect of Normal Burning Rate on the Erosive Burning Augmentation Factor

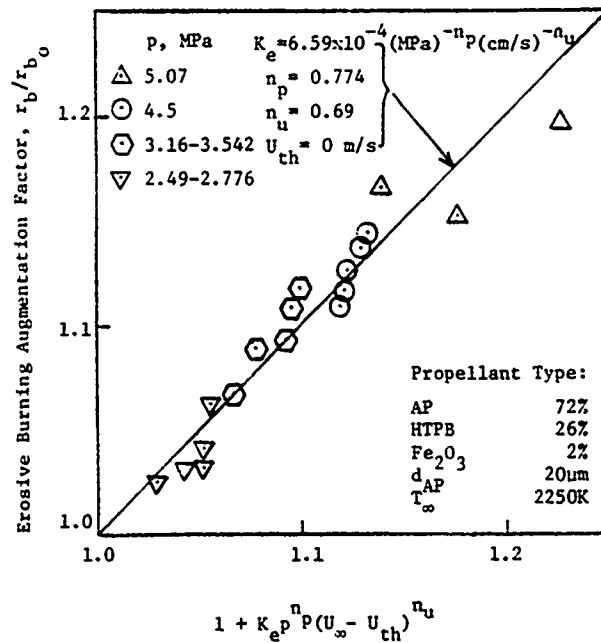


Fig. 12 Experimental Data for Erosive Burning Augmentation Factor Correlated with Pressure and Freestream Velocity for Propellant (IV)

APPENDIX F

Technical Paper on Erosive Burning
Modeling Generated at ARAP



AIAA 78-977R

**Aerothermochemical Analysis of Erosive
Burning in a Laboratory Solid-Rocket Motor**

R. A. Beddini

Reprinted from

AIAA Journal

Volume 18, Number 11, November 1980, Page 1346

Copyright American Institute of Aeronautics and Astronautics, Inc., 1978. All rights reserved

Aerothermochemical Analysis of Erosive Burning in a Laboratory Solid-Rocket Motor

Robert A. Beddini*

Aeronautical Research Associates of Princeton, Inc., Princeton, N.J.

An analysis of steady-state combustion and flow phenomena in a two-dimensional, laboratory-type solid-propellant motor is presented with emphasis on the condition of erosive burning. The problem is treated as a confined, reacting turbulent shear-flow using a second-order turbulence closure model. Low Reynolds number and propellant surface roughness effects are accounted for. Comparison of calculated results with cold flow experimental data confirms that development of the mean velocity profile is initially well described by laminar, "inviscid" theory. However, due to the rapid development of turbulence within the simulated grain-port, transition to a turbulent velocity profile is predicted to occur at center port Reynolds numbers greater than those obtained in the considered experiments. Transition of the velocity profile is theoretically found to occur prior to the onset of erosive burning in real motor environments. Comparisons of calculated results with measured static pressure distributions have been made for a composite-propellant "slab" motor. Good agreement with static pressure data is obtained for propellant roughness heights which are approximately 10% of the larger AP crystal diameters, with surface roughness significantly affecting erosive burning. Theoretical comparison with the Lenoir-Robillard model also indicates that the present model predicts a much more rapid decrease in erosive burning as the port hydraulic radius is increased.

Nomenclature

A	= Arrhenius pre-exponential coefficient
a, b	= turbulence modeling parameters (3.25, 0.125)
B_s	= effective reaction rate coefficient
c_p	= specific heat at constant pressure
c_r	= specific heat of propellant
D	= overall diffusion coefficient
g_{tm}	= metric tensor, $\partial x_i / \partial x_m$
h	= specific sensible enthalpy, $c_p T$
h_α^0	= heat of formation at 0 K
H	= total enthalpy, $H = h + u^i u_i / 2$
k	= thermal conductivity
k_s	= equivalent sand roughness height
L_s^0	= heat of decomposition at 0 K
\dot{m}_s	= surface mass flux
n	= normal burning rate pressure exponent
n_j	= surface normal vector
p	= static pressure
p^*	= reference pressure, 6.9×10^7 dyne/cm ² (1000 psi)
q	= rms intensity, $(u'^i u'^i)^{1/2}$
\dot{r}	= regression (burning) rate, \dot{m}_s / ρ_r
\dot{r}_n	= normal (nonerosive) regression rate
R	= gas constant per unit mole
Re_c	= Reynolds number, $\bar{\rho}_c \bar{u}_c \delta / \bar{\mu}_c$
Re_s	= Reynolds number, $\bar{\rho}_s \bar{v}_s \delta / \bar{\mu}_s$
t	= time
T	= static temperature
T_A	= activation temperature (energy/ R)
T_i	= interior propellant temperature
u_j	= velocity vector $\{u, v, w\}$
W_α	= molecular weight of species α
x_j	= coordinate vector $\{x, y, z\}$

Y_α	= mass fraction
β	= temperature exponent of reaction pre-exponential coefficient
δ	= half-height of port
Δh_r	= heat of reaction per unit mass
Λ	= turbulent macrolength scale
μ	= viscosity
ω	= specific reaction source term
ρ	= density
Φ	= concentration (pressure) exponent in reaction rate

Superscripts

$(\bar{\quad})$	= time average of variable
$(\quad)'$	= turbulent fluctuating value of variable

Subscripts

c	= centerline
e	= reaction end state
g	= gas phase
h	= condition at port head end
s	= condition at surface
α	= index for chemical species
π	= denotes propellant solid phase
$(,)$	= differentiation
\cdot	= reaction initial state

Introduction

CONTEMPORARY solid-propellant rocket motors often utilize a central port—the "grain port"—through which the combustion gases flow. An assumption which is almost universally used in analyses of motor performance is that the flow properties within the grain port may be represented by their bulk averages over a cross section. This assumption is practical and adequate providing closure relationships are available for describing inherently multidimensional processes occurring near the port surface (e.g., combustion and viscous friction). The closure process becomes more formidable when propellant combustion locally interacts with the fluid dynamics. One such interaction effect, which can lead to a substantial increase in the mean propellant burning

Presented as Paper 78-977 at the AIAA/SAE 14th Joint Propulsion Conference, July 25-27, 1978; submitted Aug. 25, 1978; revision received Jan. 16, 1980. Copyright © American Institute of Aeronautics and Astronautics, Inc., 1978. All rights reserved.

Index categories: Solid and Hybrid Rocket Engines; Reactive Flows; Boundary Layers and Convective Heat Transfer—Turbulent.

*Consultant, currently, Senior Research Scientist, Princeton Combustion Research Laboratories, Inc., Princeton, N.J. Member AIAA.

rate under high port velocity conditions, is termed erosive burning.

Reviews of erosive burning theoretical treatments and experimental investigations may be found in Williams et al.,¹ Kuo and Razdan,² and in the analysis of Mukunda,³ King,⁴ Beddini,⁵ and Razdan and Kuo.⁶ These analyses all assume that the flow within the grain port of a solid-rocket motor is of classical boundary-layer type. Specifically, velocity profile solutions for a turbulent boundary layer are developed (with various levels of analytic and empirical approximation) subject to matching to a uniform "core" flow which is assumed to exist within the central region of the port. The gradient of the velocity profile enters into the specification of turbulent diffusivity in the propellant flame zone, which in turn governs the magnitude and scaling of erosive burning.

To experimentally simulate the flowfield in the grain port of actual rocket motors, Dunlap et al.⁷ and Yamada et al.⁸ have investigated the flow in a porous tube and channel, respectively, with transpiration through the side wall. The Reynolds numbers (based on transpiration velocity and characteristic diameter) of these experiments were within the range associated with typical rocket motors. Based on the experimental results, both of these investigations concluded that the mean velocity profiles in actual rocket motors corresponded with self-similar solutions to the laminar Navier-Stokes equations in the inviscid limit. No evidence of a uniform core flow region was found, since the mean velocity profiles were similar in some respects to those in laminar pipe or channel flow. In addition, appreciable levels of turbulence were found, and Yamada et al. showed that the turbulence intensity profile behaved in a substantially different manner from typical turbulent channel flow. These experimental investigations have therefore posed some serious questions concerning the nature of the flowfield in actual motors, and for the assumptions used in erosive burning analyses. The mean flow behavior has also been shown by Culick⁹ to affect the aeroacoustics of the solid rocket motor.

The principal objective of the present investigation is to analyze the flowfield in the solid-rocket motor and its effects on erosive burning. It will be shown that the conflicting cold flow experimental results and prior analytical assumptions concerning the turbulent velocity profile can be substantially reconciled. In addition, the effects of propellant surface roughness and motor size on erosive burning will also be investigated. The problem is approached by extending the reacting turbulent boundary-layer analysis developed in Ref. 5. This approach utilizes a semiempirical, second-order closure description of turbulence and is sufficiently comprehensive to account for several aerothermochemical features of interest. The general model developed herein will be referred to as the solid-propellant erosive combustion (SPEC) model in the text.

Table 1 Major assumptions

1)	Single-step, homogeneous, and stoichiometric gas phase reaction.
2)	Specific heats of species are equal and independent of temperature.
3)	$k/c_p = \rho D = \mu(T)$ (Prandtl and Lewis numbers of unity).
4)	Surface decomposition of a homogeneous propellant is governed by Arrhenius kinetics.
5)	Turbulent correlations involving the temporal pressure derivative and nongradient mechanical heat production terms in the energy equation [Eq. (13) of Ref. 5] are negligible (i.e., nonhypersonic flow).
6)	The flow is quasisteady ($\partial/\partial t = 0$), and two-dimensional ($\partial/\partial z = 0 = \dot{w}$) in the plane of Fig. 1. The port half-height δ is taken to be constant.
7)	The flow is of thin shear-layer type, viz., $\partial/\partial y \gg \partial/\partial x$ with $\partial p/\partial y = 0$, and is symmetric about $y = \delta$ in the mean.

Analysis

The analysis closely follows that of Ref. 5, with the exception that boundary conditions appropriate for flow in a two-dimensional (i.e., planar) grain port and a surface roughness model will be implemented. The two-dimensional geometry (Fig. 1) approximates the configurations experimentally investigated by Yamada et al. for cold flow simulations, and by Stokes et al.¹⁰ for erosive burning. The port half-height δ (distance from surface to centerline) will be assumed constant in the present investigation.

Enthalpy and Mass Fraction Similarity

Major assumptions are summarized in Table 1. Upon invoking assumptions 1-3, and as a consequence of assumption 5, it has been shown⁵ that the general unsteady gas phase equations for species mass fraction ($Y_\alpha, \alpha = 1 \dots N$) and total (sensible plus kinetic) enthalpy H may be reduced to a single equation for a variable f , i.e.,

$$(f \cdot f)_{,t} + (\rho u^t f)_{,t} = g^{tm} (\mu f_{,m})_{,t} + \omega$$

where

$$f = (\Delta h_g)^{-1} (H - H_e + \Delta h_g) = (Y_\alpha - Y_{\alpha e}) / (Y_{\alpha e} - Y_{\alpha e})$$

$$\Delta h_g = \sum_\alpha (Y_{\alpha e} - Y_\alpha) h_\alpha^0$$

and ω is the normalized chemical production term. In the above equations, Δh_g is the heat of reaction per unit mass, and the subscripts e and e refer to conditions at the initial and end (equilibrium) states of reaction, respectively. The parameter ϕ appearing in the earlier analysis has here been absorbed into the definition of ω . It may be noted that the reaction is not required to be completed within the considered flow region, as might occur for an extremely small "motor" or a very slow reaction.

For complete similarity to exit, the boundary conditions for mass fractions and enthalpy must be identical when expressed in terms of the variable f . If the motor head end is assumed nonreactive and adiabatic, then equilibrium exists so that $f = 1$ there. Assumption 7 precludes the influence of an arbitrary downstream boundary condition on f . Hence, the behavior of thermodynamic variables (excluding pressure) within the port will be affected primarily by boundary conditions at the propellant surface. The surface boundary conditions for Y_α and H can be written for a port of rather general cross-sectional shape as⁵

$$f_s = (\dot{m}_s)^{-1} \mu n^j f_{,j} |_s$$

where \dot{m}_s is the surface mass transfer and n^j is the contravariant unit surface normal vector. As the unsteady differential equation and boundary conditions involve f alone, similarity is obtained between both mean and unsteady (turbulent) parts of Y_α and H is the gas phase.

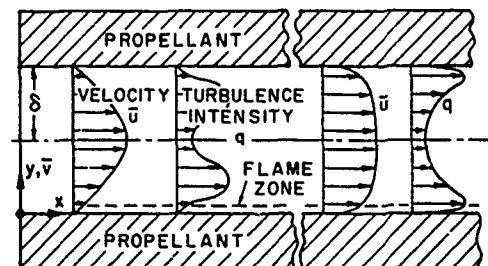


Fig. 1 Schematic representation of grain port velocity and turbulence intensity development.

The instantaneous reaction source term appearing in the f equation may be written as

$$\omega = B_z T^{\beta z} \exp(-T_{A_z}/T) \left[\frac{\rho(H_c - H)}{\Delta h_z} \right]^* \quad (4)$$

An effort has been made to improve the turbulent combustion modeling used in Ref. 5 (i.e., modeling the time average, $\bar{\omega}$, and correlations involving ω'). Specifically, a second-order Taylor expansion of ω has been used to provide $\bar{\omega}$ in terms of \bar{T} and \bar{T}'^2 , and ω' in terms of T' . The resulting correlations are determined in the final equation system without the additional empiricism often associated with turbulent combustion models. The proposed model is therefore similar to models developed by Borghi¹¹ and others. An analytically based combustion model is favored for this problem since temperature fluctuations in the combustion region are expected to be relatively small. In preliminary calculations, however, the proposed combustion model proved to be unstable. The instability is believed due to the strict numerical coupling required by the solid-propellant problem. Consequently, the results to be presented assume $\bar{\omega} = \omega(\bar{T})$ and do not indicate the possibly important effects of turbulence on reaction rate.†

Final Equations

With Y_α expressed in terms of $H = h + u'u/2$ and $h = c_p T$, use of the second-order turbulence modeling procedure of Sullivan¹³ provides differential equations which, after time averaging and in boundary-layer form, are identical to those used in Ref. 5. The empirical turbulence modeling parameters (listed in the Appendix) are also identical to the values used in Ref. 5 and in the evaluation of Sullivan's procedure by Rubesin et al.¹⁴ Overall, the complete system consists of the equations of state and continuity, and parabolic differential equations for $u, h, u'u', u'v', v'v', w'w', \rho'u', \rho'v', h'u', h'v',$ and $h'h'$. The second-order correlation equations are quite lengthy and are not listed here. They correspond with the correlation equations of Sullivan, but with the terms $\Delta h_z \chi' \omega'$ (where χ' represents $u', v', 2h'$) appearing on the right-hand sides of the $h'u', h'v',$ and $h'h'$ equations. The mean equations for conservation of mass, momentum, enthalpy, and the equation of state are

$$(\bar{\rho}\bar{u})_{,x} + (\bar{\rho}\bar{v} + \overline{\rho'v'})_{,y} = 0 \quad (1)$$

$$\bar{\rho}\bar{u}\bar{u}_{,x} + (\bar{\rho}\bar{v} + \overline{\rho'v'})\bar{u}_{,y} + (\overline{\rho'u'})_{,y} = -\bar{p}_{,x} + (\bar{\mu}\bar{u}_{,y})_{,y} \quad (2)$$

$$\begin{aligned} \bar{\rho}\bar{u}\bar{h}_{,x} + (\bar{\rho}\bar{v} + \overline{\rho'v'})\bar{h}_{,y} + (\overline{\rho'h'})_{,y} = \bar{u}\bar{p}_{,x} + \bar{\mu} \left[(\bar{u}_{,y})^2 \right. \\ \left. + \frac{q^2}{\Lambda^2} \left(a + b \frac{\rho q \Delta}{\mu} \right) \right] + (\bar{\mu}\bar{h}_{,y})_{,y} + \Delta h_z \omega \end{aligned} \quad (3)$$

†A reviewer has justifiably questioned the realism of results obtained without accounting for the effects of turbulence on reaction rate (combustion-turbulence interaction). Further research on this topic has been performed since the original manuscript was submitted, and will be presented in detail in a subsequent paper. Insofar as the present results are concerned, it has been found that combustion-turbulence interaction can affect the mean reaction rate and turbulent diffusivity profiles. However, the collective effects on the mean temperature profile and on erosive burning are, surprisingly, quite small. These results qualitatively agree with the recent findings of Borghi and Dutoya,¹² who used an empirically specified PDF to model interaction effects for an entirely gas phase problem.

$$\begin{aligned} \bar{p} = R\bar{\rho}\bar{T} \left[\sum_\alpha \bar{G}_\alpha (1 - \bar{T}'\bar{T}'/\bar{T}^2) - \sum_\alpha \overline{G'_\alpha \bar{T}'}/\bar{T} \right. \\ \left. - \sum_\alpha \sum_\beta (\overline{G'_\alpha G'_\beta}) / \sum_\alpha \bar{G}_\alpha \right] \end{aligned} \quad (4)$$

where $G_\alpha = Y_\alpha/W_\alpha$, a and b are turbulence modeling parameters, and Λ is the turbulent macrolength scale.

Initial and Boundary Conditions

The parabolic form of the differential equations requires initial conditions for the dependent variables to be established downstream of the head end. Experimental and analytical results^{7,8} suggest that an assumed initial station of $x_0 \geq 5\delta$ is more than adequately far downstream to satisfy the thin shear-layer assumption. The head-end pressure \bar{p}_h is specified, and the mean static pressure at x_0 is obtained from inviscid theory. The analytical velocity profile⁸

$$\frac{\bar{u}}{\bar{u}_c} = \sin \frac{\pi y}{2\delta} \quad (5)$$

is used at x_0 for both cold flow and erosive burning calculations. Velocity-scaled experimental profiles of turbulence intensity are used to satisfy initial conditions for the Reynolds stress variables, $\overline{u'u'}$. For reacting flows, the mean temperature profile is obtained from numerical solution of the energy equation for normal deflagration, and all thermal correlations are assumed null at x_0 . Some sensitivity to the initial conditions is obtained in the downstream calculations for particular configurations. This sensitivity is discussed in the next section.

Boundary conditions at the propellant surface ($y=0$) are: $u=0$, $\bar{p}\bar{v} = \bar{m}_s = \bar{r}\rho_s$, with all correlations assumed null. A linear pyrolysis relation,

$$\bar{m}_s = A_s T^{\beta s} \exp(-T_{A_s}/\bar{T})$$

is used in conjunction with the interface condition

$$\bar{m}_s = [L_s^0 + \bar{h} - c_s T_s]^{-1} k \frac{\partial \bar{T}}{\partial y}$$

to determine \bar{m}_s and \bar{T}_s . For cold flow calculations, the parameter \bar{v}_s is specified.

The geometric symmetry of the problem is utilized at $y=\delta$. The condition of symmetry implies that there must be no mean fluxes (convective, diffusive, or turbulent) through $y=\delta$. Hence, at $y=\delta$: $\bar{v} = \overline{u'v'} = \overline{h'v'} = \overline{\rho'v'} = 0$, with the normal gradients of all other dependent variables being null.

Pressure Gradient

As opposed to unconfined flows, wherein the pressure \bar{p} and pressure gradient, $\partial \bar{p}/\partial x$, are imposed on the boundary layer, the pressure gradient for confined boundary-layer flows evolves as part of the solution. The value of $\partial \bar{p}/\partial x$ must be consistent with the condition of conservation of mass ($\bar{v}_c = 0$) in the port. Utilizing this condition and the condition $\partial \bar{p}/\partial y = 0$, the momentum equation (2) may be integrated to yield

$$\frac{d\bar{p}}{dx} = \frac{-1}{\delta} \left[\bar{\mu} \frac{\partial \bar{u}}{\partial y} \Big|_s + \frac{d}{dx} \int_0^\delta \bar{\rho} \bar{u}^2 dy \right]$$

The first term within the brackets represents the decrease in static pressure due to surface shear, and the second term contains the effects of mass addition and change of momentum profile shape on static pressure. The latter effect

is excluded from typical one-dimensional grain port flow calculations.

Surface Roughness Model

In Ref. 15, a preliminary model for small surface roughness has been developed which is compatible with the second-order closure technique and allows direct integration to the mean surface. The model is based on the concept of Rotta (in Ref. 16) that the turbulent macrolength scale at the surface, Λ_s , tends to a nonzero value which is characteristic of the physical roughness height. It has been shown in Ref. 15 that the empirical relation $\Lambda_s = k_s/6.5$ (where k_s is the equivalent sand roughness height) satisfactorily correlates flat-plate experimental data for buffer and logarithmic region velocity profiles, and for surface friction. For "fully rough" surfaces¹⁶ the model becomes invalid, but this condition was not exceeded in the present calculations.

It will be shown that the calculations for erosive burning are quite sensitive to the value of surface roughness assumed. However, there are difficulties in implementing this—or any roughness model—for propellant surfaces. One problem is that the standard measure of surface roughness (equivalent sand roughness) is difficult to estimate for "typical" propellant surfaces undergoing combustion. Another aspect to consider is that the actual peak-to-valley roughness height can depend upon pressure. Caveny¹⁷ indicates that for composite propellants, for example, the roughness height may scale as a function of the absolute difference between oxidizer and average propellant burning rate, and hence would change from head to nozzle end along the grain. In the present work, these additional complexities are neglected by utilizing constant values of k_s equal to estimated peak-to-valley propellant roughness heights.

Results and Discussion

Grain Port Cold Flow Simulations

The cold flow simulations of Dunlap and Yamada have shown that, based on values of surface transpiration Reynolds number ($Re_s = \bar{\rho}_s \bar{v}_s \delta / \bar{\mu}_s$) which are typical of real motors (order 10^3), the mean longitudinal velocity profile in the port corresponds with self-similar solutions for inviscid, laminar flow. Yet, both experiments have also indicated that turbulence intensity profiles increase in magnitude, and that the height of maximum intensity moves closer to the port surface with increasing distance from the head end. This nonsimilar behavior of turbulence and velocity provides a critical test of grain port hydrodynamic modeling.

Mean Velocity Profiles

A comparison of present (SPEC) model predictions with the velocity profile data of Yamada is shown in Fig. 2 for $x=25$ cm. The agreement between prediction, experimental data, and the inviscid theoretical description given by Eq. (5) is quite good. Similar agreement is also obtained at the $x=15, 20,$ and 29 cm experimental stations (not shown). If allowance is made at the initial station for the fact that the calculations assume $\bar{v}_s = 1.2$ m/s, whereas \bar{v}_s changes somewhat along the experimental surface (its bulk average is 1.2 m/s), then good agreement is also obtained with the unnormalized velocity profiles shown in Fig. 2 of Ref. 8. Agreement between calculations and inviscid theory is expected when both viscous and Reynolds stresses are negligible in Eq. (2). In this case Eq. (5) is an approximate solution for incompressible flow.

In a computational experiment, it is a simple matter to "lengthen" the port. This has been done to investigate whether the inviscid profile persists at higher center port Reynolds numbers, $Re_c = \bar{\rho}_c \bar{u}_c \delta / \bar{\mu}_c$, than those obtained in the 29 cm length channel of Yamada, et al. Contrary to the conclusions of Yamada et al., the present model predicts (Fig. 2) a transition from a laminar to a turbulent velocity profile,

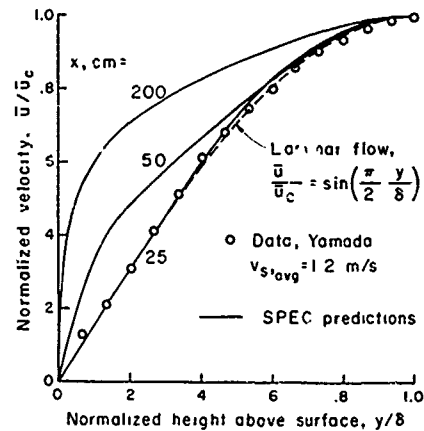


Fig. 2 Velocity profiles in cold flow simulation of two-dimensional grain port.

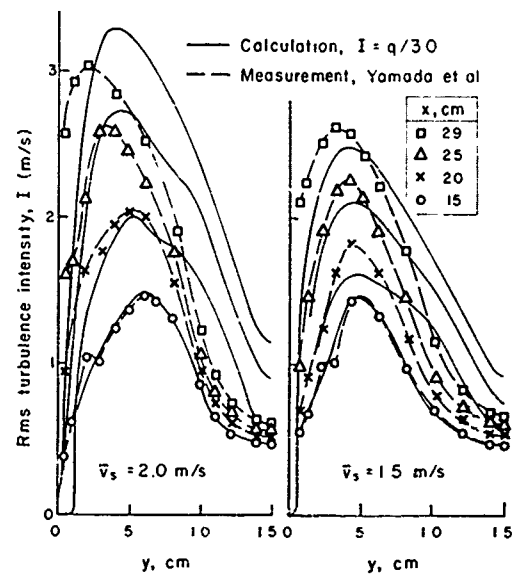


Fig. 3 Development of turbulence in cold flow simulation.

beginning at about 50 cm. The profiles continue to develop in steepness of surface gradient, such that by $x=200$ (Mach number ≈ 0.6), the velocity profile is nearly represented by a $1/7$ power law. The mechanism of transition will be discussed subsequently.

Behavior of Turbulence Intensity

A comparison between the intensity profile data of Yamada et al. and the model calculations is shown in Fig. 3 for two values of \bar{v}_s . For these calculations $x_0 = 15$ cm has been chosen to correspond with the first downstream profile, and $k_s = 65 \mu\text{m}$ is assumed to characterize the surface roughness. Qualitatively, the calculations show behavior similar to data in that turbulence increases in magnitude, with the height at which maximum intensity occurs (y_m) decreasing as x increases. Quantitatively, however, it was found necessary to multiply the intensity data (denoted by the symbol I) by a factor of 3.0 at the initial station to achieve downstream growth rates in calculated turbulence intensity (q) similar to the experimental values shown. This would appear to imply a quantitative deficiency in the modeling of turbulence development for the specific configuration. However, the calculated maximum intensities (here denoted by q_m) obtained from Fig. 3 are in the range of 12-15% of \bar{u}_c . These values are consistent with the relative intensities found in the Dunlap investigation and also in Fig. 5 of Ref. 8.

In addition to the sensitivity of the calculations to the magnitude of the turbulence initial conditions, some sensitivity to the assumed value of k_s is also observed. This sensitivity is reflected in the growth rates of the turbulent fluctuations, and in the initiation of the mean velocity profile transition process. It has also been found that the laminarization effect of the large, favorable pressure gradient exerts a strong influence on turbulence in the initial region of the flow. This leads to the question of how initial (preturbulent) disturbances are generated in the head-end region of the port. Possible mechanisms include the direct generation of vortical disturbances by the porous surface or air supply system, and the presence of acoustic disturbances which have propagated upstream in the flow. Neither of these effects has been included in the present analysis.

Notwithstanding the laminarizing effects due to large favorable pressure gradients (which diminish with axial distance in the port), an argument is now presented on why transition within a port is possible and often probable. Consider the scaling of terms in the momentum equation (2) for incompressible flow. The convective and pressure gradient terms may be scaled to within multiplicative constants as^{7,8}

$$\frac{D\bar{u}}{Dt} \sim \frac{-d\bar{p}/\rho}{dx} \sim x$$

As an approximation, the Reynolds stress term, $\overline{\partial u'v'}/\partial y$, will scale as I_m^2/y_m ($\sim q_m^2/y_m$). Both calculations and data indicate that in most cases, I_m^2/y_m grows faster than x . For example, if the data correlations of Ref. 8 are used, $I_m^2/y_m \sim \bar{u}_c^{1.6} \exp(-1/\bar{u}_c)$, which for large $\bar{u}_c \sim x^{1.6}$. Hence, given a port of sufficient length, transition should occur unless a sonic condition occurs first. Accurate prediction of the transition region will depend on the adequacy of turbulence modeling and knowledge of initial conditions. Confirmation of the transitional behavior of the velocity profile may be found in the porous tube measurements of Olson.¹⁸ These results were, however, obtained at surface transpiration Reynolds numbers lower than those associated with typical solid-propellant motors.

Reacting Flow and Erosive Burning

In the experiment of Stokes et al.,¹⁰ a "slab" motor (approximating the two-dimensional conditions of Fig. 1) was used to generate appreciable erosive burning. Assuming that the mean flow and turbulence can attain quasisteady conditions within the 0.06 s test times, and neglecting the $\approx 15\%$ variation of δ , a simulation of two-dimensional flow within the port can be obtained with the SPEC model. Greater reservations exist concerning simulation of the composite propellants used in Ref. 10 with the present homogeneous combustion model. However, the explicit appearance of a

combustion model does not occur in many erosion theories. Additionally, it has been well established that a key parameter affecting erosive burning is the normal burning rate \dot{r}_n . The SPEC model is able to represent aerochemically (over a limited range of interest) the normal burning rate pressure dependence of the EBT propellant used in Ref. 10, viz., $\dot{r}_n = 0.92 (p/p^*)^{0.55}$ cm/s. The parameters used to obtain this correlation are listed in Table 2, and have been estimated from Refs. 5 and 10.

Erosive Burning and Effect of Surface Roughness

Using the formulated initial and boundary conditions, and the physical parameters of Table 2, a comparison of SPEC model results with the experimental data of Stokes et al. is shown in Fig. 4. Comparison is made for two values of head-end pressure \bar{p}_h . Both the data and the one-dimensional, frictionless, nonerosive pressure calculations adapted from Ref. 10 have been corrected (by $\approx 3\%$) at the head end to correspond with the tabulated values,¹⁰ viz., $\bar{p}_h = 79.5$ and 60.0×10^7 dyne/cm² for tests EBT-3 and EBT-4, respectively. The corresponding values of δ (0.415, 0.404 cm) used in the calculations are obtained from the initial value plus the distance burned measurements at the head end. Initial conditions are specified at $x_0 \approx 9\delta$.

Considering the lower pressure EBT-4 results first, increasing the surface roughness height k_s produces increased erosion and hence decreased pressure along the port. For $k_s = 0$, slight erosion is obtained, such that the regression ratio \dot{r}/\dot{r}_n is only 1.07 at $x \approx 50$. Prior results⁵ of the SPEC model for smooth surfaces and unconfined boundary layers yielded underprediction of typical data by factors of two or three for lower burning rate propellants. Although this was attributed to the assumed combustion mechanism in Ref. 5, it is possible that the effects of surface roughness and combustion model are of equal importance for the quantitative prediction of erosion. One effect of surface roughness is to decrease the viscous sublayer height, thus increasing ambient turbulence levels in the flame zone. This effect can, in principle, compensate for some inadequacies of the combustion model (e.g., a lower than actual flame height). However, the value of k_s which produces the best agreement with the EBT-4 data is 46

Table 2 Thermochemical parameters

$T_e = 2976$ K (adiabatic flame temperature)
$c_p = 1.92 \times 10^{-3}$ J/kg-K
$W_o = W_{av} = 25.8$ g/g-mole
$T_{Ag} = 2.0 \times 10^4$ K
$B_g = 1.59 \times 10^{10} \text{ g}^{1-\phi} \text{ cm}^{\phi-1} \text{ s}^{-1} \text{ K}^{-\beta_g}$
$\phi = 1.10$
$\beta_g = 0$
$\mu = 4.42 \times 10^{-6} T^{0.65}$ poise
$T_i = 300$ K
$L_s^0 = 8.37 \times 10^{-2}$ J/kg
$\rho_s = 1.70$ g/cm ³
$c_s = 1.46 \times 10^{-3}$ J/kg-K
$\beta_s = 0$
$A_s = 2.50 \times 10^6$ g/cm ² -s
$T_{As} = 1.0 \times 10^4$ K

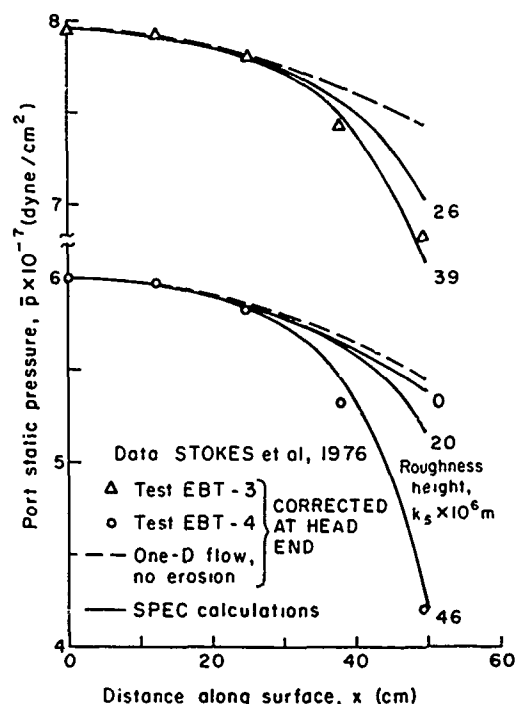


Fig. 4 Effect of surface roughness height k_s on port static pressure development with erosive burning.

μm . This value is approximately 10% of the large (400 μm) ammonium perchlorate crystal size used in the EBT formulation, and is not believed inordinate. Values of surface roughness in the 30-100 μm range (for both composite and homogeneous propellants) have been used in the erosive burning analysis of Mukunda.³

Maintaining all other conditions constant, the head-end pressure is increased from the EBT-4 to the EBT-3 test value in the top of Fig. 4. In this case a value of $k_s = 39 \mu\text{m}$ provides the best agreement with data, a slight decrease from the EBT-

4 results. The decrease is probably within the range of experimental error, although the possible effect of pressure on surface roughness noted previously in the paper may be present. (The burning rates of EBT and pure AP are more equivalent at this pressure.)

Profile Development in Grain Port

Figure 5 shows the predicted development of key dependent variables within the slab-motor port. Computational conditions correspond to the EBT-4 run in Fig. 4 with $k_s = 46 \mu\text{m}$. Elements of the basic interaction mechanisms between mean and turbulent variables have been discussed in Ref. 5. Qualitative differences between the present and prior results will be discussed herein.

The temperature profile at $x = 5 \text{ cm}$ in Fig. 5a is identical to the normal (strand) burning profile. It persists (being scaled in height by change in pressure) until the start of erosive burning at $x = 20$. By $x = 35$, the propellant regression ratio \dot{r}/\dot{r}_n has reached 1.9, which is reflected by the change in temperature gradient near the surface. Considering the rapidly changing pressure, the temperature profile at $x = 50$ ($\dot{r}/\dot{r}_n \approx 3.5$) reflects severe diffusive broadening due to turbulence. The temperature profile in the main portion of the port is decreased somewhat due to adiabatic acceleration (Mach number = 0.69 at $x = 50$), but this does not perceptibly affect the flame zone.

The turbulent contribution to heat flux may be written as $\rho \bar{h}'v'$ to second order. Figure 5b shows that $\bar{h}'v'$ is correlated with flame position and temperature gradient. This suggests that a diffusive approximation of turbulent heat flux may be valid for alternative erosive burning analyses.

Normalized velocity profiles are shown in Fig. 5c. Utilizing Eq. (5) as an initial condition at $x_0 = 3.5$, the velocity profile shows signs of a transitional "bulge" in the lower portion of the boundary layer at $x = 5$. By $x = 35$, transition has been completed and erosion is severe. In this and other calculations to be presented for this propellant, erosive burning consistently occurs subsequent to transition. Apparently, it is the large increase in surface velocity gradient which enables the production of sufficient turbulence (Fig. 5d) to enter the flame zone (Fig. 5a).

It is also noted that the calculations shown in Fig. 5 are much less sensitive to the initial conditions placed on the Reynolds stresses than are the cold flow calculations previously discussed. The precise reason for this has not been determined, but may well be related to the gas-phase density change induced by combustion.

Effect of Port Size on Erosive Burning

Mihlfeith¹⁹ has observed that the widely used Lenoir-Robillard (L-R) theory,²⁰ as well as some other theories, are deficient in their ability to scale erosive burning as a function of port size. Specifically, it was noted that the L-R theory overpredicts erosive burning in full-scale motors when initially correlated with subscale data. A comparison of the present theory with that of Lenoir and Robillard is therefore warranted, with particular interest in the geometric scaling of erosive burning. Stokes et al. have correlated the L-R theory to the experimental static pressure results shown in Fig. 4. In the present notation, the L-R expression for regression rate may be written as¹⁰

$$\dot{r}_{LR} = \dot{r}_n + \alpha_L (\bar{\rho}_c \bar{u}_c)^{0.8} (2\delta)^{-0.2} \exp(-\beta_L \dot{r}_{LR} \rho_x / \bar{\rho}_c \bar{u}_c)$$

The parameters $\alpha_L = 0.0245$ and $\beta_L = 42$ were evaluated¹⁰ using a least-squares procedure. Theoretical comparisons have been made by utilizing SPEC-calculated values of $\bar{\rho}_c$ and \bar{u}_c along the port.

Results of the comparison are shown in Fig. 6. The regression ratios for increasing values of δ have been plotted as a function of centerline mass flux, $\bar{\rho}_c \bar{u}_c$. Considering the

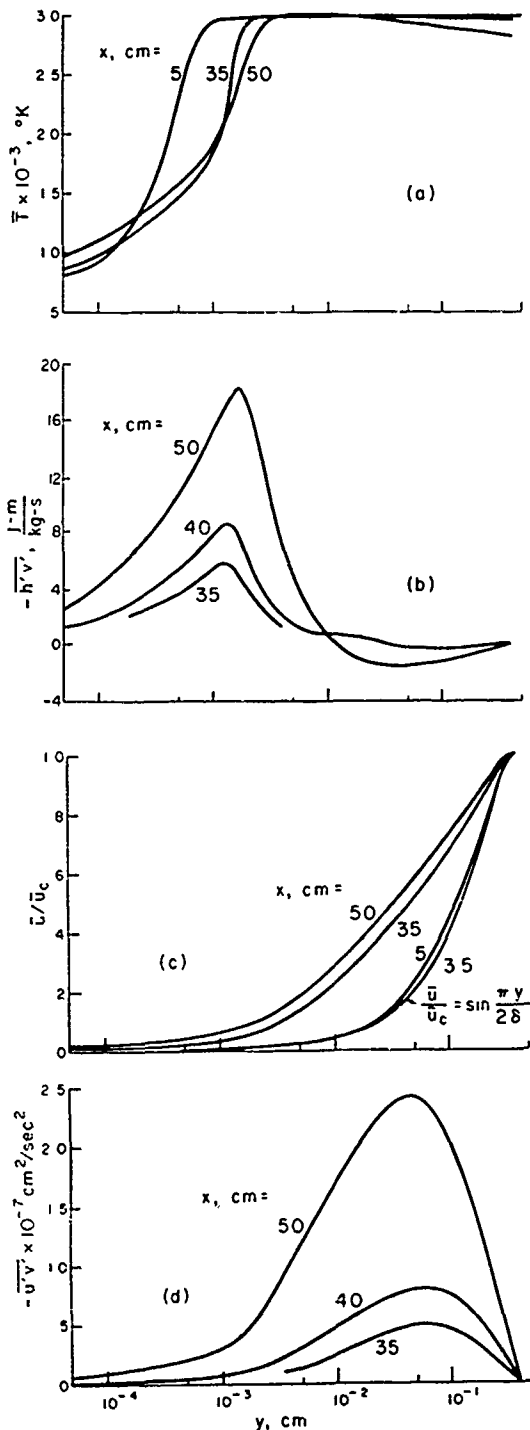


Fig. 5 Profile development in two-dimensional grain port: a) mean temperature; b) turbulent heat transfer correlation; c) normalized mean velocity; d) turbulent shear stress correlation, EBT-4 conditions, $k_s = 46 \mu\text{m}$.

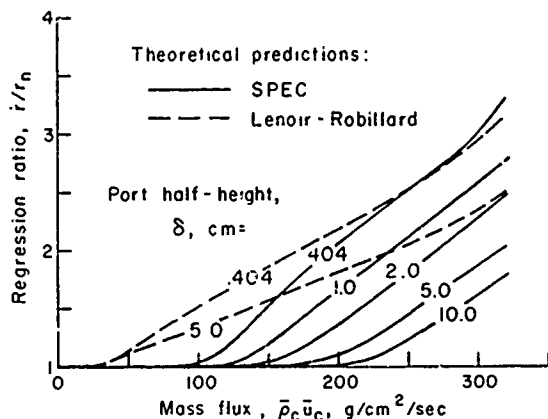


Fig. 6 Effect of port size on erosive burning as function of centerline mass flux, $k_s = 46 \mu\text{m}$.

$\delta = 0.404$ case, both theories show similar regression ratios at higher values of mass flux, this being required to produce the experimental static pressure results of Fig. 4. At lower values of mass flux, the L-R theory predicts greater erosion. This is partly due to the use of centerline rather than bulk average velocities in the expression for \dot{r}_{LR} . The centerline velocities become within 20% of bulk velocities subsequent to transition, i.e., at mass velocities where the SPEC model shows erosion.

As the port half-height δ is increased, SPEC calculations (denoted by solid lines) show a continuous decrease in regression ratio at constant mass flux. For the given motor, most of the decrease in regression ratio is attributed to a translational increase in threshold mass flux. Although there is a slight decrease in slope for large δ , SPEC-calculated regression ratios appear to scale with the shift in threshold mass velocity. By comparing the L-R and SPEC calculations for $\delta = 5$ cm, the SPEC model is shown to predict less erosion with geometric scale-up. Qualitatively, this behavior in the L-R model is largely due to the lack of threshold velocity dependence upon scale. Similar results are obtained for other values of δ .

Conclusions

The major conclusions of this research may be summarized as follows.

1) The SPEC model has been compared with experimental data in cold flow simulations of a two-dimensional grain port. These comparisons show good agreement with laminar theoretical description for mean velocity profile in the Reynolds number range of data.

2) At higher center port Reynolds numbers, transition to a turbulent velocity profile is predicted to occur. This prediction contradicts the conclusions of recent experimental investigations, i.e., the inviscid velocity profile does not necessarily persist throughout laboratory or full-scale motors. The plausibility of transitional behavior is justified with an argument based on the development of turbulence within the port.

3) The completion of transition is followed by the start of erosive burning in theoretical comparisons with laboratory motor data. The intricate connection between transition and erosive burning warrants further experimental investigation with cold flow apparatus.

4) The effects of surface roughness on erosive burning are indicated to be quite important. Although possibly compensating for some inadequacies in combustion modeling, realistic values of roughness have provided good agreement with experimental static pressure data under severe erosion conditions.

5) The effect of geometric scaling on erosive burning has been theoretically investigated for a two-dimensional motor. As port half-height (hydraulic radius) is increased, the SPEC model is shown to produce less erosion than the Lenoir-Robillard model for a specific mass velocity. This observation qualitatively agrees with recent criticisms concerning geometric scaling deficiencies in the Lenoir-Robillard model.

Appendix: Turbulence Modeling Parameters

Listed below are the non-null parameters used for the second-order closure modeling of Sullivan.¹³ Note that some of the parameters appear only as collective products in the final equations. The uppercase notation is consistent with the computer generated format of the equations.

$$\begin{aligned}
 A &= 3.25 \\
 B &= 0.125 \\
 \text{CLAMB} &= 0.17 \\
 \text{DIN} &= 0.65 \\
 \text{AHH} &= 5.85 \\
 \text{AHU} &= \text{ARU} = 3.25 \\
 \text{BHH} &= 0.225 \\
 \text{VUU} &= \text{VUH} = \text{VHH} = 0.1 \\
 \text{VRU} &= \text{VRH} = \text{VRR} = 0.1 \\
 \text{PMU2} &= \text{PMH2} = \text{PMR2} = 1.0 \\
 \text{PTHM} &= \text{PTUM} = 0.15 \\
 \text{PGH2} &= \text{PGR2} = 0.8 \\
 \text{PGU} &= \text{PGU2} = 1.0 \\
 \text{WWU1} &= \text{WWR1} = \text{WWH1} = -0.1 \\
 \text{WWGU} &= -0.5 \\
 \text{WWGR} &= \text{WWGH} = -1.0
 \end{aligned}$$

Acknowledgment

This research has been supported by the Air Force Office of Scientific Research under prime Contract F44620-78-C-0016; Capt. R. F. Sperlein, program manager. The assistance of Mr. Asad Khan of Rutgers University in performing the calculations was appreciated.

References

- Williams, F. A., Barrere, M., and Huang, N. C., "Fundamental Aspects of Solid Rockets," AGARDograph 116, Chaps. 4, 6, and 7, Oct. 1969, pp. 339-456.
- Kuo, K. K. and Razdan, M. K., "Review of Erosive Burning of Solid Propellants," *Proceedings of 12th JANNAF Combustion Meeting*, Aug. 1975, pp. 323-338.
- Mukunda, H. S., "A Comprehensive Theory of Erosive Burning in Solid Rocket Propellants," *Combustion Science and Technology*, Vol. 18, 1978, pp. 105-118.
- King, M., "A Model of the Erosive Burning of Composite Propellants," *Journal of Spacecraft and Rockets*, Vol. 15, May-June 1978, pp. 139-146.
- Beddini, R. A., "A Reacting Turbulent Boundary Layer Approach to Solid Propellant Erosive Burning," *AIAA Journal*, Vol. 16, Sept. 1978, pp. 898-905.
- Razdan, M. K. and Kuo, K. K., "Erosive Burning Study of Composite Solid Propellants by Turbulent Boundary-Layer Approach," *AIAA Journal*, Vol. 17, Nov. 1979, pp. 1225-1233.
- Dunlap, R., Willoughby, P. G., and Hermesen, R. W., "Flowfield in the Combustion Chamber of a Solid Propellant Rocket Motor," *AIAA Journal*, Vol. 12, Oct. 1974, pp. 1440-1442.
- Yamada, K., Goto, M., and Ishikawa, N., "Simulative Study on the Erosive Burning of Solid Rocket Motors," *AIAA Journal*, Vol. 14, Sept. 1976, pp. 1170-1177.
- Culick, F.E.C., "Rotational Axisymmetric Mean Flow and Damping of Acoustic Waves in a Solid Propellant Rocket," *AIAA Journal*, Vol. 4, Aug. 1966, pp. 1462-1464.
- Stokes, B. B., Hessler, R. O., and Caveny, L. H., "Erosive Burning of Nonmetalized Composite Propellants—Data Acquisition and Analysis," *Proceedings of 13th JANNAF Combustion Meeting*, CPIA Pub. 281, Vol. II, Dec. 1976, p. 437.
- Borghini, R., "Chemical Reaction Calculations in Turbulent Flows Applicable to a CO-containing Turbojet Plume," *Advances in Geophysics*, Vol. 18, 1974, p. 349.

¹²Borghi, R. and Dutoya, D., "On the Scales of the Fluctuations in Turbulent Combustion," *Proceedings of 17th Symposium (International) on Combustion*, The Combustion Institute, Pittsburgh, Pa., 1979, pp. 235-244.

¹³Sullivan, R. D., "GYC—A Program to Compute the Turbulent Boundary Layer on a Rotating Cone," A.R.A.P. Working Paper 76-2, Aeronautical Research Associates of Princeton, Inc., Princeton, N.J., Aug. 1976.

¹⁴Rubesin, M. W., Crisalli, A. J., Lanfranco, M. J., Horstman, C. C. and Acharya, M., "A Critical Evaluation of Second-Order Closure Models for Incompressible Boundary Layers with Axial Pressure Gradients," AIAA Paper 77-128, Aerospace Sciences Meeting, Jan. 1977.

¹⁵Beddini, R. A., "Preliminary Studies of Roughness and Free-Stream Disturbance Effects on Boundary Layer Skin Friction," A.R.A.P. Technical Memo. 77-11, Aeronautical Research Associates of Princeton, Inc., Princeton, N.J., June 1977.

¹⁶Hinze, J. O., *Turbulence*, 2nd ed., McGraw-Hill Book Co., New York, 1975, pp. 614-624.

¹⁷Caveny, L. H., personal communication, June 19, 1978.

¹⁸Olson, R. M., "Experimental Studies of Turbulent Flow in a Porous Circular Tube with Uniform Mass Transfer through the Tube Wall," Ph.D. Thesis, University of Minnesota, Minneapolis, July 1964; also, Huesmann, K. and Eckert, E.R.G., "Untersuchungen über die laminare Stromung und den Umschlag zur Turbulenz in porösen Rohren mit gleichmässiger Einblasung durch die Rohrwand," *Wärme- und Stoffübertragung*, Bd. 1, 1968, p. S2.

¹⁹Mihlfeith, C. M., "JANNAF Erosive Burning Workshop Report," *Proceedings of 14th JANNAF Combustion Meeting*, CPIA Publication 292, Vol. 1, Dec. 1977, pp. 379-392.

²⁰Lenoir, J. M. and Robillard, G., "A Mathematical Method to Predict the Effects of Erosive Burning in Solid Propellant Rockets," *Proceedings of 6th Symposium (International) on Combustion*, Reinhold Publishing, Stanford, Conn., 1957, pp. 663-667.